Chapter 4

Synthetic Phase with the Structure of Apatite

Petr Ptáček

Additional information is available at the end of the chapter

http://dx.doi.org/10.5772/62212

Abstract

The previous chapters were dedicated to description of structure and properties of minerals from supergroup of apatite and introduction of method for identification and investigation of properties of phosphate minerals. The first synthesis of apatite was performed by Daubrée by passing the PCl_3 vapor over red-hot lime. The fourth chapter of this book introduces techniques for the preparation of synthetic analogs of apatite minerals including solid-state synthesis, wet chemical methods, hydrothermal synthesis as well as methods for preparation of single crystals. Chapter continues with description of structure and properties of synthetic compounds of apatite type and ends with incorporation of 3d-metal ions into the hexagonal channel of apatite.

Keywords: Apatite, Solid-State Synthesis, Wet Chemical Methods, Hydrothermal Synthesis, Single crystal, Lacunar Apatite

The first synthesis of apatite was performed by DAUBRÉE [1], who obtained it in crystals by passing the vapor of phosphorus trichloride (PCl_3) over red-hot lime. The synthetic mineral analogues of chlorapatite, fluorapatite, or the mixtures of these phases were prepared by MANROSS [2] via fusing of sodium phosphate either with calcium chloride, calcium fluoride, or both together. The similar process was also successfully used by BRIEGLEB [3]. FORCHHAMMER [4] prepared chlorapatite by fusing calcium phosphate with sodium chloride. When bone ash or marl was used instead of artificial calcium phosphate, mixed apatite was formed. Similar results were reported by DEVILLE and CARON [5], who fused bone ash with ammonium chloride and either calcium chloride or fluoride, and also by DITTE [6], who repeated Forchhammer's

experiment [7]. Zambonini and Ferrucio [8] found that the fusion of $Ca_3(PO_4)_2$ with $CaCl_2$ produced apatite with very weak birefringence. Fusing $Ca_3(PO_4)_2$ with an excess of NaCl gave crystals with the birefringence of 0.0050–0.0058.

By heating calcium phosphate with calcium chloride and water, under the pressure at 250°C, Debray prepared chlorapatite [9]. Weinshenk [10] also prepared chlorapatite by heating calcium chloride, ammonium phosphate and ammonium chloride at the temperature of 150 to 180°C in a sealed tube.[1] Cameron and McCaughey [11] prepared fluorapatite by dissolving calcium fluoride in fused disodium phosphate and lixiviating[2] the cooled melt. Artificial fluorapatite sometimes exhibits the peculiarity of re-entrant pyramidal ends or phantom crystals. Spodiosite ($Ca_2(PO_4)F$) is orthorhombic, chlorspodiosite ($Ca_2(PO_4)Cl$ [12],[13]) being much less developed along the *c*-axis than fluorspodiosite [14]. Chlorapatite was formed when dicalcium phosphate was added in excess to molten calcium chloride. When precipitated calcium phosphate was used, chlorspodiosite[3] ($Ca_3(PO_4)_2 \cdot CaCl_2$, $Ca_2(PO_4)Cl$ [14]) was obtained. Apatite was reported by Hutchins [15] and Voght [16] as present in lead-furnace slag [7].

The history of synthesis of various apatite compounds and substitution in the apatite structure including the preparation of didymium bearing chlorapatite and chlorspodiosite is described in the work of Zambonini and Ferrucio [17]. The paper describes three of those apatite syntheses using the mixture of $Ca_3(PO_4)_2$, $DiPO_4$ [4] and $CaCl_2$ in the weight ratio of 1:0.07:2.19 (1), 1:0.15:8.76 (2) and 1:0.67:2 (3). These mixtures were heated to the temperature of 1180, 1000 and 1100°C, respectively. Transparent, colorless apatite with the content of 3% $DiPO_4$ results from the first experiment. The second experiment leads to the pale-violet crystal of chlorspodiosite3. The crystals of $DiPO_4$ and only little amount of chlorapatite and chlorspodiosite with 9% of $DiPO_4$ were recognized in the third mixture.

Hendricks et al [19] reported the preparation of hydroxylapatite by the hydrolysis of tricalcium phosphate[5] with neutral ammonium citrate. Oxoapatite was then prepared by the ignition of hydroxylapatite to constant weight at 50°C.[6]

[1] The method is described in **Section 4.1.1**.

[2] The separation techniques based on leaching of minerals from a solid by dissolving them in a liquid.

[3] Chlorine analog of spodiosite [14]. Calcium chlorspodiosite is colorless crystalline compound structurally related to the mineral wagnerite ($Mg_2(PO_4)F$). It was reported by Nacken in his study of the phase relationships which was obtained in the system $CaCl_2$-CaO-P_2O_5 [12]. The synthesis of the compound by dissolving $Ca_3(PO_4)_2$ in fused $CaCl_2$ was reported by Klement and Gembruch [13]. Since the mineral was recognized as the mixture of fluorapatite, calcite and serpentine, it was discredited (IMA action 2003-03-B).

[4] Didymium (Di) was recognized as the mixture of element of neodymium and praseodymium [18].

[5] Tricalcium phosphate was prepared by slow addition of Na_3PO_4 solution to the solution with the excess of $Ca(NO_3)_2$. The precipitate was washed with saturated solution of $Ca_3(PO_4)_2$ until the filtrate was free of nitrates. The salt was then dried at 50°C [19],[18].

[6] Hydroxylapatite is very difficult to dehydrate, even at high temperature (**Section 1.5.2**). As a consequence of this, many workers have mistaken it for oxyapatite [18].

http://dx.doi.org/10.5772/62212

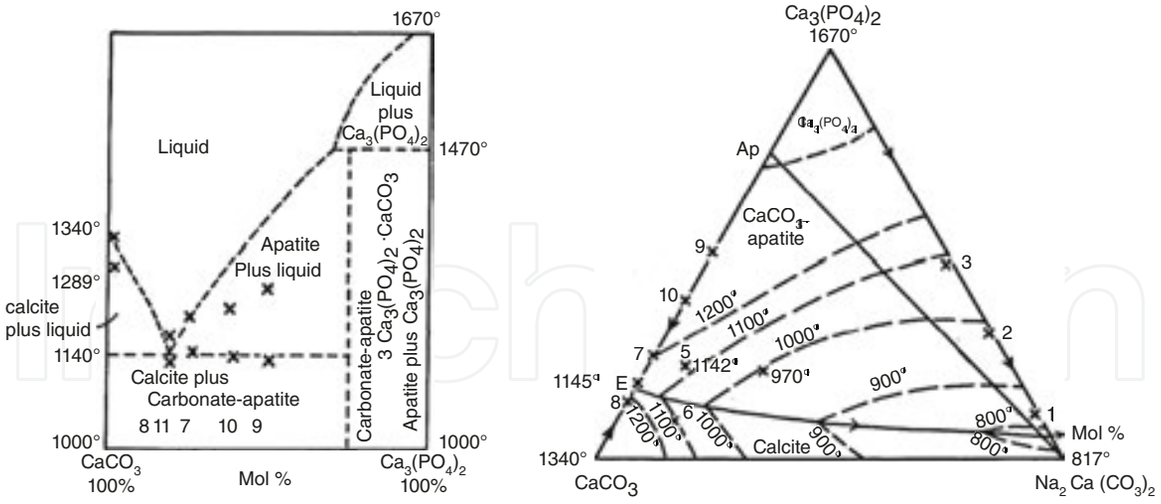

Fig. 1. The phase equilibrium in carbonate-apatite–$CaCO_3$ (a) and carbonate-apatite–$CaCO_3$–Na_2CO_3 systems (b) [20].

Eitel [20] investigated the binary systems $Ca_3(PO_4)_2$–$CaCO_3$ (**Fig. 1**(**a**)) and $Ca_3(PO_4)_2$–$CaCO_3$–Na_2CO_3[7] (**b**) and claimed to have crystallized carbonate-apatite from a melt, but he determined CO_2 only qualitatively and on a sample that may have been impure. The structure of prepared carbonate-apatite is not known [18].

The equilibrium given by the following scheme was predicted- for carbonate-apatite [20]:

$$CaCO_3 + \text{liquid} \leftrightarrow \text{carbonate} - \text{apatite} + Na_2Ca\left(CO_3\right)_2 \tag{1}$$

$$\begin{aligned} &\text{liquid} \leftrightarrow \text{carbonate} - \text{apatite} + Na_2Ca\left(CO_3\right)_2 \\ &+Na_2\left(CO_3\right)_2 \ \left(\text{mix of crystals}\right) \end{aligned} \tag{2}$$

The prepared crystals are typically long or short lengths with hexagonal prism $\{10\bar{1}0\}$, dipyramid $\{10\bar{1}1\}$ and pinacoid {0001}. The skeletal crystals had inclusions along the central canals parallel to the *c*-axis. The refractive index is uniaxial (-), $\varepsilon = 1.635$, $\omega = 1.626$, $\delta = 0.009$.

4.1. Common synthetic techniques for the preparation of apatites

The literature on the preparation of synthetic analogues of minerals from the supergroup of apatite[8] (**Section 1.1**) is very extensive, but can be divided into three main categories [18],[21], [22],[23],[24]:

[7] Introduced as double salt of $Na_2Ca(CO_3)_2$. Prepared mixtures were heated under the pressure of CO_2 in the range from 55 to 100 and from 23 to 54 kg·cm^{-2} (kg·cm^{-2} = 98066.5 Pa) for binary and ternary system, respectively [20].

[8] In older literature termed as apatite-like substances.

1. **Solid-State Synthesis**[9] (**Dry Method**) usually requires rather high temperature ≥ 1200°C and the product is characterized by a gradient of composition in the grain of material. The method and special techniques, conditions and devices used to control the product properties and to improve the reaction rate and homogeneity of the products are described in **Section 4.1.1**.

2. **Wet chemical method**[10] (precipitation from the solution): requires a long time period (10 hour or more) and often results in amorphous and non-stoichiometric products.

3. **Hydrothermal synthesis**[11]: involves heating of reactants with water in closed vessel, an autoclave

Other methods (**Section 4.1.1**) such as microwave synthesis, combustion synthesis and high pressure method or deposition techniques are used much rarely.

The pressure-temperature ranges of these methods are shown in **Fig. 2**. Some of the most applied techniques are described in this chapter. The methods for the preparation of single crystals are described separately in the next **Section 4.2**.

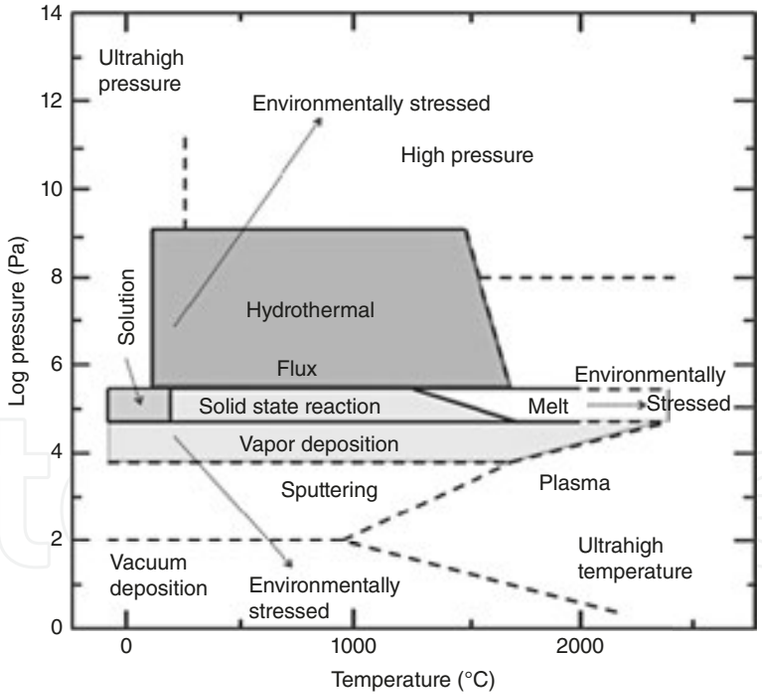

Fig. 2. Pressure-temperature range for the material preparation [21].

[9] Various alternative names, such as Shake 'n Bake Methods or Beat 'n Heat, are used for the solid state synthesis (reaction) in literature [23].

[10] Jaffe [18] recognized the precipitation by metathesis and the precipitation by hydrolysis.

[11] Sometimes are included among high-pressure methods [24].

http://dx.doi.org/10.5772/62212

4.1.1. Solid-State Synthesis

Solid-phase reactions (syntheses) are usually activated by high-temperature treatment [25]. The preparation of materials in solid-state is rather different form the synthesis of discrete molecules. The process involves the treatment of the whole lattice. Often, the post-synthesis purification of materials is not possible due to low solubility of formed phases. Hence, all effort must be made to avoid the excess of reagents. These methods are usually slow due to entire reaction which occurs in the solid state and requires the diffusion across the points of contact in a mixture [26],[27]. Special techniques can also be used based on the reduction of particle size or on the preparation of precursor in order to reduce the particle size, improve the product homogeneity and lower the temperature of thermal treatment [24].

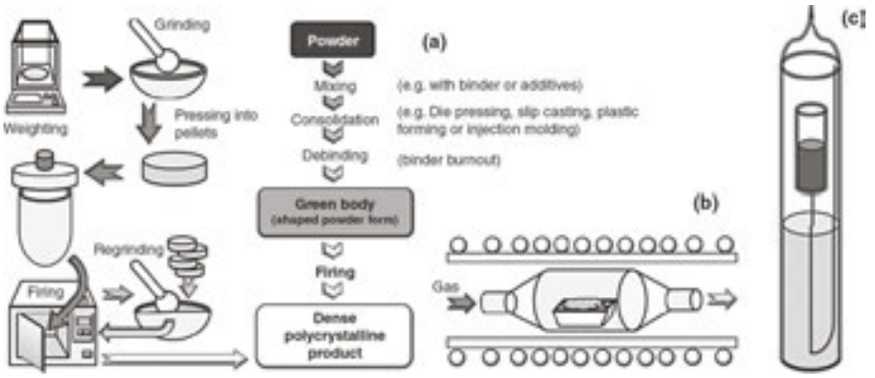

Fig. 3. Reaction scheme for solid-state synthesis: (a) ceramic method [26], (b) reaction of solids under special gas atmosphere [24] and (c) sealed glass tube [21],[33].

The most applied techniques[12] in solid-state synthesis are [23],[26],[24],[29],[28],[30],[31],[32]:

a. Ceramic method[13]: is the most common way of preparation of solids (metal oxides, aluminosilicates, sulfides, nitrides, etc.) that is based on thermal treatment of compacted powder[14] of two or more nonvolatile solids, which react to reach required composition and desired microstructure of the product **Fig. 3(a)**. Since the reaction can occur only at the interface of solids, once the surface layer has reacted, the reaction continues as the reactants diffuse from the bulk to the interface. The rate of reaction is then often limited by the diffusion hence it is important to prepare raw meal from fine and well mixed particles in order to maximize the contact area and minimize the diffusion path. It also decreases the temperature required for the thermal treatment. The repeating of regrind-

[12] Solid-state synthesis is classified among physical methods (together with vapor phase synthesis, laser ablation, etc.) some of other techniques listed below (sol-gel process, precipitation method, etc.) are considered as chemical methods [28].

[13] Since ceramic can be fabricated by a variety of methods, some of which have their origin in early civilizations, ceramic methods must be distinguished from the ceramic fabrication processes.

[14] The consolidation of ceramic powder to produce a **green body** is commonly referred to as forming. The main methods include dry of semidry pressing (1), plastic forming with water or organic polymers (2) and casting from a concentrated suspension or slurry (3) [30].

ing of the sample and the repeating of its thermal treatment is usually required to improve the homogeneity of the product.

The nucleation of a new phase, the epitactic[15] and topotactic[16] phenomenon's (oriented nucleation), crystal growth, phase transformation[17] and the sintration[18] are common during the thermal treatment.[19]

b. **Sealed tube** (**pipe**) **method** (**reaction**): is applied in the cases when direct reaction under ambient conditions (in air at one atmosphere pressure) cannot be performed due to high volatility of reactants, air sensitivity of starting materials and/or products, or the desire to form a compound with a metal in an unusually low oxidation state. Typically for this type of reactions, the components are loaded into a glass (method was first applied by De Sénarmont [33], **Fig. 3**(**c**)) or quartz ampoule (tube) in a glass box, evacuated and sealed off by melting the glass/quartz using a blow torch. The whole tube is heated to required temperature and time. Cooled tube is then broken up to get the product. The reaction of material inside with the tube may cause that the side-wall of tube is weaken. In the combination with pressure in the tube, these reactions can be hazardous. The synthesis can be also performed with metal capsules (solvothermal reactions, **Section 4.1.3**) sealed by welding.

c. **Synthesis under controlled** (**special**) **atmosphere**: the preparation of some compounds must be carried out under a special atmosphere, but not necessarily at high pressures. The oxidation (O_2), inert (Ar, N_2) or reduction atmosphere (CO/CO_2 or H_2/H_2O) is used to prepare the compounds in required oxidation state.

d. **Solid-state synthesis under high-pressure**: high pressure can be applied [24],[30],[34], [35]:

- **Directly applied pressure** (external pressure, pressure sintering, or pressure-assisted sintering): includes the techniques known as hot pressing (pressure is applied uniax-

[15] There is a structural similarity between the substrate and the nucleus that is limited to 2D interface and referred to as epitaxy [23].

[16] There is a structural similarity between the substrate and the nucleus (like for epitaxy[15])) that extends to 3D for topotaxy [23].

[17] Phase transformation has usually significant effects on the reaction rate. The reaction rate is strongly increased at the temperatures near the phase transformation because the mobility of atoms is also increased. This phenomenon is termed as **Hedvall effect** [29].

[18] Sintering is defined as the bonding of adjacent surfaces in a mass of powder or a compact by heating [29]. In general there are three types of sintering process including Solid-Phase (Dry) Sintering (1), Liquid-Phase Sintering (2) and Reactive (Reaction) Sintering (3) [29]. The process can also be divided according to applied conditions and densification practice to Conventional Sintering (1), Microwave Sintering (2) and Pressure Sintering (3). The stages of the sintering process include: (1) initial stage (formation and growth of necks), (2) intermediate stage (pores reached their equilibrium shapes, continuous porosity), (3) final stage (pores reached their equilibrium shapes, isolated (enclosed) porosity) [30]. The process can also be divided according to the mass transport mechanism to viscous sintering and diffusion sintering (further divided according to dominant type of diffusion to surface diffusion, volume diffusion, intergranular diffusion, grain-boundary diffusion, but gas transport (diffusion) of matter can also occur).

[19] Generally, the term **firing** is used when the processes occurring during thermal treatment of green body are fairly complex, as in many traditional ceramics produced from clay-based materials. In less complex cases the term sintering[18] is used [30].

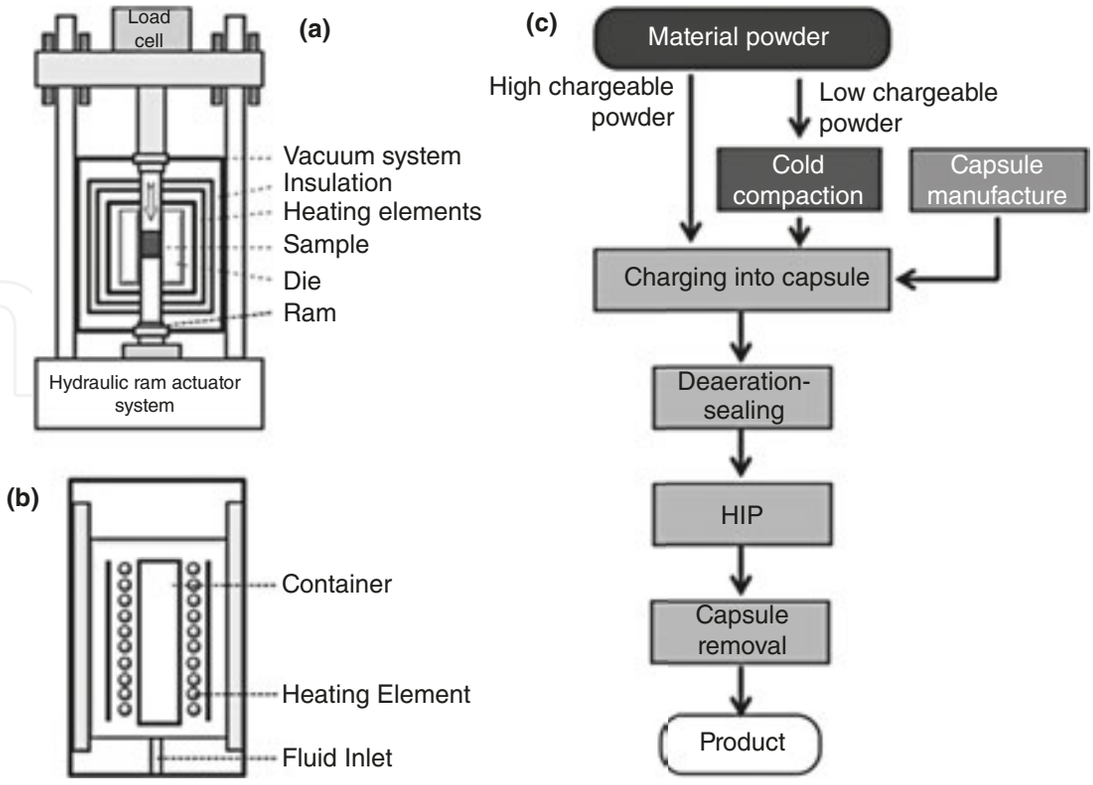

Fig. 4. Schematic diagram of hot pressing process [30], hot isostatic pressing [36] and the example of metallic capsule method [37].

ially or biaxially to the powder in a die, **Fig. 4**(**a**)) and sinter forging (similar to hot-pressing but without confining the sample in a die).

- **Indirectly applied pressure** can be applied through inert (hot isostatic pressing, HIP, **Fig. 4**(**b**)) or reactive gas, through ultrasound, by milling equipment (mechanochemical (powder) synthesis and activation) and by detonation.

The method is particularly important for the preparation of dense sample of ceramics with high degree of covalent bonding such as SiC and Si_3N_4.

Normal process of compaction of powder material involves uniaxial pressing in a die followed by sintering for densification. However better densification can be achieved by exerting a uniform pressure from all directions through a fluid medium onto the powder material retained in container (die), i.e. the pressure is generated by heating of medium. The process is termed as isostatic compaction, and as **hot isostatic pressing** (HIP) if performed at high temperature. The diffusion of medium from the container to the sample is avoided by its encapsulation by metal or glass (metallic or glass capsule method, **Fig. 4**(**c**) [36],[37].

In the case of **ultrasound (cavitation) methods** the phenomenon known as cavitation[20] takes place. Traveling the ultrasound wave leads to high pressure volume (compression) of the liquid which is followed by low pressure. Sudden expansion (rarefaction) leads to the formation of tiny bubbles. The bubbles expand to an unsustainable size and then collapse. The expansion and the collapse of bubbles create very localized hot spots, which reach instantaneous pressures of more than 100 MPa and temperatures of up to 5000°C (**Section 9.2.2**) [24], [28].

By **detonation methods** usually the nano-sized particles are prepared. The detonation is a superfast (with the velocity exceeding that of sound) exothermic reaction through the substance. The detonation wave consisting of the shock front, chemical reaction zone and the region where the products are scattered, spreads at constant rate due to continuous supply of energy from the chemical transformation of new portions of the explosive to the shock wave. The temperature (in the range from 2000 to 5000 K) and the pressure (shock wave) are reached by detonation in a suitably strong vessel. For example, the change of pressure at the end of the reaction zone ranges from 9.5 to 30 GPa for hexogen. This method was used for the preparation of nano-sized synthetic diamond,[21] graphite, boron nitride, etc. [24],[38].

Mechanochemical synthesis[22] is a solid-state synthesis method that takes advantage of the perturbation of surface-bonded species by pressure to enhance the thermodynamic and kinetic reactions between solids. The pressure can be applied at ambient temperature by friction and impact via milling equipment (**Fig. 5**) ranging from low energy ball mills to high energy stirred mills.[23] The main advantage of this method is the simplicity and low cost. The method was successfully used for the synthesis of oxides, phosphates, carbides, complexes, intermetalides [44],[45],[46],[47],[48],[24] alloys, etc.

---

[20] Generally, the cavitation can be divided into four types on the basis of the mode of generation of cavitation conditions: (1) acoustic cavitation (sound waves of high frequency 16 kHz–1 MHz), (2) Hydrodynamic cavitation (pressure variation is obtained by changing the geometry of the system), (3) optic cavitation (passing of photons of high intensity) and (4) particle cavitation (produced by the bombardments of other types of elementary particles, e.g. protons) [28].

[21] The method for the detonation transformation of graphite into diamond was earlier developed at the Institute of Chemical Physics of the Academy of Sciences of the USSR [38].

[22] Mechanochemical synthesis (reaction) of solids in the presence of water can be considered as hydrothermal one [25].

[23] Mechanochemistry is a branch of chemistry which is concerned with chemical and physico-chemical changes of substances of all stages of aggregation due to the influence of mechanical energy (Ostwald [39]). Colloid mills can be classified into three main groups with regard to the mechanism utilized for production of dispersion: beater-type mills (1), the smooth-surface type (2) and the rough-surface type. Beater-type mills include the original Plauson machine and some modified mills [48].

[24] Also intermetallic compounds, i.e. substances composed of two or more metallic elements with given stoichiometry and structure. Different atomic species occupy different lattice sites [44].

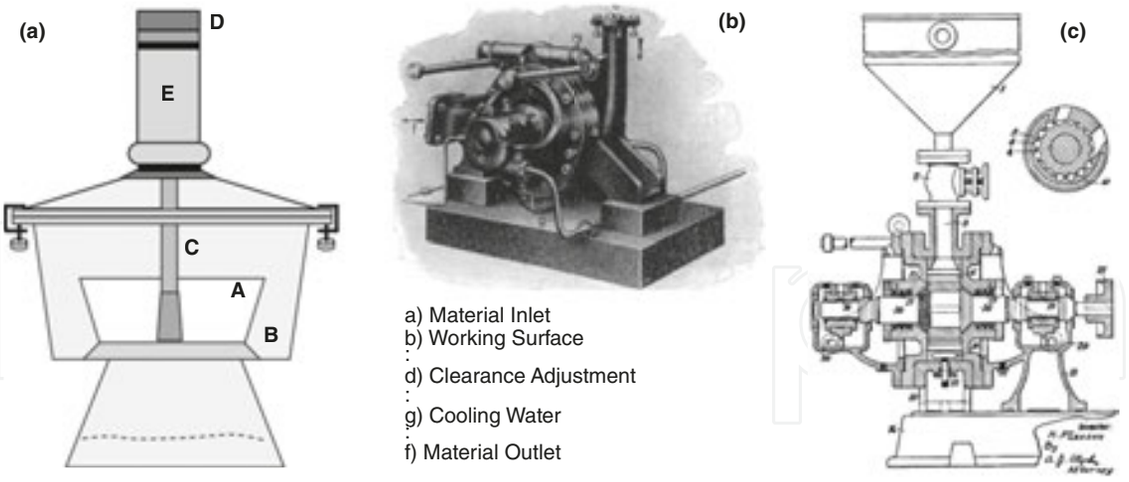

Fig. 5. The first mechanochemical reactor[25] (a): mortar (A), iron collar (B), pestle (C), handle (D) and rubber tube (E) [32],[39], Plauson-Oderberg (beater-type [48][23]) colloid mill for wet milling (b) and longitudinal section through Plauson colloidal mill [47] (c).

Mechanochemical activation involves the dispersion of solids and their deformation. These processes cause the generation of defects in solids, and also accelerate the migration of defects in the bulk, increase the number of contacts between particles and renew the contacts [25],[32], [34],[39],[40],[41],[42],[43],[49].

The advanced preparation techniques used for the reduction of particle size, activation of starting material or preparation of nano-scale[26] precursor are a broad group of methods with complicated nomenclature. The most known methods are:

i. **Sol-gel process** [26],[30],[50],[51],[52]: in this method, a solution of metal compounds (usually alkoxides of $M(OR)_4$ type, such as TMOS ($Si(OCH_3)_4$), TEOS ($Si(OC_2H_5)_4$), TEOT ($Ti(OC_2H_5)_4$), etc.,[27] or $(RO)_xMR'_{4-x}$ type, such as $(H_3CO)_3SiCH_3$, $(H_3CO)_3Si(CH{=}CH_2)$, etc.[28]) or suspension of very fine particles in a liquid (sol) is converted into rigid gel by removing the solvent or by adding a component which causes the gel to solidify. Two different sol-gel processes can be distinguished,[29] depending on whether the sol or the solution of alkoxides (alkoxide methods) is used **Fig. 6**(**a**,**b**).

[25] Constructed by PARKER [39] for the study of solid–solid reaction of the type: $Na_2CO_3 + BaSO_4 \rightarrow Na_2SO_4 + BaCO_3$ [41]. Earlier works were concerned with the decomposition of solids by high pressure and by grinding in a mortar with the pestle [42],[43].

[26] Nano it the Greek word for dwarf. In the International System of Units (SI) it is the decimal multiple 10^{-9} used as prefix. Nanoscience refers to the range from one to several hundred manometers and the nanotechnologies are the technologies in which atoms are manipulated in quantities of one to several thousand atoms. Nanoscience probably first gained the attention in 1959 in the lecture of the American Nobel laureate of 1965 in physics R. Feynman, who stated: *…that the day was no far off, when substances could be assembled at an atomic level* [27].

[27] Tetrametoxysilane, tetraetoxysilane, tetraethyl orthotitanate, etc.

[28] Methyltrimethoxysilane, vinyltrimethodxysilane, etc. **R**′ can also be reactive (polymerizable) groups such as (3-aminopropyl)trietoxysilane (APTES) or (3-glycidopropyl)trimetoxysilane (GLYMO) which can be used to prepare interconnected inorganic-organic networks. These materials are known as ORMOCERS (organically modified ceramics).

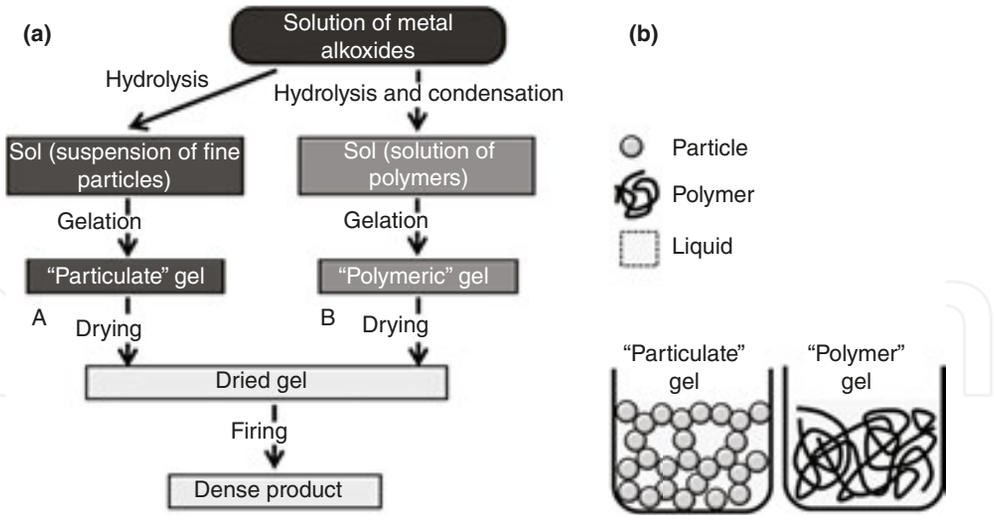

Fig. 6. Basic flow charts for sol-gel processes using a sol (a) and a solution of alkoxides (b). Schematic diagram of the structure of particulate gel formed from a sol (c) and polymeric gel from a solution (d) [30].

Starting with a sol, gelled material consists of identifiable colloidal particles which were joined together by the surface forces to form a network **Fig. 6**(**c**). When the solution of metal-alkoxides is used (**d**), the gel consist of a network of polymer chains formed via the reaction of hydrolysis (**Eq. 3**[30]) and condensation (**Eq. 4**[31]):

$$\mathrm{M(OR)_4 + H_2O' \leftrightarrow M(OR)_3\,O'H + ROH} \tag{3}$$

[29] This classification [30] does not set aside often used group of semi-alkoxide methods (using the mixture of soluble salt and metal alkoxide), Pechini type polymeric gel methods (liquid mix techniques) as well as modified Pechini methods. The Pechini process usually uses soluble nitrates, acetates, chlorides, carbonates, isopropoxides or other metal compounds which are dissolved in the solution of citric acid (in general in polycarboxylic acids) and ethylene glycol (in general glycol). The polycondensation reaction leads to the polymeric gel accommodating the stable chelates of metal cations [50]:

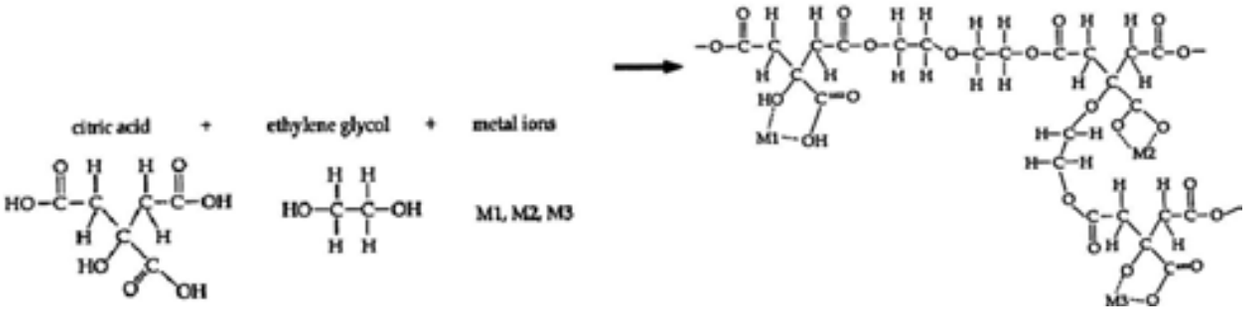

[30] The first step is the hydrolysis, the equilibrium constant for higher degree of hydrolysis decreases depending on the nature of –OR (increasing length of hydrocarbon chain and its branching). The process is also affected by the temperature, the solvent composition and applied water to alkoxide ratio, the type of catalysis, the application of ultrasound energy, etc. [52].

[31] Due to the formation of ROH molecule is termed as "alcohol producing condensation", i.e. the reaction between alkoxy (nonhydrolyzed) and hydrolyzed groups. The reaction with two hydrolyzed groups leads to the formation of –M–O–M– bridge and water, i.e. is termed as "water producing condensation".

http://dx.doi.org/10.5772/62212

$$M(OR)_3OH + M(OR)_4 \leftrightarrow (RO)_3 - M - O - M - (RO)_3 + ROH \quad (4)$$

Drying of gel leads to xerogel. The process is usually followed by shrinkage and formation of cracks. The thermal treatment of xerogel often involves the pyrolysis and calcination. If monolith is needed (aerogel [51]) the supercritical drying is usually applied.

ii. **Precipitation (co-precipitation) methods**[32] [26],[53]: the main reason why the precipitation is used to make ceramic powder is that it gives pure solid product, rejecting to the supernatant most of the impurities. In addition the particle morphology and the particle size distribution can be controlled to some degree. Mixed ion solution can be precipitated to produce a solid precursor containing required ions, although care must be taken to ensure correct ration of ions in the precipitate. The precipitation of powder involves the nucleation and the growth from supersaturated solution.

iii. **Solvation of metal salts** [26]: this method is based on dissolving the metal salt (often nitrates, hydroxides or oxalates) in suitable solvent followed by evaporating the mixture to dryness. Dried residue is then processed as in the ceramic method. In the case that the components have similar solubility, the method ensures better mixing than usual ceramic method.

iv. **Polymer pyrolysis** [30],[54]: reefers to the pyrolytic decomposition of metal-organic polymeric compounds (so-called preceramic polymers) to produce ceramics. The properties of the products depend on the nature of polymer and applied pyrolysis conditions. The polymer pyrolysis is an extension of well-known method for the production of carbon fibers by the pyrolysis of carbon-based polymers.

v. **Combustion methods** [55],[56],[57]: are characterized by high-temperatures, fast heating rates and short reaction times. The techniques involve an exothermic decomposition of fuel-oxidant precursor which results in either finely dispersed powder of precursor or direct product. Nitrates of required metals and urea, glycin or glucose as the most applied fuel are used as starting materials. The advantages of the sol-gel process and the combustion method are combined in the **gel combustion**.

vi. **Self-propagating high temperature synthesis (SHS)** [57],[58],[59]: was discovered in 1967 by Merzhanov [60],[61] and is based on the exothermic reaction[33] between two or more reagents that after the initiation to ignition temperature (T_{ig}) does not require any external source of heat and rapidly propagates thorough the reaction mixture.[34]

[32] The precipitation method is used for the preparation of precursor that is further treated by solid-state synthesis. The techniques of direct precipitation of apatite are described in **Section 4.1.2**.

[33] Therefore often associated with combustion techniques [56].

[34] The process is analogous to the process of frontal polymerization in which localized polymerization reaction zone propagates thorough the mixture of solution of a monomer and initiator due to the heat diffusion and the occurrence of exothermic reaction [59].

vii. **Spray pyrolysis** [62],[63]: small droplets of a solution containing desired precursor are introduced into the hot zone to the furnace to obtain required product. According to applied conditions in different stages of the thermal cycle (**Fig. 7**) the aerosol will form non-coherent powder and solid particles.

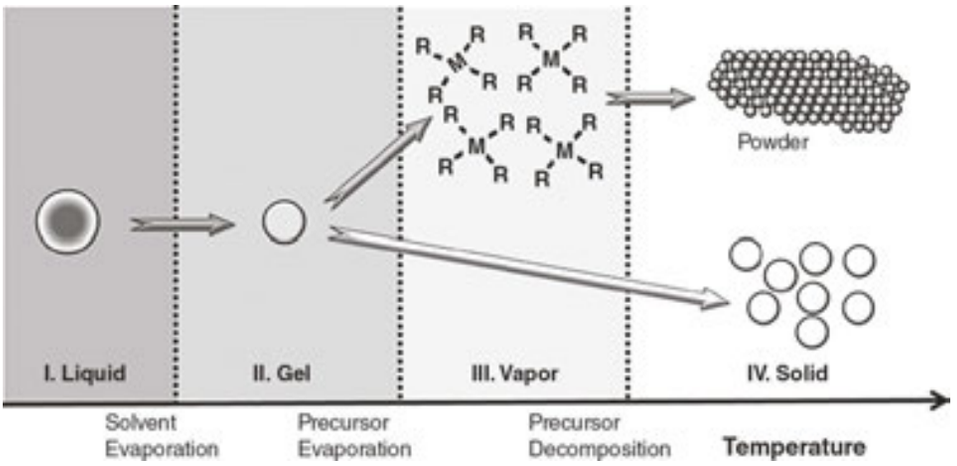

Fig. 7. Thermal cycle of spray pyrolysis [63].

viii. **Freeze drying** [35],[64]: the method discovered in 1965 that consists of fast freezing of the precursor solution (ensures preservation of maximum chemical homogeneity achieved in the starting solution), sublimation of solvent and final calcination. The main characteristics of the freeze drying method are that the drying is not accompanied by the coagulation of particles and the shrinkage of particles usually does not occur. The method produces fine and reactive powder of high purity

The reaction schemes for the solid-state synthesis of apatite structured compounds were published by Knyazev et al [65]:

$$\begin{aligned} &4.5\ M^{II}\left(NO_3\right)_2\cdot nH_2O + 0.5\ M^{II}L_2\cdot mH_2O + 3\left(NH_4\right)_2HPO_4 \rightarrow \\ &M^{II}_5\left(PO_4\right)_3L + 9\ NO_2 + 2.25\ O_2 + 6\ NH_3 + \left(4.5 + 4.5n + 0.5m\right)\ H_2O \end{aligned} \tag{5}$$

where M^{II} = Ca, Sr, Ba, Cd, Pb and L = OH, F, Cl, Br and I.

$$\begin{aligned} &3\ M^{II}\left(NO_3\right)_2\cdot nH_2O + 2\ NH_4VO_3 \rightarrow M^{II}_3\left(VO_4\right)_2 + 6\ NO_2 + 1.5\ O_2 \\ &+2\ NH_3 + \left(3n+1\right)\ H_2O \end{aligned} \tag{6}$$

$$1.5\ M^{II}_3\left(VO_4\right)_2 + 0.5\ M^{II}L_2\cdot mH_2O \rightarrow M^{II}_5\left(VO_4\right)_3L + 0.5m\ H_2O \tag{7}$$

where M^{II} = Ca, Sr, Ba, Cd, Pb and L = F, Cl and Br.

http://dx.doi.org/10.5772/62212

$$4.5\ M^{II}CO_3 + 3\ CrO_3 + 0.5\ M^{II}L_2 \cdot mH_2O \rightarrow M^{II}_5\left(CrO_4\right)_3 L + 4.5\ CO_2 + 0.75\ O_2 + 0.5m\ H_2O \quad (8)$$

where M^{II} = Ca, Sr and L = F and Cl.

$$4.5\ Ba^{II}CO_3 + 3\ MnO_2 + 0.5\ Ba^{II}L_2 \cdot mH_2O + 0.75\ O_2 \rightarrow Ba^{II}_5\left(MnO_4\right)_3 L + 4.5\ CO_2 + 0.5m\ H_2O \quad (9)$$

The temperature effect (**Table 1**) observed during the synthesis includes [65]:

1. synthesis;

2. polymorphic transition;

3. thermal decomposition; and

4. melting.

Compound	T_s	T_r	T_d	T_m
	[K]			
$Ca_5(PO_4)_3OH$	310	992	–	–
	1173	–	1523	–
$Ca_5(PO_4)_3Cl$	1073	953	–	>1723
$Ca_5(VO_4)_3Cl$	1073	794	–	>1723
$Ca_5(CrO_4)_3Cl$	1123	9007	–	1616
$Sr_5(PO_4)_3Br$	1473	–	1661	–
$Sr_5(VO_4)_3Cl$	1023	–	–	>1723
$Sr_5(CrO_4)_3F$	1373	–	–	1705
$Ba_5(VO_4)_3Cl$	1073	–	–	>1723
$Ba_5(MnO_4)_3F$	1123	–	1163	–
$Pb_5(PO_4)_3I$	973	–	–	256
$Pb_5(VO_4)_3F$	923	–	1044	–

Table 1. Temperature of synthesis (T_s), polymorphic transition (T_{tr}), decomposition (T_d) and melting (T_m) of some apatite-structured compounds [65].

The temperatures of these effects for some apatites are listed in **Table 1**.

The phase transformation and the thermal expansion coefficient of apatite-structured compound with the composition given by the formula $\mathbf{M}_5(\mathbf{XO}_4)_3\mathbf{Z}_q$ (M = Ca, Sr, Cd, Ba, Pb) were investigated by CHERNORUKOV et al [66]. Pb-containing apatites are shown to undergo the

phase transition involving the reduction in unit-cell symmetry from hexagonal to monoclinic. The thermal expansion anisotropy in the hexagonal phases increases in the order:

$$Ca<Sr<Ba<Pb<Cd,$$

and the monoclinic phases are less anisotropic but have larger thermal expansion coefficients in comparison with the hexagonal phases.

4.1.2. Precipitation method

The precipitation method is based on the combination reaction(s) when cations and anions in the solution combine to form insoluble ionic solid, so-called precipitate. The method can be divided to [35]:

i. **Direct precipitation method** is based on the reaction of neutralization and precipitation. The precipitate is then separated from the solution via filtration.

ii. **Homogeneous precipitation method** does not need precipitants because decomposed chemical acts as the precipitant, e.g. urea is decomposed in ammonium hydroxide and formed NH_4OH acts as the precipitant:

$$\left(NH_2\right)_2 CO + 3\ H_2O \overset{70°C}{\rightarrow} 2\ NH_4OH + CO_2 \tag{10}$$

iii. **Coprecipitation method** is initiated by the addition of precipitant to mixed-salt solution.

iv. **Compound precipitation method** is the precipitation of stoichiometric compounds from the solution.

Wet techniques of apatite preparation are based on the precipitation from solution at ambient temperature [67]. The preparation techniques based on aqueous precipitation at moderate temperatures often lead to non-stoichiometric apatites [68]. Hydroxylapatite close to the ideal formula, can be precipitated by the addition of $Ca(OH)_2$ to diluted phosphoric acid and complete neutralization at the boiling point [69]

$$6\ H_3PO_4 + 10\ Ca\left(OH\right)_2 \rightarrow Ca_{10}\left(PO_4\right)_6\left(OH\right)_2 + 18\ H_2O \tag{11}$$

Precipitated hydroxylapatite shows extremely small crystal sizes (hexagonal plates ~200Å sides) and large surface area from 50 to 200 $m^2 \cdot g^{-1}$.

The Eh-pH diagrams for the Ca-P-H_2O system at 25 and 300°C for 1.67 mol activity of Ca and 1 mol activity of P ($\boldsymbol{a}_{Ca} = 1.67\boldsymbol{a}_P$) under the pressure of 1 bar are shown in **Fig. 8**(**a**) and (**b**), respectively. The P$\boldsymbol{a}_{Ca}$-pH diagrams, where P$\boldsymbol{a}_{Ca}$ = *-log* $\boldsymbol{a}_{Ca}$ for this system show that the pH of minimum solubility of HAP clearly decreases with increasing temperature. At each tempera-

http://dx.doi.org/10.5772/62212

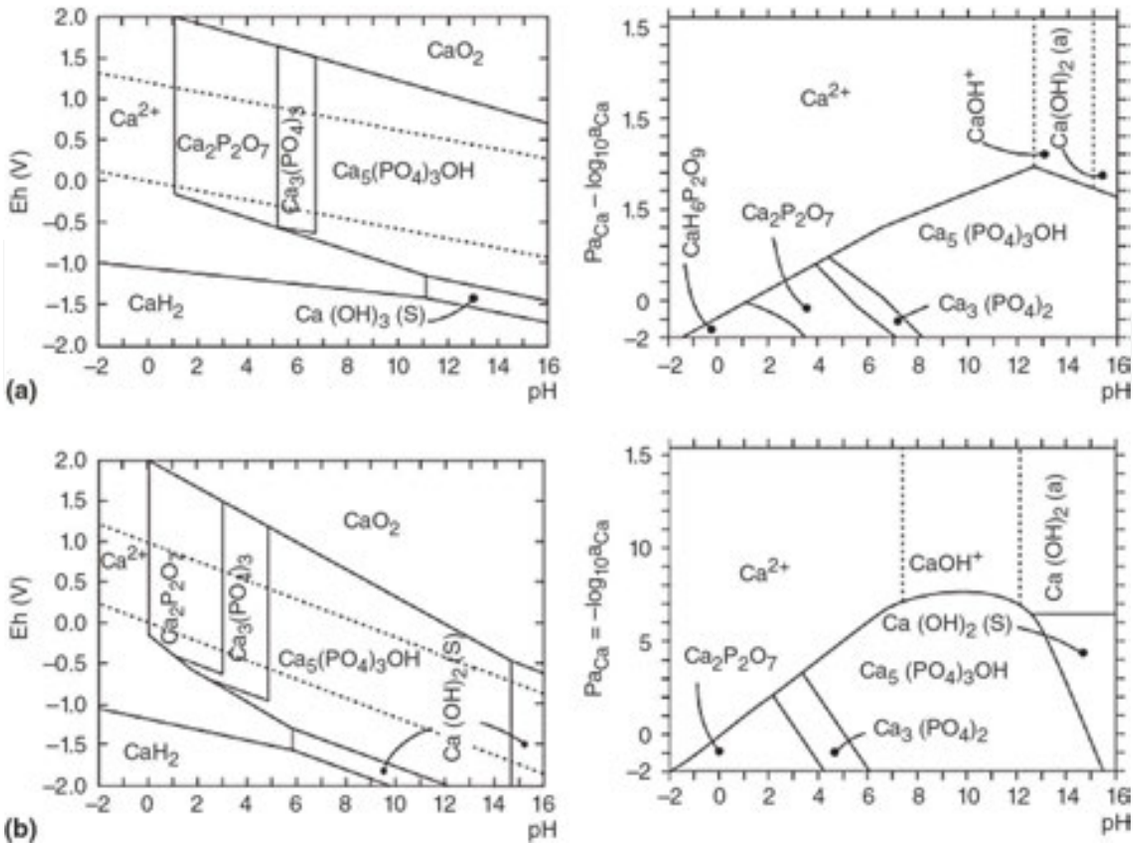

Fig. 8. Eh-pH and Pa_{Ca}-pH diagram of Ca-P-H_2O system at 25°C (a) and 300°C (b).

ture, HAP predominates in higher pH range, while $Ca_3(PO_4)_2$, $Ca_2P_2O_7$ and $CaH_6P_2O_9$ have predominates at lower pH [21].

The stability of calcium phosphates at higher temperatures is shown in **Fig. 9**. The equation numbers refer to the following reactions [21]:

$$3\ CaHPO_4 \leftrightarrow Ca_3(PO_4)_2 + H_3PO_4 \tag{12}$$

$$3\ Ca(H_2PO_4)_2 \leftrightarrow Ca_3(PO_4)_2 + 4\ H_3PO_4 \tag{13}$$

$$Ca_{10}H_2P_6O_{26} \leftrightarrow 3\ Ca_3(PO_4)_2 + CaO + H_2O \tag{14}$$

$$CaH_5PO_6 \leftrightarrow CaHPO_4 + 2\ H_2O \tag{15}$$

$$CaH_6P_2O_9 \leftrightarrow Ca(H_2PO_4)_2 + H_2O \tag{16}$$

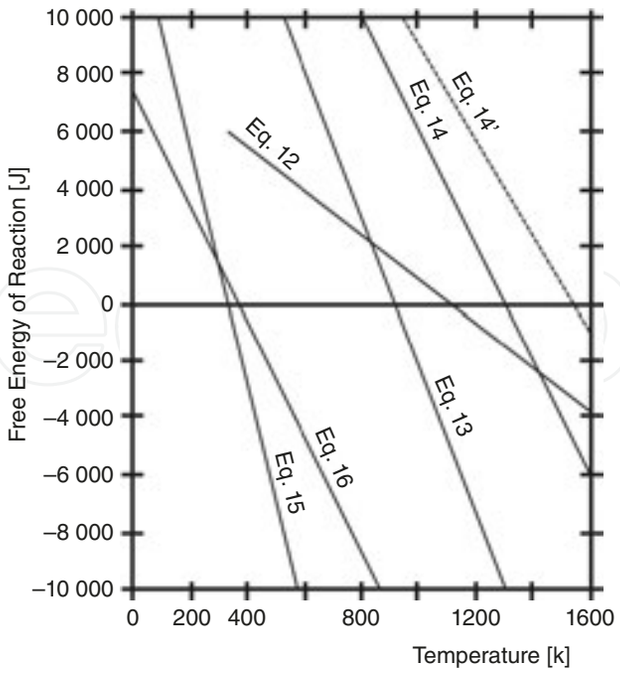

Fig. 9. Temperature dependence of free energy of reaction for some calcium phosphates according to **Eqs. 12–23** for water vapor fugacity equal to 0.03 atm., except for the dashed line **Eq. 14′**, which corresponds to water vapor fugacity equal to 1 atm. [21].

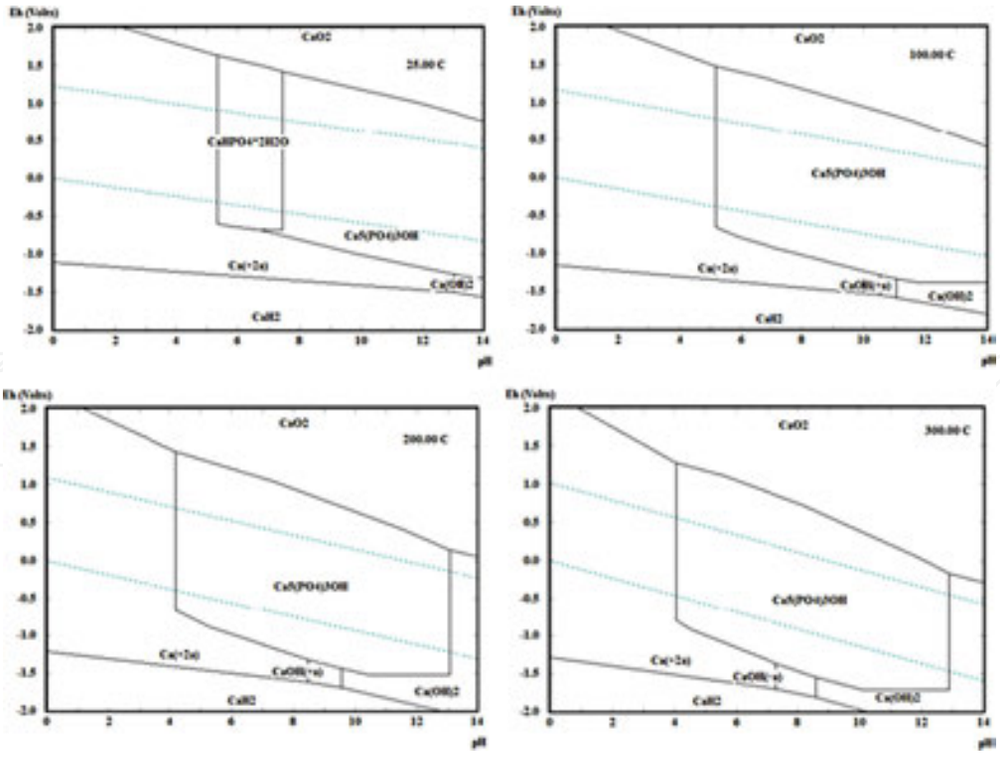

Fig. 10. Eh-pH diagram of Ca-P-H_2O system at 25°C (a), 100°C (b), 200°C (c) and 300°C (d).

For the purpose of this book the calculation of Eh-pH diagram for the solution where the concentration of ions (Ca^{2+}, PO_4^{3-} and OH^-) is equivalent to the system containing $5 \cdot 10^{-3}$ mol·dm $^{-3}$ of apatite was performed. The ionic strength (refer to **Footnote 31** in **Section 3.4.1**) of that solution enables the calculation of activity of Ca and P using the activity coefficient estimated from modified Davies equation (refer to **Footnote 31** in **Section 3.4.1**) and the concentration of calcium as follows: $a_{Ca} = 1.062 \cdot 10^{-3}$ and $a_P = 1.67 \cdot a_{Ca} = 6.36 \cdot 10^{-4}$. If the activity of ions is used instead of its concentration, the Eh-pH in **Fig. 10** can be calculated.

In this system,[35] $CaHPO_4 \cdot 2H_2O$ is stable under ambient temperature and nearly neutral pH. Hydroxylapatite becomes stable at the pH higher than 7.5. With increasing temperature, the formation of HAP instead of $CaHPO_4 \cdot 2H_2O$ is more probable. Minimal solubility of hydroxylapatite is then shifted to significantly lower pH than for **Fig. 8**.

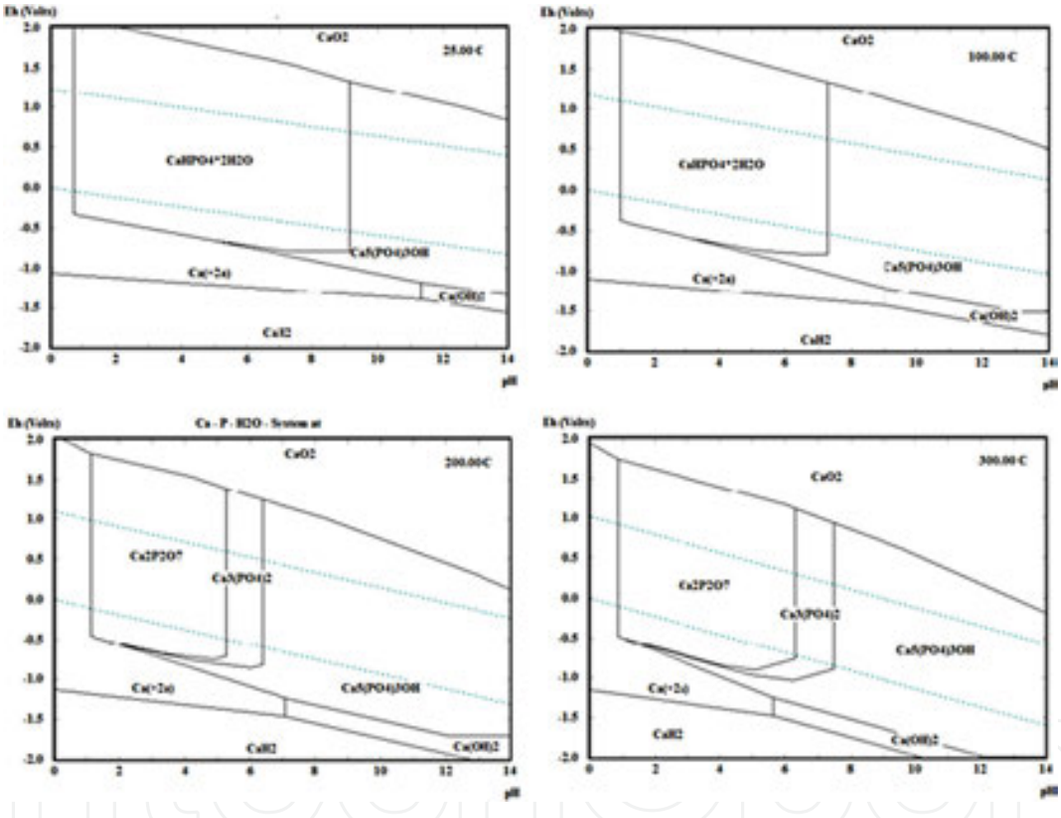

Fig. 11. Eh-pH diagram of Ca-P-H_2O system with the concentration 20× higher than for that in **Fig. 10** at 25°C (a), 100°C (b), 200°C (c) and 300°C (d).

Other difference is a fact, that the field of stability of $Ca(OH)_2$ starts at the pH = 13 for the system with elevated temperature. The formation of $CaHPO_4 \cdot 2H_2O$, $Ca_2P_2O_7$ and $Ca_3(PO_4)_2$ was not predicted.

The calculation for 20-times higher concentration **Fig. 11** than for the system mentioned above shows broadening field of $CaHPO_4 \cdot 2H_2O$. $Ca_2P_2O_7$ was formed by the thermal condensation

[35] The main difference against to the systems on **Fig. 8** and **Fig. 11** is significantly lower ionic strength.

of $CaHPO_4$ at temperatures higher than 164°C in acidic environment and $Ca_3(PO_4)_2$ precipitated from the solution at nearly neutral conditions. Hydroxylapatite again predominates at higher pH and $Ca(OH)_2$ does not appear at higher temperatures and the pH below 14 (the same as for **Fig. 8**).

The phase equilibrium in the system $CaO\text{-}P_2O_5\text{-}H_2O$ was extensively studied by the solid-state reaction method under the atmospheric pressure of water vapor by Van Wazrer [70] and in aqueous systems at temperatures lower than 100°C by Brown et al [71],[72]. Biggar [73] studied the $CaO\text{-}P_2O_5\text{-}H_2O$ system in the temperature range from 700 to 950°C and the pressure of 1 kbar. Feng and Rockett [74] studied the system $CaO\text{-}P_2O_5\text{-}H_2O$ at 1000 bar with 50%wt. and 200°C (**Fig. 12**).

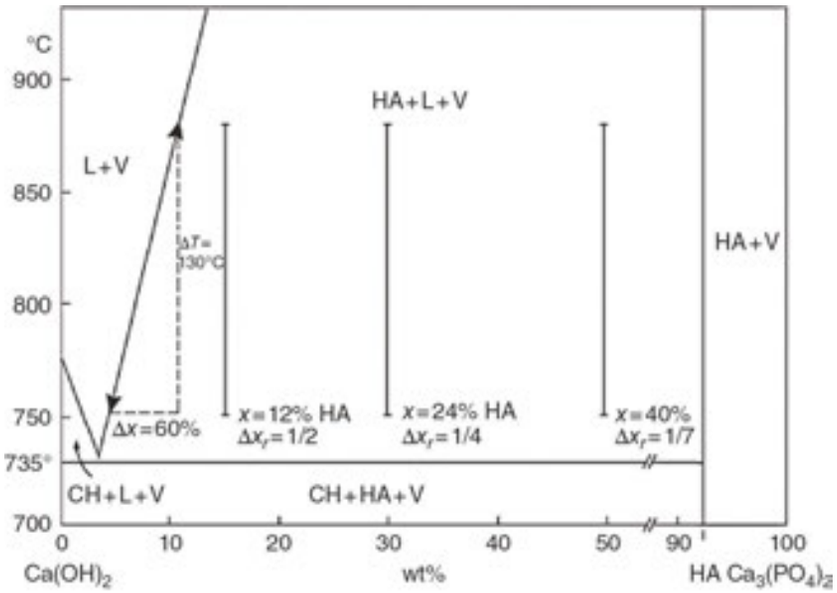

Fig. 12. Phase diagram of $Ca(OH)_2\text{-}Ca_3(PO_4)_2\text{-}H_2O$ system [21].

The **molten** (**fused**) **salts**[36] **precipitation method** uses the precursor mixed with low melting point salt such as NaCl, KCl, or their eutectics. Upon the melting of the mixture, reactant oxides dissolve in the salt and desired compound precipitates due to its low solubility in molten salt.

[36] Fused salts are widely used in many industrial processes requiring to free the limitations arising from the use of aqueous solutions. Their thermal stability and generally low vapor pressure enable fast reaction rates and ability to dissolve many inorganic compounds making them useful solvents in electrometallurgy, metal coating, treatment of by-products, and energy conversion. It is recalled that one of the most important chemicals produced worldwide, sulfuric acid, is made by the molten salt catalysis. The electrolysis of molten salt is a technique used by H. Moissan for the isolation of element fluorine from the melt of KF·2HF (Moissan's method is used for industrial production of fluorine). It was also used by H. Davy to discover several new elements (sodium, potassium, alkali metals) and to prove the chlorine as a new element (originally discovered by C.W. Sheelle who considered it as "*dephlogisticated marine acid*"). Today the industrial production of Li and Na is based on the electrolysis of eutectic melt of LiCl–KCl (or $CaCl_2$) and NaCl–KCl (or $CaCl_2$), respectively. The production of K, Rb and Cs is based on the reduction of molten KCl, RbCl and CsCl by Na at the temperature of 600°C. Molten salt method also plays significant role in the development of energy resources, including the reprocessing of nuclear wastes, molten carbonate/solid oxide fuel cells (**Section 10.4**), and high temperature molten salt batteries. Fused alkali nitrates/nitrites are valuable materials for the heat transport and storage in solar plants. Molten salt bathes remain of large use in industry for the treatment of steel and variety of other metals as well as nonmetals, such as glass, plastics and rubber [75].

The melt is cooled down, and the salt is dissolved to yield the powder product of synthesis [75], [76].

The structure of a molten salt is characterized by an alteration of positively and negatively charged ionic solvation shells around a given ion. This arises from the predominance of Coulombic effects, which results in a strong attraction between oppositely charged species and a strong repulsion otherwise [75].

The utilization of molten salt precipitation method for the synthesis of apatites at "moderate temperatures" in the range from 500 to 700°C was also reported. Based on its principle, the method combines the advantages of thermal hydrolysis ("dry method") and the precipitation from the solution ("wet method"). As a reaction media, the chloride melt of the equimolar NaCl-KCl (665°C) composition as well as eutectic melt (390°C) in the system Li_2CO_3 (27)–Na_2CO_3 (28)–K_2CO_3 (45% mol.) can be used. The most probable reactions are estimated from the thermodynamic consideration as follows [22]:

$$6\ KPO_3 + 6\ CaO + 3\ CaCO_3 + Ca(OH)_2 \rightarrow HAP + 3\ K_2CO_3 \quad (17)$$

$$6\ NaPO_3 + 6\ CaO + 3\ CaCO_3 + Ca(OH)_2 \rightarrow HAP + 3\ Na_2CO_3 \quad (18)$$

$$6\ KPO_3 + 6\ CaO + 3\ CaCO_3 + CaF_2 \rightarrow FAP + 3\ K_2CO_3 \quad (19)$$

$$6\ NaPO_3 + 6\ CaO + 3\ CaCO_3 + CaF_2 \rightarrow FAP + 3\ Na_2CO_3 \quad (20)$$

4.1.3 Hydrothermal synthesis

The original hydrothermal[37] method involves heating of the reactants in a closed vessel, an autoclave, with water (heterogeneous reaction). Autoclave is usually constructed from thick stainless steel to withstand the high pressures and is fitted with safety valves; it may be lined with nonreactive materials, such as noble metals, quartz or Teflon. When the autoclave is heated, the pressure increases and the water remains liquid above its normal boiling temperature of 100°C, so-called superheated water. These conditions, in which the pressure is raised above atmospheric pressure and the temperature is raised above the boiling temperature of water are known as hydrothermal conditions (high-pressure-high-temperature, HPHT). HPHT conditions enable to dissolve and recrystallize (recover) the materials which are relatively insoluble under ordinary conditions. The methods enable [21],[24],[67]:

1. Synthesis of new phases or stabilization of new complexes.

[37] The term hydrothermal is of purely geological origin. It was first used by British geologist, Sir Roderick Murchison, to describe the action of water at elevated temperature and pressure in bringing about changes in the Earth´s crust, and leading to the formation of various rocks and minerals. Materials scientists popularized the technique, particularly during 1940s. The first hydrothermal synthesis was performed by Schafhautl in Papin's digester, who obtained quartz crystals upon hydrothermal treatment of freshly precipitated silic acid [21].

2. Crystal growth of several inorganic compounds.
3. Preparation of finely divided materials and microcrystallites with well-defined size and morphology for specific applications.
4. In situ fabrication of materials with desired size, shape and also dispersity in case of nanomaterials.
5. Leaching of ores in metal extraction.
6. Decomposition, alteration, corrosion and technique.

Several definitions of hydrothermal synthesis use aqueous solvent under HPHT conditions [21]:

a. In hydrothermal synthesis the material is subjected to the action of water, at temperatures generally near, though often considerably above the critical temperature[38] of water (~370°C) in closed bombs, and therefore, under the corresponding high pressures developed by such solution [77].
b. Hydrothermal synthesis is a heterogeneous reaction in aqueous media above 100°C and the pressure higher than 1 bar [78].
c. Hydrothermal synthesis involves water as a catalyst and occasionally as a component of solid phases in the synthesis at elevated temperature (>100°C) and pressure greater than a few atmospheres [79].

Depending on the type of solvent used in the heterogeneous reaction the glycothermal, alcothermal, ammonothermal, lyothermal, carbothermal, etc., methods are recognized. According to applied solvent and condition, the hydrothermal methods can be further divided as follows [21].

i. **Conventional hydrothermal techniques**, which use aqueous solvent.
ii. **Solvothermal techniques or methods**, which use nonaqueous solvent.
iii. **Supercritical hydrothermal** methods use aqueous and nonaqueous solvent under critical to supercritical conditions.
iv. **Multienergy hydrothermal methods** combine hydrothermal method with additional microwave, electrochemical, sonar, mechanochemical, etc. energy.

Hydrothermal conditions exist in nature, and numerous minerals including naturally occurring zeolites and gemstones, are formed by this process. The term has been extended to other systems with moderately raised conditions and temperatures lower than those typically used in ceramics and sol-gel syntheses. Lower temperatures used are one of the advantages of the method. Other methods include the preparation of compounds in unusual oxidation states or phases, which are stabilized by raised temperature and pressure [24].

[38] The temperature and the pressure at critical point of water are 373.946°C and 22.064 MPa, respectively.

http://dx.doi.org/10.5772/62212

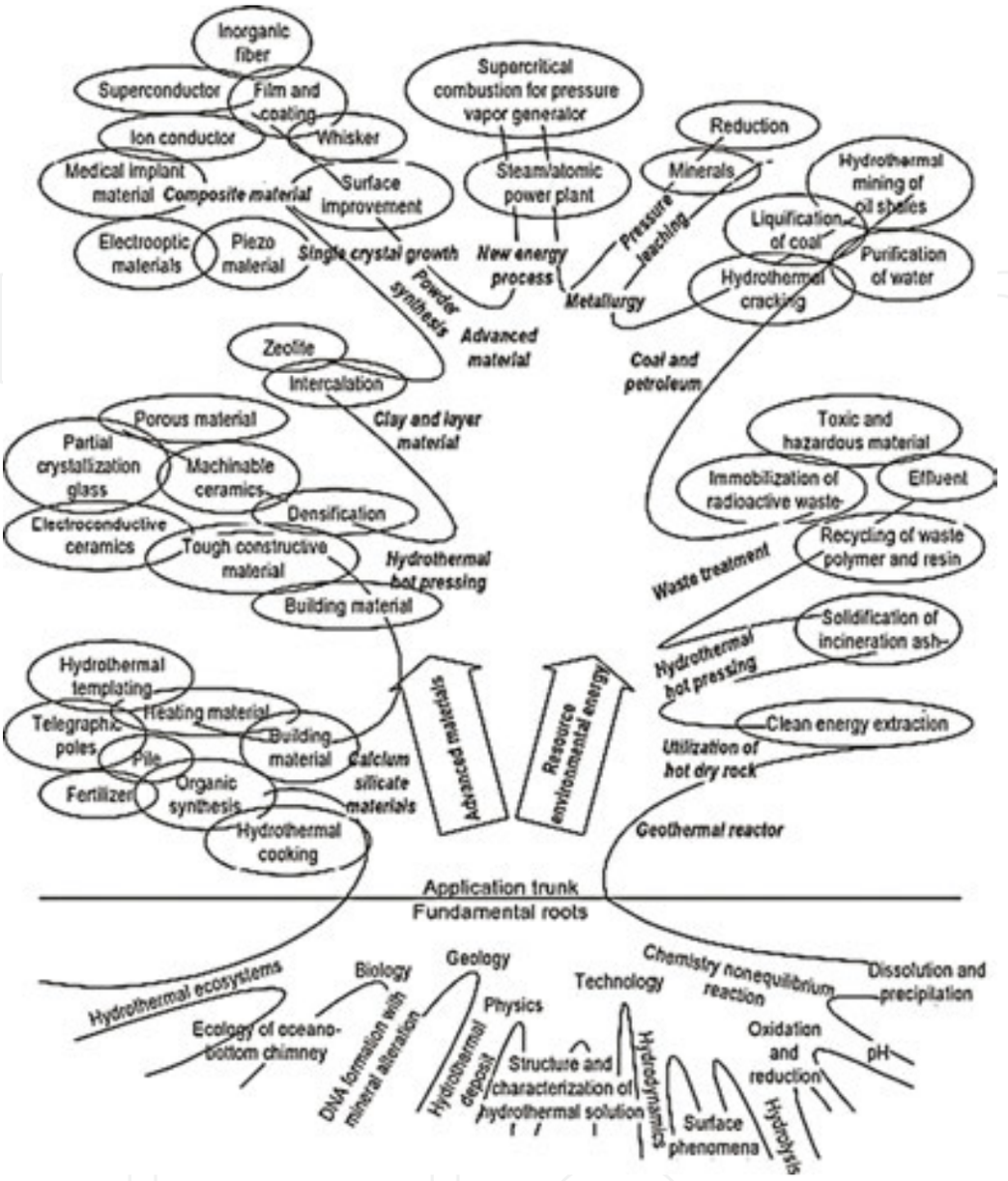

Fig. 13. Tree showing the interdisciplinary nature of hydrothermal technology [21].

Hydrothermal synthesis was used industrially[39] to prepare large crystals of quartz and synthetic gemstones. It is useful in metal oxide systems, where oxides are not soluble in water at atmospheric pressure but dissolve in superheated water under hydrothermal conditions. Where even these temperatures and pressures are insufficient to dissolve the starting materials, alkali or metal salts as mineralizers can be added, the anions of which form complexes with the solid and render it soluble [24].

[39] The first successful commercial application of hydrothermal technology was in mineral extraction or in ore beneficiation. The method was used to leach bauxite by sodium hydroxide by Karl Josef Bayer in 1892. The product of so-called Bayer´s process, aluminum hydroxide, is then converted to Al_2O_3 and used to produce aluminum metal or in ceramics [21].

Throughout the course of evolution of hydrothermal synthesis from the geoscientific applications to modern technologies, the hydrothermal technique has captured the attention of scientists and technologists from different branches of science. The hydrothermal technique is popularly used by geologists, biologists, physicists, chemists, ceramists, hydro-metallurgists, materials scientists, engineers, etc. **Fig. 13** shows different branches of science either emerging out from the hydrothermal technique or closely linked up with the hydrothermal technique. One could firmly say that this family tree will keep expanding its branches and roots in the years to come [21].

The hydrothermal techniques for the preparation of compounds with the structure of apatite should be divided to:

1. low-temperature hydrothermal synthesis (LHS);

2. high-temperature hydrothermal synthesis.

The hydrothermal synthesis of all three normal apatite end-members was reported by Baumer and Argiolas [80]. They prepared crystallites of sizes from 50 to 500 μm. The synthesis of chlorapatite at 400°C and the pressure <3 kbar proceeds via the reaction:

$$10\ CaCl_2 + 6\ H_3PO_4 \Leftrightarrow Ca_{10}\left(PO_4\right)_6 Cl_2 + 18\ HCl \tag{21}$$

The synthesis and the stability of carbonate-fluorapatite were examined by Jahnke [81]. The carbonate-apatite phase is stable in solutions relatively rich in carbonate such as sea-water. When exposed to low-carbonate solutions, the carbonate-apatite should lose the CO_3^{2-} ion [82].

During the hydrothermal synthesis of HAP whisker, the acetamide was used by Zhang and Darvell [83] as an agent to drive homogeneous precipitation at temperatures below 100°C. Acetamide shows low hydrolysis rate in both acidic and basic conditions, releasing acetate and ammonia:

$$CH_3CONH_2 + H_3O^+ \rightarrow CH_3CO_2H + NH_4^+ \tag{22}$$

which do no substitute in HAP lattice. The precipitation of hydroxylapatite from the solution of $Ca(NO_3)_2{\cdot}4H_2O$ and $(NH_4)_2HPO_4$ in 0.05 mol·dm^{-3} (Ca:P = 1.67) treated to the temperature of 180°C for 10–15 hours yielded to large rod-like and well-crystallized particles of hydroxylapatite.

The stoichiometric single crystals of hydroxylapatite nanorods with mono-dispersion and narrow-size distribution in diameter were successfully synthesized by Lin et al [84] via the hydrothermal microemulsion method [85].[40] The microemulsion was prepared using CTAB as the surfactant and *n*-pentanol as the cosurfactant. First, 0.5 M $Ca(NO_3)_2$ solutions and 0.3 M $(NH_4)_2HPO_4$ solutions were obtained by dissolving $Ca(NO_3)_2{\cdot}4H_2O$ and $(NH_4)_2HPO_4$ in

[40] The emulsification consists in dispersing of one fluid in another, non-miscible one, via the creation of interface [85].

distilled water, respectively, and the pH of both solutions was adjusted to 11.0 by adding ammonia solution. These aqueous solutions were used as the water phase and n-hexane was used as oil phase. The mixture of surfactants [86][41] and $Ca(NO_3)_2$ solution was stirred, ultrasonicated and optically transparent microemulsion was obtained. The solution of $(NH_4)_2HPO_4$ was drop wisely added into the $Ca(NO_3)_2$ microemulsion solution to obtain a suspension, and the pH of the suspension was maintained at 11.0 using ammonia solution. Then the suspension of the microemulsion was transferred into stainless steel autoclaves and maintained at 180°C for 18 h. Washed hydroxylapatite powder was then calcined at 600°C for 2 h [84].

4.2 Preparation of single crystals

The first technique that was used for the production of crystals **Fig. 14**(**a**) was described by Verneuil [90],[91],[92],[93] at the turn of the 20th century,[42] but there is an evidence that the so-called Geneva ruby had been grown by a similar technique almost 20 years earlier. The second technique for single crystal growth was introduced by Czochralsky [94] few years later, who needed materials with small dimensions[43] in order to study the growth kinetics of metal (**Fig. 14**(**b**)). This technique is based on pulling thin wires from the melt at various speeds and obtaining single crystals. Beginning in 1950s, it eventually developed into the complex technology required in order to obtain large-diameter prefect crystals which are a raw material for the electronics industry, but controlling the dimension of the crystal was very difficult. The idea of using a shaping device floating on the melt surface to stabilize the crystal growth was introduced by Gomperz [95], who used a drilled mica plate. Since that time, numerous types of shaping devices have been used to get crystals of various shapes [26],[87],[88].

Kyropoulos developed the melt growth techniques (**Fig. 15**) for growing large crystal from the melt using a cooled seed in 1926 [96],[97],[98]. The method was demonstrated via the production of large single crystals of alkali halides [99].

---

[41] The name surfactant is a contraction of the term: **surf**ace-**act**ive-**a**ge**nt**. It can be defined as the substance that, even if present at low concentration, has ability to be adsorbed onto the surface or interface of the system and significantly alter (usually decrease) its surface or interface free energy. While the term **surface** usually means the interface between condensed phase and gas, the interface is considered as a boundary between two immiscible phases. The molecular structure of surfactant contains lyophobic group (little attraction for solvent) and lyophilic group (strong attraction for solvent), i.e. amphipathic structure [86].

[42] Verneuil in fact wished to study the properties of ruby and other alumina-based crystals and was aware of very high melting temperatures of these materials, which prevented the use of any crucible material known in that time. This problem was solved- by melting alumina powder in a hydrogen-oxygen flame and solidifying the droplets on a colder seed. Nowadays this technique is used for the production of single crystals of sapphire (single crystal of Al_2O_3 in **Chapter 3** (**Fig. 14**) was prepared by this method) and spinel with only little changes [87]. The crystal grows from the melt film, which thickness is defined by the crystal diameter and the thermal conditions at the crystallization front [93].

The scheme of Verneuil's growth unit [87],[90],[93]: electromagnet (A, or camshaft) operating the hammer (M), supply chamber of fine Al_2O_3 powder (P), feeder (C, D), oxygen (O) and hydrogen (H) inlet, growing crystal (R), crystal holder (S) and device for the crystal adjustment (V).

[43] Small dimension is necessary to dissipate the latent heat of solidification efficiently and rapidly [87].

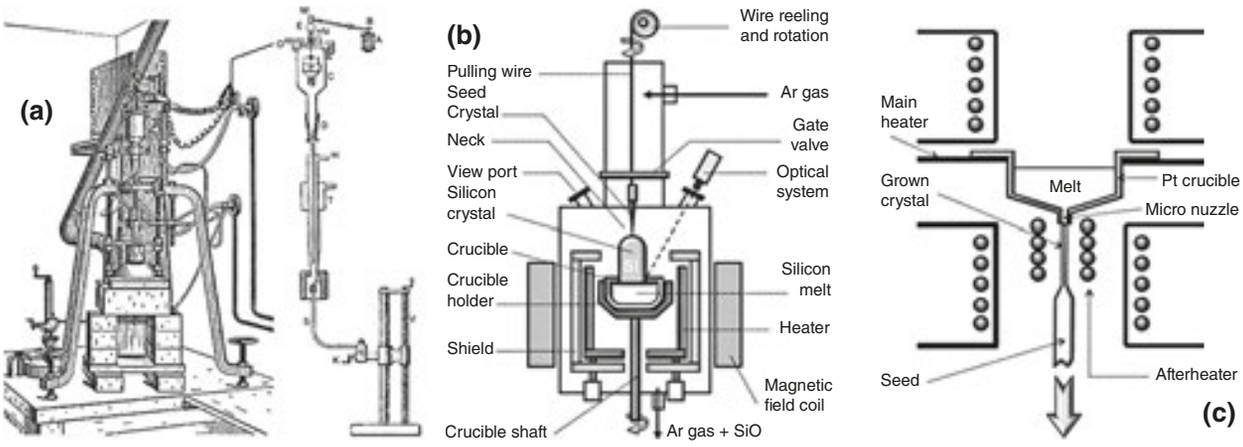

Fig. 14. Scheme of Verneuil's method[42] (a) [87],[90], Czochralsky growth apparatus (b) [88] and μ-PD apparatus (c) [89].

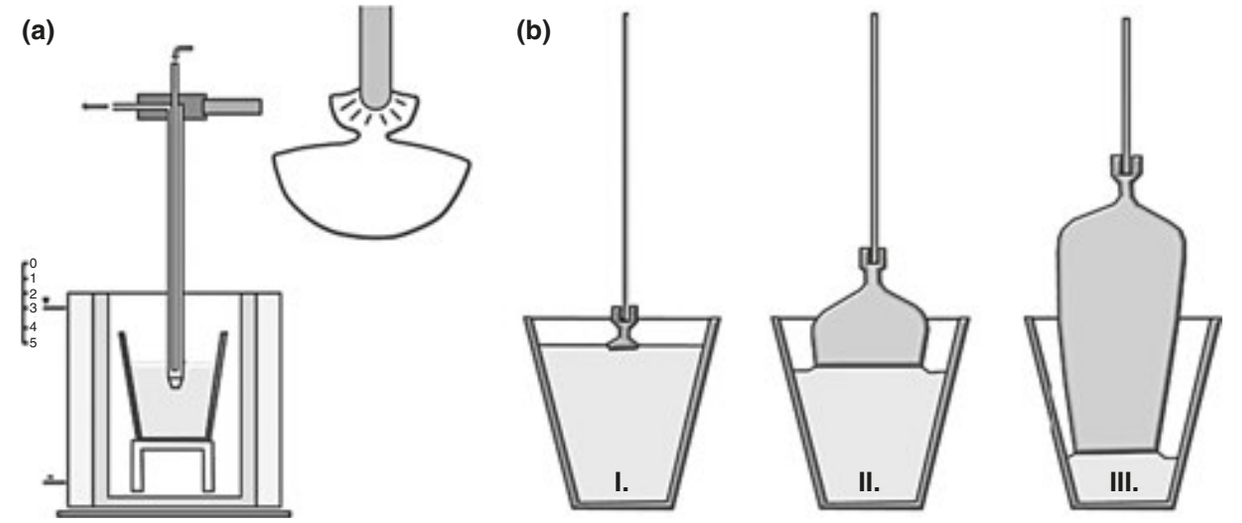

Fig. 15. Schematic illustration of Kyropoulos method [96] and three stages of Kyropoulos method [98].

After important growth processes based on capillarity, historically the next development was the Bridgman method [100], aiming at increasing the crystal size and consisting in growing the crystal in crucible. The next method to be invented in 1952 by Phann [101] was the floating zone (FZ) technique.[44] This method is capillary-based technique that was originally developed for the material purification [87]. The schematic representation of convection in the molten zone according to Higuchi et al [102] is shown in **Fig. 16**. The Marangoni convection[45] in molten zone leads to the formation of tiny bubbles, which are not arranged randomly, but form a ring inside the crystal.

[44] The floating zone is generated by means of water-cooled induction coil fed by radio frequency power in the megahertz range [103].

[45] Marangoni convection, which is caused by the differences in the surface tension over the melt surface, flows along the interface from the surface to a central region of the melt. On the other hand, forced convection, which is caused by the crystal rotation, flows towards the periphery from the center [102].

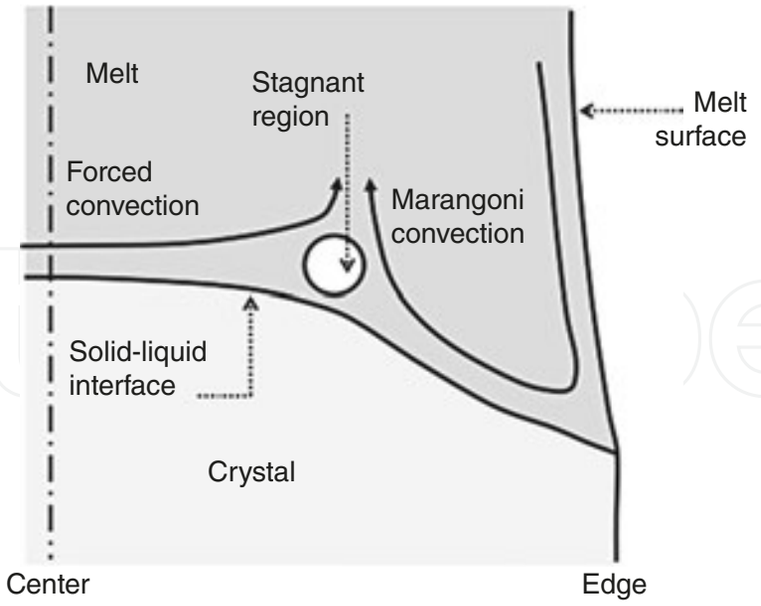

Fig. 16. Schematic representation of convection in the molten zone [102].

Since then various modifications of these basic methods have been proposed, such as the pedestal growth, edge-defined film-fed growth (EFG) process, inverted EFG process, micro-pulling down (μ-PD, **Fig. 14**(**c**)), etc., all based on the use of capillary force in order to maintain and shape the liquid. **Fig. 17** show the classification of these methods based on the presence or absence of the crucible or shaping die in contact with molten material and on the direction of pulling [87],[89],[103],[104].

Whiskers can be described as long filamentary defect-free single crystals of great mechanical strength, which is attributed to their high structural perfection. The explanation of whisker growth is based on the screw dislocation theory. The dislocation appears only along the whisker axis, while in another two dimensions the faces will stay perfect. Consequently, no growth will occur at an appreciable rate on the side faces of whisker. Due to the presence of axial screw dislocation the whisker grows only along its axis [105]. Apatite whiskers are usually prepared by hydrothermal synthesis [83],[106],[107],[108], molten salt method [109] and also via the precipitation method [110].

Dendrites[46] are normally single crystals, and the branches follow definite crystallographic orientation. The branches are regularly oriented and the opposite sides of the primary stem show marked symmetry. The growth of dendritic crystal is controlled by the diffusion of latent heat from growing crystal-melt interface [110],[111]. The dendritic growth of apatite crystal is described in glass ceramics [111],[112] and the formation of comb-shaped acicular and dendritic apatite was also observed as a product of quenching of trapped phosphate melt inclusions [113].

[46] The name was derived from the Greek word "tree like".

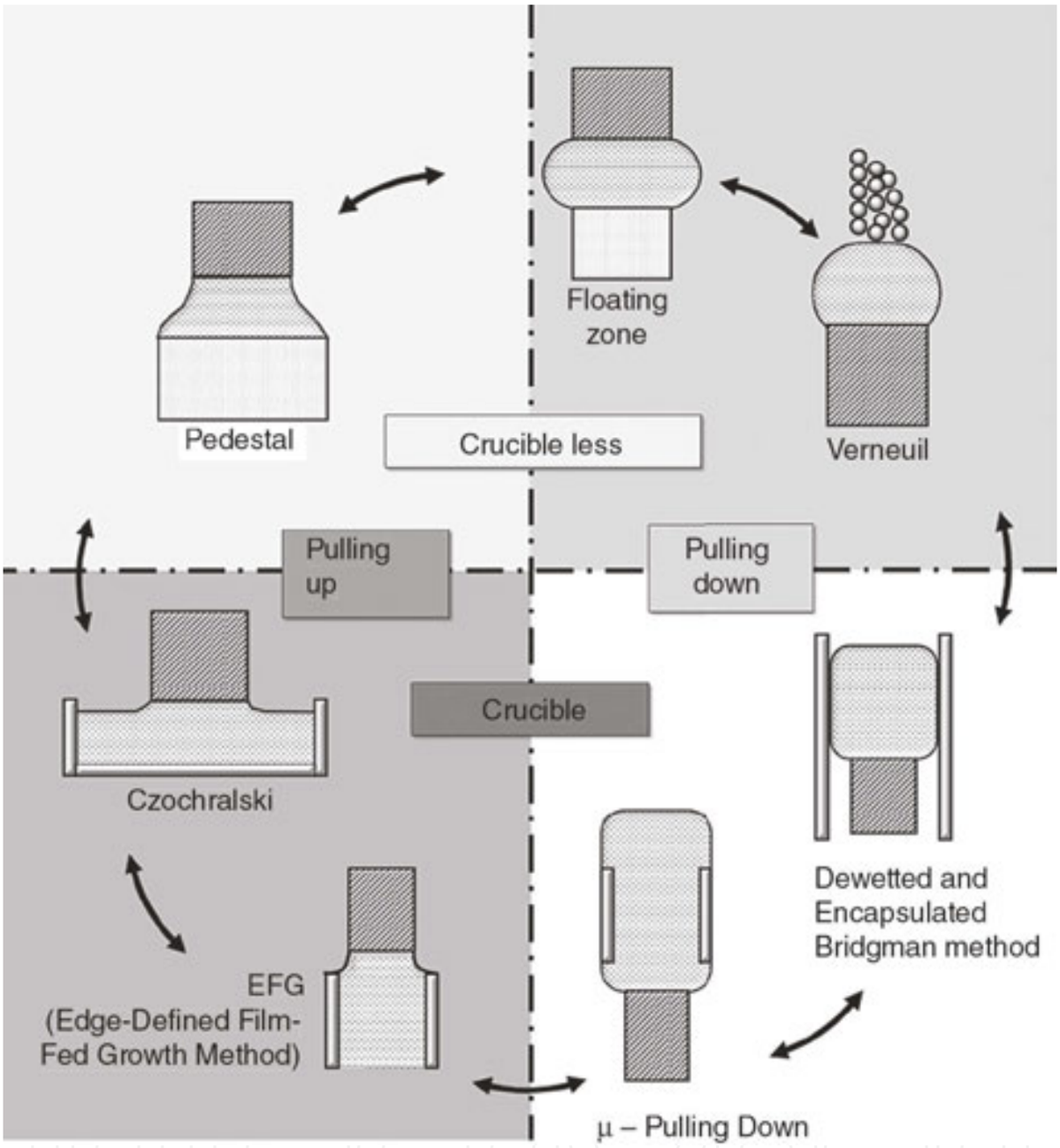

Fig. 17. Classification of various crystal growth processes using capillary forces for maintaining or shaping the molten material [87].

4.2.1 Fluorapatite

Single crystals of fluorapatite up to 5 cm long and of 1 cm maximum diameter were first prepared via the Kyropoulos method (pulling the crystal from the melt) by JOHNSON [114]. The Czochralsky method was used by MAZELSKI et al [114],[115] to grow the crystals up to 30 cm long. The ratio of CaF_2 to $Ca_3(PO_4)_2$ as determined by chemical analysis of crystals depends upon the value of the same ration in the melt. Even if the melt had correct stoichiometric

http://dx.doi.org/10.5772/62212

composition, grown fluorapatite would appear to have the deficiency of CaF_2 of about 5%. Fluorapatite as well as chlorapatite crystal with the length from 5 to 6 mm were grown by PRENER [116] from the solutions of apatite in molten calcium fluoride and chloride, respectively. The analyses of these flux-grown crystals agreed with theoretical values within 0.1% [114], [117].

4.2.2 Other compounds of apatite type

Single crystals of apatite-type $Nd_{9.33}(SiO_4)_6O_2$, $Pr_{9.33}(SiO_4)_6O_2$ and $Sm_{9.33}(SiO_4)_6O_2$ were prepared by HIGUCHI et al [102],[118],[119] from the stoichiometric mixture of Nd_2O_3, Pr_6O_{11} and Sm_2O_3 with SiO_2 (9.33 : 6) via the floating zone method. The crystal growth using the optical floating zone technique (a) was extensively used to grow a variety of bulk crystals, particularly single crystals of metal oxides [120],[121].

The pseudobinary phase diagram for the Nd_2O_3–SiO_2 system around the apatite phase is shown in **Fig. 19** [118],[122]. With the except of the end-member Nd_2O_3 and SiO_2, the apatite phase (Nd_2O_3 : SiO_2 = 7:9), Nd_2SiO_5 and $Nd_2Si_2O_7$ are observed. Both, Nd_2SiO_5 and $Nd_2Si_2O_7$ melt incongruently, while the apatite phase melts congruently.

YOSHIKAWA et al [123] prepared <0001> oriented $Ca_8La_2(PO_4)_6O_2$ (CLPA) single crystals with the apatite structure, which were grown by the Czochralsky method. This material can be used as substrate for the growth of <0001> GaN epitaxial layers.

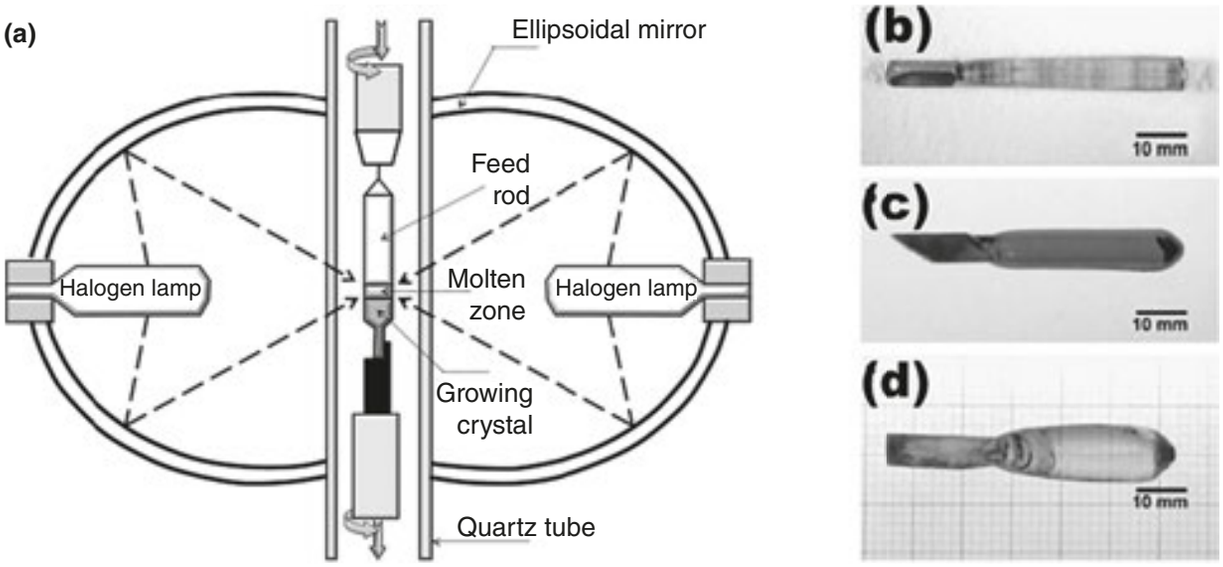

Fig. 18. Schematic diagram of the furnace with double ellipsoidal mirrors (a) and single grown crystals of $Pr_{9.33}(SiO_4)_6O_2$ (b), $Nd_{9.33}(SiO_4)_6O_2$ (c) and $Sm_{9.33}(SiO_4)_6O_2$ (d) [118].

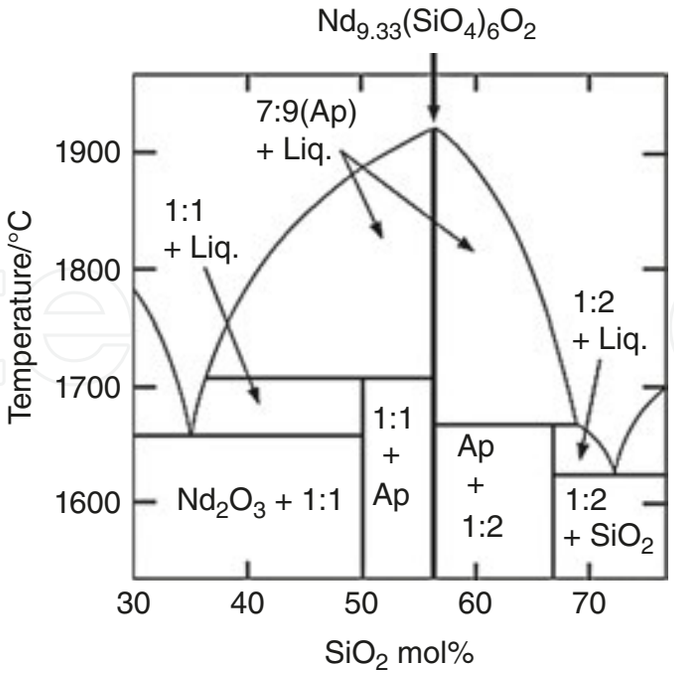

Fig. 19. Reconstructed pseudobinary phase diagram around the apatite phase $Nd_{9.33}(SiO_4)_6O_2$ in the Nd_2O_3-SiO system [118].

The growth of single crystal of synthetic analogue of vanadinite (lead vanado-chlorapatite, $Pb_5(VO_4)_3Cl$) using the CsCl flux method was performed by Masaoka and Kyono [124]. No impurity phases were formed from this crystal growth method. Crystals obtained via this method exhibit well-developed hexagonal prismatic form of the size of several millimeters along the [0001] direction. The largest crystals were approximately 6×1×1 mm.

The first hydrothermal growth of single crystals of chlorapatite was reported by Roufosse et al [125]. Crystals grown from the system chlorapatite-HCl-H_2O at 50 000 psi and pH = 1 with the growth zone at 465°C and dissolution zone at 360°C were found to be of high stoichiometry.

4.3 Synthetic analogues of the mineral hydroxylapatite

The synthetic analogue of the mineral hydroxylapatite can by prepared by the reaction [126]:

$$10\ Ca(NO_3)_2 + 6\ (NH_4)_2HPO_4 + 8\ NH_4OH \rightarrow Ca_{10}(PO_4)_6(OH)_2 + 20\ NH_4NO_3 + 6\ H_2O \quad (23)$$

Aqueous solutions of 0.167 mol·cm^{-3} of $Ca(NO_3)_2$ and 0.100 mol·cm^{-3} of $(NH_4)_2HPO_4$ were prepared, and their pH values were adjusted to above 8 by the addition of ammonium hydroxide. $(NH_4)_2HPO_4$ solution was heated to about 85°C and then slowly dropped into equal volume of vigorously stirred solution of $Ca(NO_3)_2$. The temperature of the reaction mixture

http://dx.doi.org/10.5772/62212

was kept at 85°C and stirring was maintained for further 3 days. In order to remove CO_2, the flow of N_2 was introduced to the suspension in reaction vessel. The suspension was then filtered and washed.

The survey of known chemical reactions successfully used for the synthesis of hydroxylapatite was provided by Shojai et al [32]. Depending on applied method (**Table 2**) and conditions (**Fig. 20**), different shapes of apatite particles can be prepared.

Shape*		**Approximated size range**	**Method(s) of synthesis****
	Irregular, formless, sphere	5 nm–200 μm	ss, mch, cc, hl, sg, hth, em, sch, ht, bs, cp
	Sphere, microsphere, nanosphere, ball	10 nm–1000 μm	mch, cc, sg, hth, em, sch, ht, bs, cp
	Rod, needle, tube, filament, fibber, wire, whisker, prism, worm, hexagonal prism, platelet, lath, strip	length: 10 nm–150 μm diameter: 3 nm–50 μm aspect ratio: 2–1200	ss, mch, cc, hl, sg, hth, em, sch, ht, bs, cp
	Plate, flake, sheet	length: 40 nm–50 μm width: 20 nm–35 μm thickness: 3 nm–5 μm	cc, hth, bs, cp
	Self-assembled nanorods, bundles of nanorods, oriented bundle, oriented raft, enamel prism-like structures, clusters of nanotubes, oriented array of bundled needles, packed nanorods	length: 200 nm–80 μm width: 100 nm–50 μm (oriented nanorods of 10 nm–13 μm diameter and 600 nm–5 μm length).	cc, hl, tht, bs, cp
	Dandelion, chrysanthemum, flower, feathery structure, bundle of fibers, self-assembled nanorods, rosette	1–8 μm (oriented nanorods of 80–500 nm diameter and 600 nm–5 μm length)	hth, em, bs, cp
	Leaf, flake, sheet, plate	800 nm–10 μm (organized nanoplates of 20–100 nm thickness)	cc, hl, cp
	Flower	700 nm–60 μm (organized petals of 20 nm–10 μm width and 180 nm–50 μm length)	cc, hth, bs

Shape*	Approximated size range	Method(s) of synthesis**
Porous microsphere, mesoporous sphere	0.5–7 μm (pores 20–150 nm)	hth, cp
Bowknot, self-assembled nanorods	1.5–2.5 μm (organized nanorods of 100–150 nm diameter and 1–2 μm length)	cp
Dumbbell	2–3 μm (organized nanoparticles of ~50 nm size)	cc

* Consult with **Section 3.1.14**.
** Solid-state synthesis (ss), mechanochemical method (mch), conventional chemical precipitation (cc), hydrolysis method (hl), sol-gel method (sg), hydrothermal method (hth), emulsion method (em), sonochemical method (sch), high-temperature processes (ht), synthesis from biogenic sources (bs), combination procedures (cp).

Table 2. Shape of hydroxylapatite particles prepared by given synthesis methods [32].

The influence of conditions on the morphology of hydroxylapatite particles is shown in **Fig. 20**. During hydrothermal synthesis, the particle size of HAP decreases with increasing pH value [32],[127],[128].

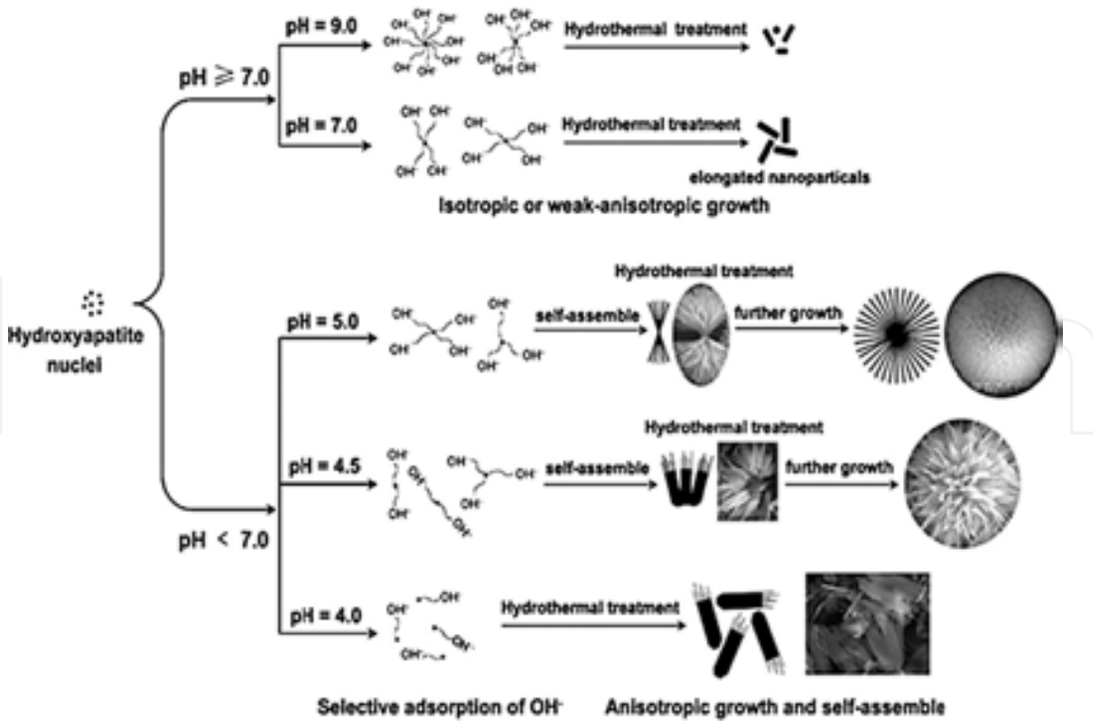

Fig. 20. The formation and the morphology evolution mechanism of $Ca_5(PO_4)_3OH$ samples with various morphologies based upon different pH values [127],[128].

http://dx.doi.org/10.5772/62212

Complete replacement of halogen occurs when either fluorapatite or chlorapatite is heated in the steam of H_2 or H_2O at high temperatures [69]:

$$Ca_{10}(PO_4)_6F_2 \overset{H_2,\ 1630°C}{\rightarrow} Ca_{10}(PO_4)_6(OH)_2 \overset{H_2O,\ 800°C}{\leftarrow} Ca_{10}(PO_4)_6Cl_2 \quad (24)$$

4.4 Fluorapatites

4.4.1 Synthetic analogues of the mineral fluorapatite

In literature various routes for the preparation of synthetic analogues of fluorapatite are described which include solid-state reactions of the type [129]:

$$3\ Ca_3(PO_4)_2 + CaF_2 \rightarrow Ca_{10}(PO_4)_6F_2 \quad (25)$$

At the temperature of 900°C hydroxylapatite reacts with calcium fluoride to give fluorapatite [69]:

$$Ca_{10}(PO_4)_6(OH)_2 + CaF_2 \rightarrow Ca_{10}(PO_4)_6F_2 + CaO + H_2O(g) \quad (26)$$

Fluorapatite can be also prepared directly by firing a mix of $3Ca_3(PO_4)_2$ with CaF_2 at 1600°C, or from calcium pyrophosphate and calcium fluoride:

$$18\ Ca_2P_2O_7 + 14\ CaF_2 \rightarrow 5\ Ca_{10}(PO_4)_6F_2 + 6\ POF_3 \quad (27)$$

Chlorapatite can be prepared by similar method using calcium chloride. It can also be produced in the reversible reaction according to **Eq. 21**.

Original phase diagram **Fig. 21**(a) for the section $Ca_3(PO_4)_2$–CaF_2 of the ternary system CaO–P_2O_5–CaF_2 was published by Nacken [130]. The range of compositions was extended by Berak [131] (b), and further refined (**Fig. 22**) by Berak and T.-Hudina [132]. Important features are congruent melting of $Ca_{10}(PO_4)_3F_2$ at 1650°C, eutectics with $Ca_3(PO_4)_2$ at 1620°C and second one with CaF_2 at 1203°C. Sufficiently precise phase diagram enables to determine necessary information on the flux growth of fluorapatite, so the crystal with only slight deficiency in fluorine compared to the theoretical one can be prepared. The problem concerning possible stable existence of spodiosite ($Ca_2(PO_4)F$) analogous to naturally occurring mineral remains unsettled, but it appears unlikely to be stable at liquidus temperatures [133].

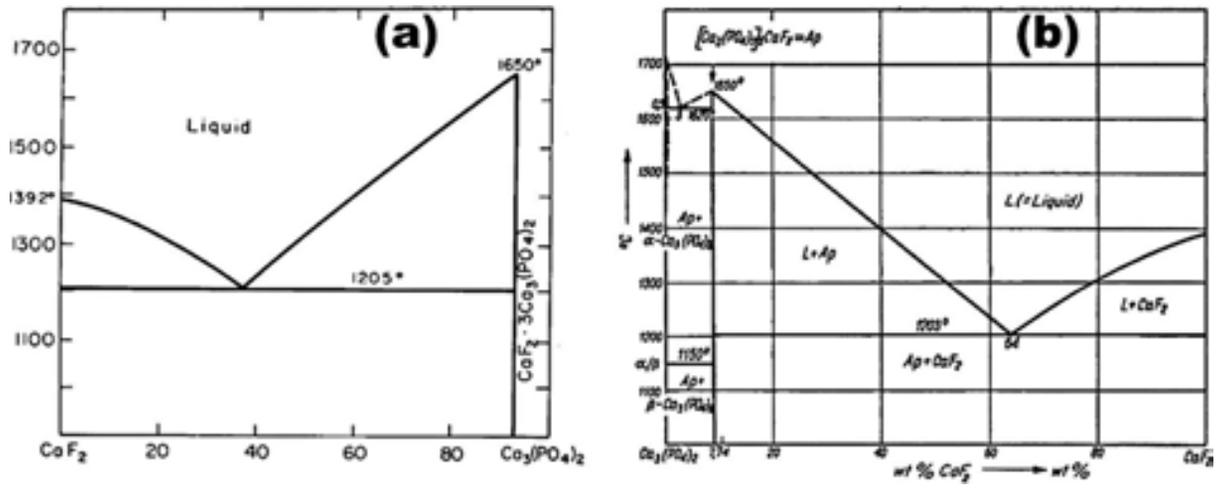

Fig. 21. Phase diagram of $Ca_3(PO_4)_2$–CaF_2 section by NACKEN [130] (a) and BERAK [131] (b).

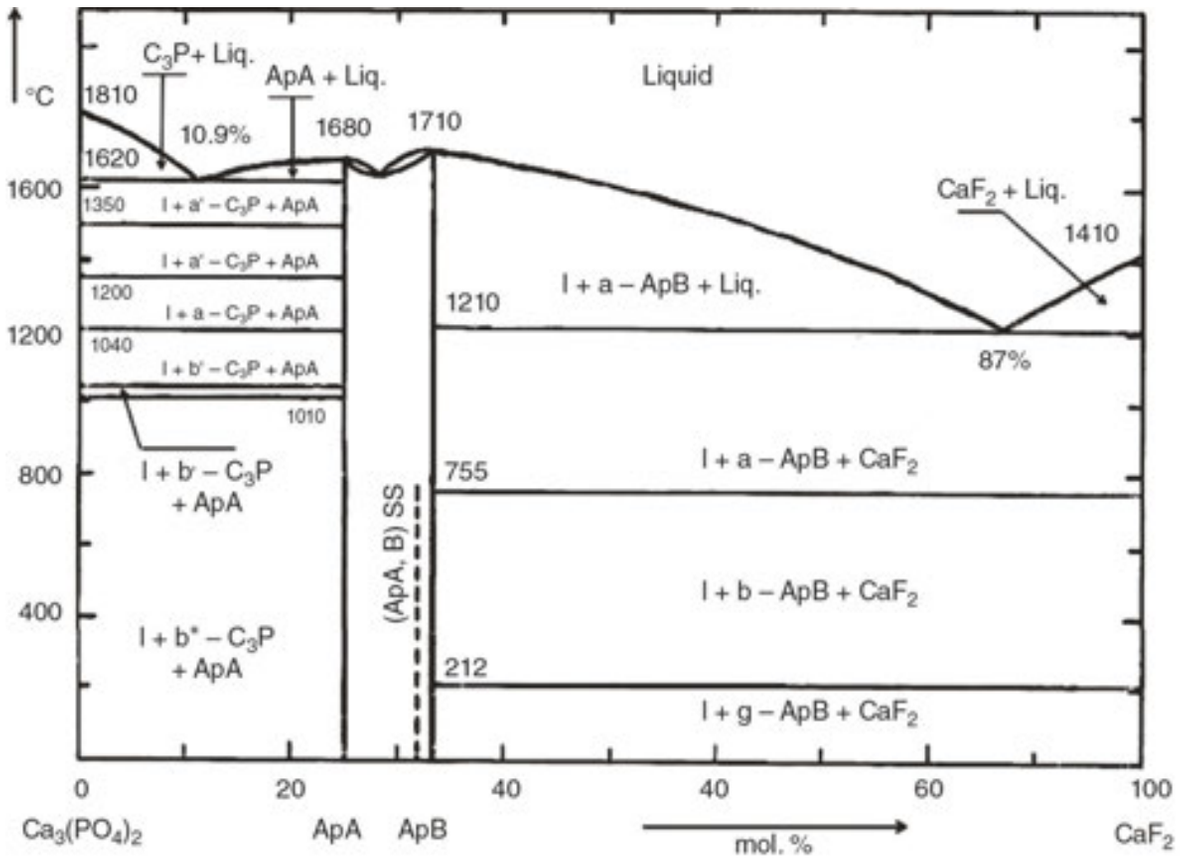

Fig. 22. Phase equilibrium in the system $Ca_3(PO_4)_2$–CaF_2: $Ca_{10}(PO_4)_6F_2$ (ApA) and $Ca_7(PO_4)_4F_2$ (ApB) [132].

The implication of the crystal growth of apatite and calcite in the systems $Ca_3(PO_4)_2$–$CaCO_3$–$Ca(OH)_2$–CaF_2 (**Fig. 23**(**a**)) and $Ca_3(PO_4)_2$–$Ca(OH)_2$–CaF_2–H_2O (**b**) enables the quaternary phase diagram provided by WILLIE [134].

http://dx.doi.org/10.5772/62212

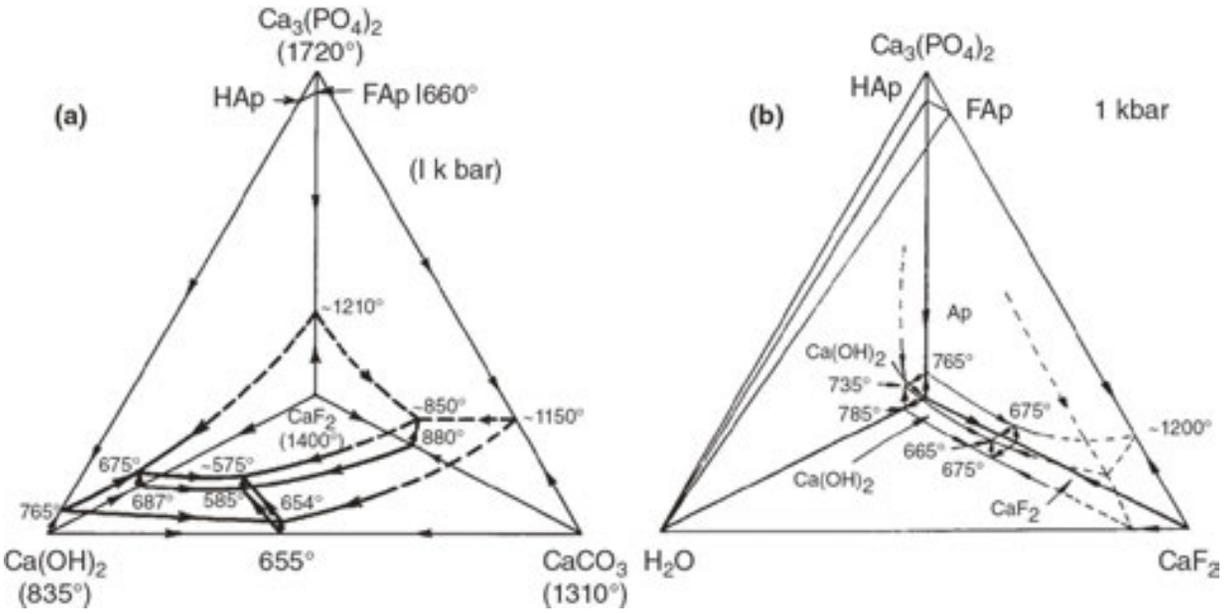

Fig. 23. System $Ca_3(PO_4)_2$–$CaCO_3$–$Ca(OH)_2$–CaF_2 (a) and $Ca_3(PO_4)_2$–$Ca(OH)_2$–CaF_2–H_2O (b) at the pressure of 1 kbar [134].

Long and uniform HAP whiskers with high crystallinity, controlled morphology and high aspect ratio were synthesized by ZHANG and DARWELL [83] via the hydrothermal method using acetamide. Compared to urea as an additive, which is commonly used to raise the pH in order to drive the nucleation and growth of HA crystals [106], acetamide has low hydrolysis rate under required hydrothermal conditions. This allows better and easier control, giving rise to rapid growth of whiskers at low supersaturation. The whisker length and width were in turn given by the solution conditions, including the concentration of Ca and PO_4 [83].

4.4.2 Barium fluorapatite

Barium apatite can be prepared by solid-state reaction [135]:

$$6\ BaHPO_4 + 3BaCO_3 + BaF_2 \xrightarrow{heat} Ba_{10}(PO_4)_6F_2 + 3CO_2 + 3H_2O \quad (28)$$

It possesses typical hexagonal structure with the space group $P6_3/M$ and a = 10.153 Å, c = 7.733 Å, c:a = 1:0.722, V = 10.153 Å^3 and Z = 2 [135].

Ba(1) atoms are located in columns on three threefold axes and are coordinated by nine oxygen atoms. The Ba(2) sites form triangles around the F site and are coordinated by six oxygen atoms and one fluoride ion. Fluoride ions are statistically displaced by ~0.25 Å from the Ba(2) triangles. This displacement of F ions is analogous to the displacement of OH ion in $Ca_{10}(PO_4)_6(OH)_2$ [138].

4.5 Chlorapatites

4.5.1 Synthetic analogues of the mineral chlorapatite

The stoichiometric Ca:P ratio in the composition of chlorapatite, the mole ratio of calcium to phosphorous was equal to 1.67 [139]. The reaction of $CaCl_2$ with H_3PO_4 under hydrothermal conditions including the temperature of 400°C and the pressure < 3 kbar leads to chlorapatite (**Eq. 21**) [82],[140].

The mechanochemical synthesis of chlorapatite in a high energy planetary mill should be described by the reaction [139]:

$$9CaO + CaCl_2 + 3\ P_2O_5 \rightarrow Ca_{10}\left(PO_4\right)_6 Cl_2 \tag{29}$$

Nacken [141] determined the phase diagram for the section $Ca_3(PO_4)_2$–$CaCl_2$ of the ternary system CaO–P_2O_5–$CaCl_2$ (**Fig. 24**). Chlorapatite crystallized from melts of its own composition is highly deficient in Cl, while lower temperatures near 1040°C lead to the crystallization of stoichiometric chlorapatite [133].

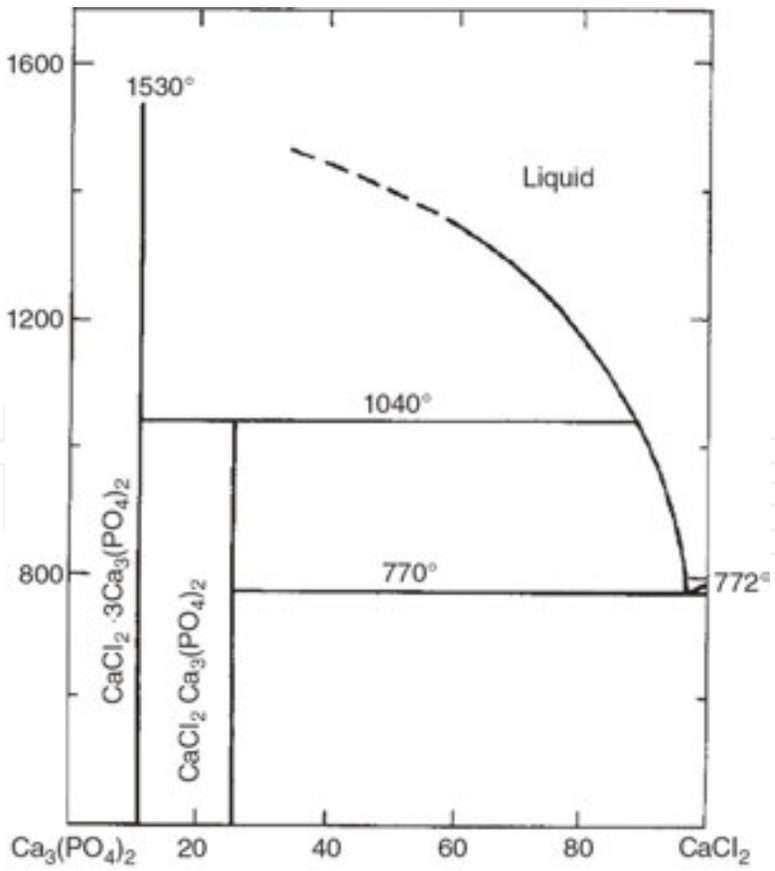

Fig. 24. Phase equilibrium in the system $Ca_3(PO_4)_2$–$CaCl_2$ by Nacken [133].

The mechanosynthesis and the characterization of chlorapatite nanopowders were performed by Fahami et al [139]. The formation of chlorapatite takes place according to the reaction 29. At the beginning of milling, the main products were stoichiometrically deficient chlorapatite and calcium oxide. Eventually, high crystalline CAP nanopowder was obtained after 300 min of milling. By increasing the milling time to 300 min, the lattice strain significantly increased.

4.5.2 Cadmium chlorapatite

Large crystals of $Cd_5(PO_4)_3Cl$ (space group $P6_3/M$, a = 9.633 Å, c = 6.484 Å and Z = 2) grow hydrothermally at 500°C and 800–1400 atm. from Na- and NH_4-containing solutions [142], [143]. The phase transition in cadmium chlorapatite from $P6_3/M$ to $P6_c/MCM$ was confirmed through the temperature dependent Raman measurements. The phase transition temperature from lower temperature phase ($P6_3/M$) to high temperature phase ($P6_3/MCM$) is approximately 700°C and was detected through the disappearance of low-temperature phase A_g Raman bands as the temperature approached the transformation temperature [144].

4.5.3 Other chlorapatites

The structure of apatite phase of the composition $Ba_5(OsO_5)_3Cl$ ($P6_3CM$, $\boldsymbol{a}$ = 10.928 Å, $\boldsymbol{c}$ = 7.824 Å, $\boldsymbol{V}$ =809.2 Å^3, Z = 2 and $\boldsymbol{\rho}$ = 6.29 g·cm^{-3}) where PO_4 tetrahedra are replaced by pyramidal OsO_5 groups was reported by Plaisier et al [145] as isomorphous with $Ba_5(ReO_5)_3Cl$ (Besse et al [146]) and $Ba_5(ReO_5)_3I$ (Baud et al [147]). The structure (**Fig. 25**) consists of columns of Ba(1) atoms parallel to the ***c***-axis and chains of $ClBa_6$ octahedra with common faces along the ***c***-axis. Among these are isolated pyramidal OsO_5 groups. Ba(1) atoms lie on the threefold-axis and are surrounded by nine oxygen atoms. Ba(1)-O distances vary between 2.74 and 2.76 Å. Atom of Ba(2) is surrounded by seven oxygen atoms and two atoms of chlorine.

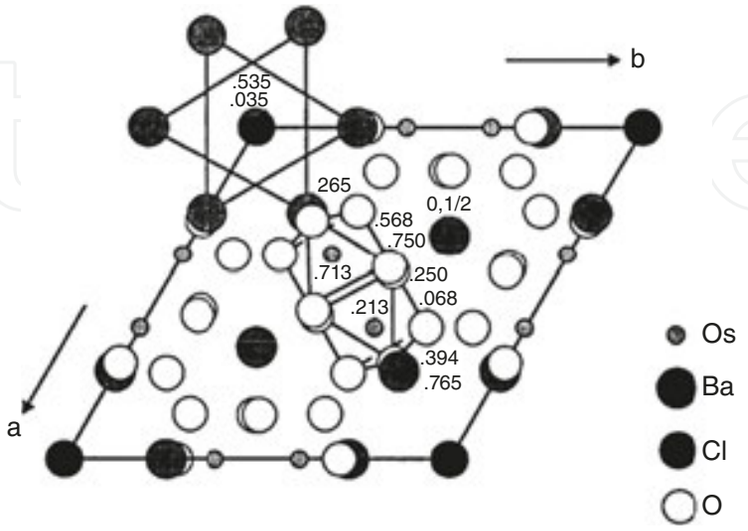

Fig. 25. Projection of the structure of $Ba_5(OsO_5)_3Cl$ along the c-axis [145].

Suzuky and Kibe [148] used the NaCl flux method to prepare barium ($Ba_5(PO_4)_3Cl$) and strontium chlorapatite ($Sr_5(PO_4)_3Cl$) crystals and modified.[47] Wilhelmy method [149],[150], [151][48] for the determination of surface free energy (~26 $mN \cdot m^{-1}$ for both apatite crystals[49]). The determination of specific surface free energies (surface tension) for single crystal of $Sr_5(PO_4)_3Cl$ [152] (aspect ratio is 3.2) via the measurement of contact angles of water and formamide (CH_3NO) shows that ideal flat surface without a step should have uniform specific surface free energy, estimated to ≤ 26 and ≤ 50 $mN \cdot m^{-1}$ for (101⊚0) and (101⊚1) faces,[50] respectively. Experimentally obtained specific surface free energies roughly satisfy the Wulff's relationship [153],[154]:

$$\frac{\gamma_i}{h_i} = \text{const}, \tag{30}$$

where γ_i is the specific surface free energy of the *i*-th face of the crystal and h_i is the distance of face from the Wulff's (central) point of crystal.

4.6 Carbonated (biological) apatites

It seems now to be generally accepted that CO_3^{2-} dominantly replaces PO_4^{3-} in biological apatite (BAP, BAp) [155]. Carbonate-hydroxyl-apatite ($Ca_{10}(PO_4,CO_3)_6(OH)_2$), can be found mainly on islands and in caves, as a part of bird and bat excrements, guano [156].

4.6.1 Carbonated hydroxyl$^-$ and fluorapatite

Carbonated hydroxylapatite is the most important mineral in human dental enamel and bone [157],[158],[159],[160],[161],[162],[163],[164]. The presence of highly carbonated apatite was also proposed as a marker of the presence of bacteria (infectious microorganism) in kidney stones[51] [165],[166]. According to the position of planar bivalent carbonate ion (CO_3^{2-}) with anionic radius of 0.176 nm in the structure of apatite, three kinds of carbonate apatite are recognized in literature [157],[158],[167],[168],[169].

[47] The weight of liquid was measured instead of the weight of crystal.

[48] Since measured parameter is force (***F***, measured by tensiometer or microbalance), the Wilhelmy plate (or rod) method can be easily applied for small contact angles. The surface tension (γ) is calculated from the equation: $\gamma = F/(l \cos \Theta)$, where l = 2×length + 2×width of the plate, and wetting angle Θ is usually not determined but its value is taken for zero (complete wetting is assumed) or the value from either literature is used [149],[150],[151].

[49] The value should be affected by the estimation of value of aspect ratio.

[50] First-order hexagonal prism and first-order dipyramid, respectively.

[51] From the medical point of view, pathological calcifications refer to a concretion, e.g. a kidney stone, often associated with the tissue alteration. Additionally, normal physiological calcifications such as bone may become pathological through the influence of diseases such as arthrosis or osteoporosis Different chemical phases constitute the pathological calcifications, but calcium phosphate apatites are present in most of them [166]. Biological apatites (BAP) are described in **Section 7.1.3**.

http://dx.doi.org/10.5772/62212

1. **Type A**: CO_3^{2-} substitutes for OH^- (or Z^- anion in general) in the apatite channel at z ≈ 0.5 (**Fig. 27**(**a**)) by two triad clusters of Ca^{2+} atoms z ≈ 0.25 (1/4) and 0.75 (3/4). The composition of CCAP is given by the formula: $Ca_{10}(PO_4)_6(CO_3)_x(OH)_{2-2x}$. The TYPE-A substitution can be described as follows [170]:

$$\begin{aligned} &Ca_{10}(PO_4)_6(OH)_2 + CO_3^{2-} \rightarrow Ca_{10}(PO_4)_6CO_3 + 2\ OH^- \\ &\text{or}\quad \left[{}^{A}CO_3^{2-} + {}^{A}[V] \Leftrightarrow 2\left(OH^-, F^-, Cl^-\right)\right] \end{aligned} \tag{31}$$

The crystal structure of type-A carbonate apatite is controversial [172]. There are three different structures: with the space group $P\bar{6}$ in hexagonal symmetry (**Fig. 27**) [171], with the space group $P\bar{3}$ [159],[173] and with the space group Pb in monoclinic symmetry [174], [175].

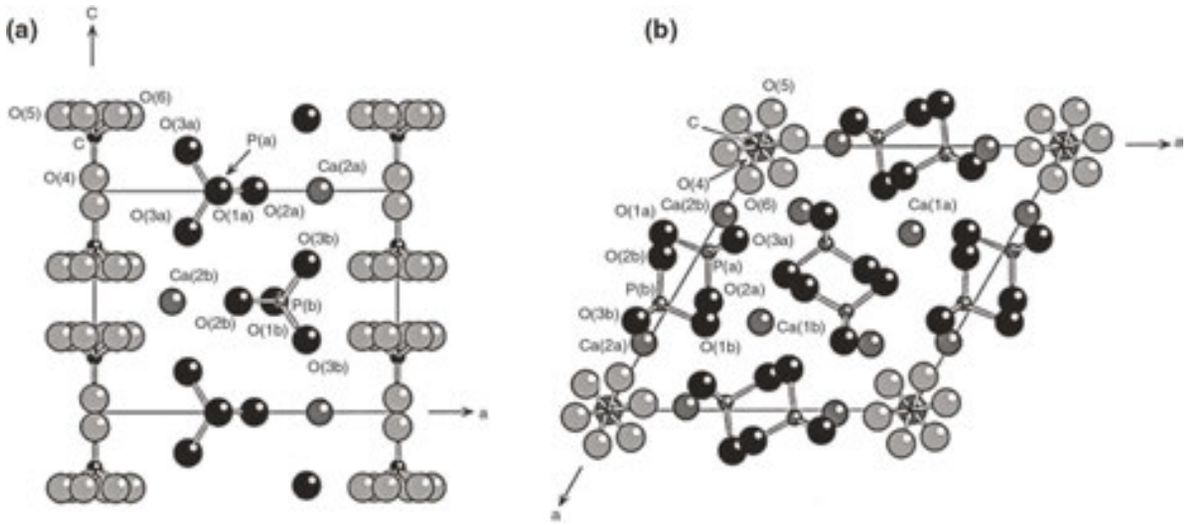

Fig. 26. The atomic configuration of type-A carbonated apatite on the (010) plane (a) and (001) plane (b) according to SUETSUGU et al [171].

2. **Type B**: CO_3^{2-} substitutes for phosphate ion (PO_4^{3-}). Different chemical formula is used to describe B-type carbonate apatite, the simplest and often used is [176]: $Ca_{10-x}(PO_4)_{6-x}(CO_3)_x(OH)_{2-x}$. The interpretation of the location of type-B carbonate ion is also problematical [158]. The carbonate ion is located in the vicinity of substituted phosphate group and occupies as many phosphate oxygen sites as possible. Some examples of the B-TYPE substitutions are described by equations [170],[177]:

$$\begin{aligned} &Ca_{10}(PO_4)_6(OH)_2 + Na^+ + CO_3^{2-} \rightarrow Ca_9Na(PO_4)_5CO_3(OH)_2 \\ &+Ca^{2+} + PO_4^{3-} \end{aligned} \tag{32}$$

$$\begin{aligned} &Ca_{10}(PO_4)_6(OH)_2 + CO_3^{2-} \rightarrow Ca_9[V_{Ca}](PO_4)_5 CO_3(OH)[V_{OH}] \\ &+PO_4^{3-} + OH^- + Ca^{2+} \end{aligned} \tag{33}$$

$$\begin{aligned} &Ca_{10}(PO_4)_6(OH)_2 + HPO_4^{2-} + CO_3^{2-} \rightarrow \\ &Ca_9[V_{Ca}]HPO_4(PO_4)_4 CO_3(OH)[V_{OH}] + 2\ PO_4^{3-} + Ca^{2+} \end{aligned} \tag{34}$$

where ***V*** denotes the vacancy. There is no clear energetic preference of CO_3^{2-} to substitute for any particular PO_4^{3-} group [178]. Sodium (**Eq. 33**) or other alkali metal cation (AM = Li, Na, K, Rb and Cs) is also known to increase the maximum ratio of carbonate substitution in B-site because its incorporation in calcium sites induces favorable electrical charge balance [176]:

$$\left[{}^{B}CO_3^{2-} + AM^+ \Leftrightarrow Ca^{2+} + PO_4^{3-}\right] \tag{35}$$

3. **Type AB**: mixed A-B type of apatite, where the composition can be described as: $Ca_{10}(PO_4)_{6-y}(CO_3)_{x+(3/2)y}(OH)_{2-2x}$. If both PO_4^{3-} ($z \approx 0.25$ or 0.75) and OH^- anions were replaced by two CO_3^{2-}, the process can be described as follows:

$$\begin{aligned} &Ca_{10}(PO_4)_6(OH)_2 + 2\ CO_3^{2-} \rightarrow Ca_{10}(PO_4)_5(CO_3)_2(OH) \\ &+OH^- + PO_4^{3-} \end{aligned} \tag{36}$$

Two different structural roles of CO_3^{2-} anion result in characteristic infrared (IR) signatures: type A carbonate having a doublet band at about 1545 and 1450 cm^{-1} (asymmetric stretching vibration, ν_3) and a singlet band at 880 cm^{-1} (out-of-plane bending vibration, ν_2), and type B having these bands at about 1455, 1410 and 875 cm^{-1}, respectively [158].

Published structural studies [158] of carbonated apatites were performed with the synthetic phases. Ren et al [171] investigated the structure of carbonated apatite using the ab initio simulation (**Fig. 27**) with the conclusion that the most energetically stable substitutions is type-AB in which two carbonate ions replace one phosphate group and one hydroxyl group respectively. The crystal structure of A-type of carbonated apatite is energetically more favorable than B-type of substitution. The most stable configuration of type-A is carbonate triangular plane almost parallel to the ***c***-axis at $z = 0.46$. Type-A substitution tends to increase the lattice parameter ***a*** but decreases ***c*** whereas type-B substitution shows the opposite effect. The lowest energy configuration of type-B has calcium ion replaced by a sodium ion to balance the charge (**Eq. 33**) and the carbonate lying almost flat on the ***b***/***c*** plane.

http://dx.doi.org/10.5772/62212

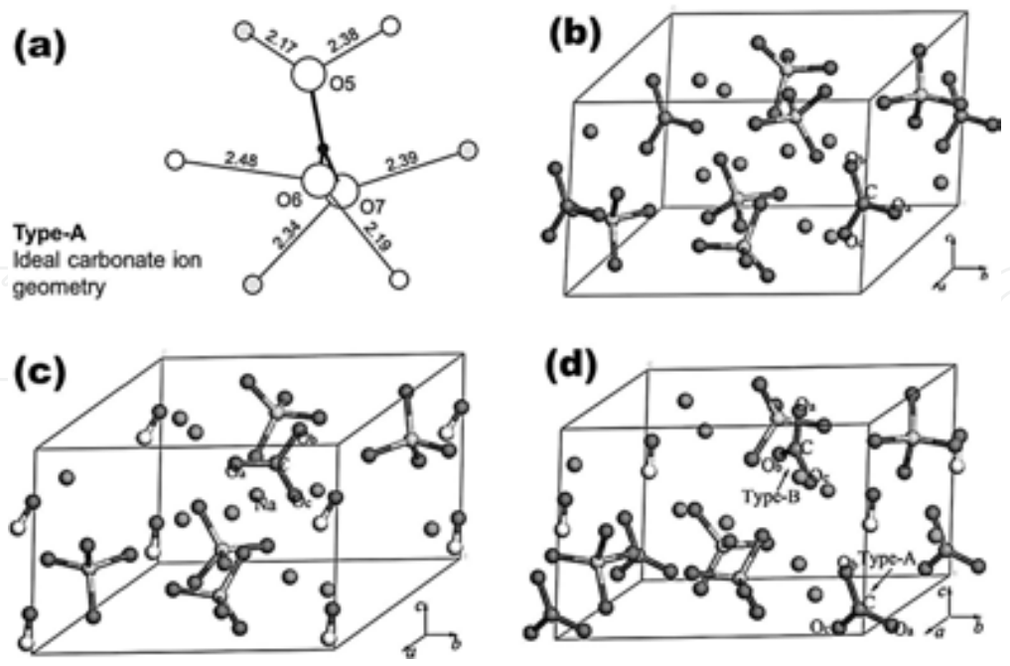

Fig. 27. The model of channel structure for ideal carbonate ion geometry of TYPE-A (a) [101] and the energetically favored configuration of TYPE-A carbonated apatite (b), the most stable structure of TYPE-B carbonated apatite (c) and the configuration of TYPE-AB after the geometry optimization (d) [170].

The type-A of carbonated apatite in which carbonate ion was completely substituted for the hydroxyl site, was synthesized by heating low crystalline and stoichiometric synthetic analogue of hydroxylapatite powder in the flow of dry carbon dioxide gas at 1000°C for 24 h by TONEGAWA et al [172]. The chemical composition of this phase can be described by the formula: $Ca_{10}(PO_4)_6(CO_3)_{0.93\pm0.06}$. The crystal structure was determined to be of monoclinic symmetry with the space group P_B in the temperature range from 25 to 500°C.

The synthesis of type-A carbonate apatite can be performed by heating of pure HAP at temperatures from 800 to 1000°C for several hours in dry CO_2 atmosphere according to the reaction [176],[179]:

$$Ca_{10}(PO_4)_6(OH)_2 + y\ CO_2 \leftrightarrow Ca_{10}(PO_4)_6(OH)_{2-y}(CO_3)_y + y\ H_2O \quad (37)$$

Type-B carbonated apatite powders are generally synthesized from the precipitation reaction in aqueous media [176]. The reaction **38** (or **Eq. 4** as was described in **Section 1.5.2**) can be used for the capture of carbon dioxide at high temperature over the operation limit of CaO-based sorbents.

The mechanochemical synthesis of B-type carbonated fluorapatite under argon atmosphere using high-energy planetary ball mill was described by N.-TABRIZI and FAHAMI [180]. The process can be described by the reaction:

$$\left(9-x/2\right)\ CaCO_3+\left(3-x/2\right)\ P_2O_5+CaF_2\rightarrow Ca_{10-x/2}\left(PO_4\right)_{6-x}\left(CO_3\right)_x\ F_2 \\ +\left(9-3x/2\right)CO_2 \tag{38}$$

4.6.2 Carbonate-chlorapatites

Carbonated chlorapatite nanopowders can be synthesized by the mechanochemical process under argon atmosphere using the mixture of calcite ($CaCO_3$), phosphorus pentoxide (P_2O_5) and calcium chloride ($CaCl_2$) as raw materials [181],[182]:

$$\left(9-x/2\right)\ CaCO_3+\left(3-x/2\right)\ P_2O_5+CaCl_2\rightarrow \\ Ca_{10-x/2}\left(PO_4\right)_{6-x}\left(CO_3\right)_x\ Cl_2+\left(9-3x/2\right)\ CO_2 \tag{39}$$

The substitution degree of PO_4^{3-} was given by the *x* value in the general formula of TYPE-B of $Ca_{10-x/2}(PO_4)_{6-x}(CO_3)_xCl_2$.

The high-pressure (1 GPa) synthesis of sodium-bearing carbonate chlorapatite of TYPE A-B (CCLAP, $Ca_{10-(y+z)}Na_y[V]_z[(PO_4)_{6-(y+2z)}(CO_3)_{y+2z}][Cl_{2-2x}(CO_3)_x]$, where $x \approx y \approx 4z \approx 0.4$) from carbonate rich melt in the temperature range from 1000 to 1350°C, was described by FLEET et al [169].

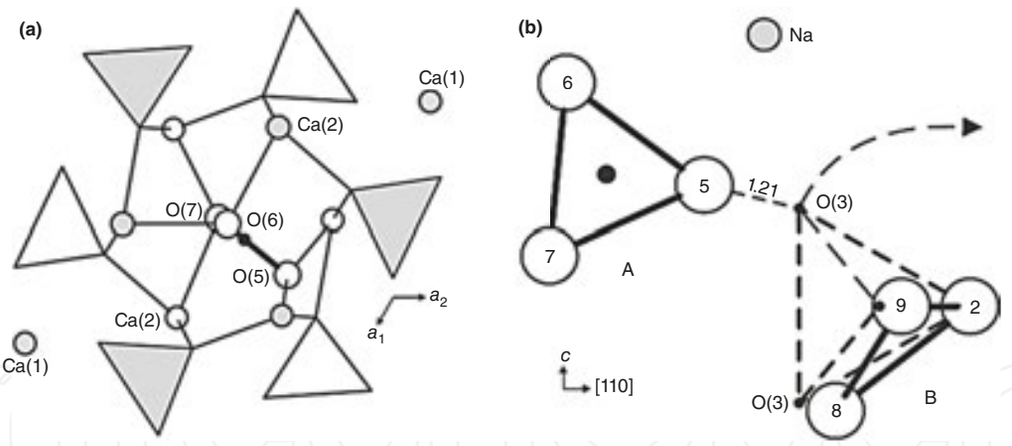

Fig. 28. The structure of carbonate chlorapatite showing one of 12 possible orientations of the type-A carbonate ion in apatite channel: the unit-cell origin is in the center of figure, shaded phosphate polyhedra and Ca(2) atoms are centered at *z* = 3/4 (a) and the fragment of CCLAP structure showing the location of B carbonate ion close to the sloping faces of substituted phosphate tetrahedron (b) according to FLEET AND LIU [169].

The structure of Na-bearing CCLAP crystals (**Fig. 28**(**a**)) with the contents of Na and A and B-type of carbonate ranges between those of Na-bearing carbonated fluorapatite (CFAP) and carbonated hydroxylapatite (CHAP). The stoichiometric amount of Na and A-type of carbonate is consistent with the near linear (1:1) correlation reported for CHAP and CFAP and provides the evidence of active role of Na in the substitution of carbonate into the apatite channel, even if Na does not appear in usual charge-balanced substitution scheme [169]:

$$\left[{}^{A}CO_3^{2-} \Leftrightarrow 2\ Cl^- \right] \tag{40}$$

On the other hand, the B : Na ratio is higher than one (approximately 1 : 1.5) and is located between the values determined for CHAP (B : Na = 1) and CFAP (B : Na = 2). The substitutions of B carbonate ion into CCLAP seem to be more complex than those into CHAP, which is expressed by **Fig. 28** or by the following charge-balanced substitutions scheme:

$$\left[Na^+ + {}^{B}CO_3^{2-} \Leftrightarrow Ca^{2+} + PO_4^{3-} \right] \tag{41}$$

There should be additional vacancies including the charge-balancing mechanism:

$$\left[1/2\ [V] + {}^{B}CO_3^{2-} \Leftrightarrow 1/2\ Ca^{2+} + PO_4^{3-} \right] \tag{42}$$

This leads to the formula of sodium-bearing carbonate chlorapatite mentioned above.

Similar profiles of ν_3 bands in FT-IR spectra for all carbonate apatite composition series and carbonated contents, together with common X-ray structure suggest that Na cation and A and B carbonate ion substituents are present as randomly distributed defect clusters within host apatite structure. The defect cluster depicted in **Fig. 28** (**b**) facilitates local charge compensation by Na-for-Ca substitution, explains the linear 1:1 correlation between Na and A carbonate, and minimizes the effects of spatial accommodation [169].

The synthesis of hydroxyl-chlorapatite solid solution via the precipitation method can be presented as follows [183]:

$$\begin{aligned} &10\ Ca(NO_3)_2 + 6\ (NH_4)_2 HPO_4 + 2\ NH_4Cl + 6\ NH_4OH \rightarrow \\ &Ca_{10}(PO_4)_6\left[(OH)_{2-x}\ Cl_x\right] + 20\ NH_4NO_3 + H_2O \end{aligned} \tag{43}$$

Also fluorine and chlorine co-substituted hydroxylapatites can be prepared by aqueous precipitation method [184]:

$$\begin{aligned} &10\ Ca(NO_3)_2 + 6\ (NH_4)_2 HPO_4 + \ NH_4F + NH_4Cl + 6\ NH_4OH \rightarrow \\ &Ca_{10}(PO_4)_6(F,Cl) + 20\ NH_4NO_3 + 6\ H_2O \end{aligned} \tag{44}$$

$$\begin{aligned} &10\ Ca(NO_3)_2 + 6\ (NH_4)_2 HPO_4 + x\ NH_4F + \\ &y\ NH_4Cl + \left[8 - (x+y)\right]\ NH_4OH \rightarrow Ca_{10}(PO_4)_6\left(OH_{2-(x+y)}F_xCl_y\right) \\ &+20\ NH_4NO_3 + 6\ H_2O \end{aligned} \tag{45}$$

Carbonate can be introduced into the structure of carbonated barium-chlorapatite by stirring apatite in an $(NH_4)_2CO_3$ solution for 1 week [185]:

$$Ba_{10}(PO_4)_6Cl_2 + CO_3^{2-} \rightarrow Ba_9(PO_4)_5Cl + PO_4^{3-} + Cl^- + Ba^{2+} \quad (46)$$

The attempts to prepare carbonated barium-chlorapatite in a one-step synthesis results in a mixture of $BaCO_3$ and $Ba_3(PO_4)_3$. The variations in the manner in which carbonate was added to the reaction mixture, such as co-titrating a carbonate solution along with $BaCl_2$ and $NH_4H_2PO_4$, pre-mixing it with $NH_4H_2PO_4$, or adding it first or last did not eliminate the precipitation of simple salts. The inability at 60°C and at the pH of 10 to produce carbonated barium-chlorapatite at any ratio of carbonate to phosphate in the aqueous solution is probably due to close molar solubility of simple salts [185].

4.7 Bromoapatites

4.7.1 Calcium bromapatite

Calcium bromapatite has typical hexagonal apatite structure with the space group $P6_3/M$, ***a*** = 9.761 Å, ***c*** = 6.739 Å, c:a = 1: 0.6904, ***V*** = 556.06 Å^3 and ***Z*** = 2 (**Fig. 29**) [186]. The synthesis of **calcium bromapatite** ($Ca_{10}(PO_4)_6Br_2$) in the tubular quartz reactor (sealed-tube method) can be described by the reaction [135],[187],[188],[189]:

$$Ca_{10}(PO_4)_6OH_2 + 2\ HBr \xrightarrow{1193\ K,\ 15\ h} Ca_{10}(PO_4)_6Br_2 + 2\ H_2O \quad (47)$$

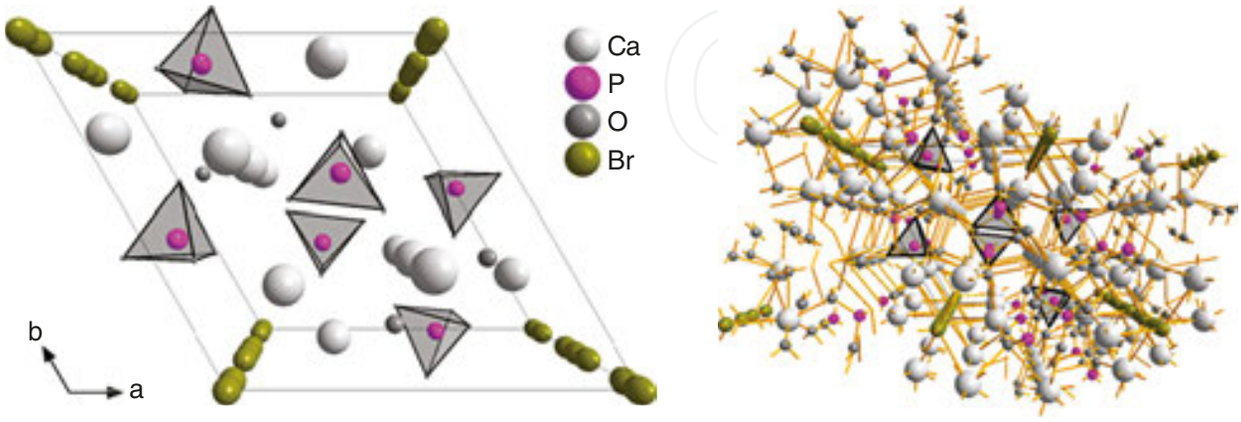

Fig. 29. The structure of $Ca_5(PO_4)_3Br$ (perspective view along the c-axis).

The phase can also be prepared via solid-state synthesis reaction [135]:

http://dx.doi.org/10.5772/62212

$$6\ CaHPO_4 + 3\ CaCO_3 + CaBr_2 \xrightarrow{heat} Ca_{10}\left(PO_4\right)_6 Br_2 + 3\ CO_2 + 3\ H_2O \quad (48)$$

4.7.2 Lead bromapatite

The synthesis of **lead bromapatite** ($Pb_{10}(PO_4)_6Br_2$) by solid-state synthesis via sintering of equal amount of $Pb_9(PO_4)_6$ and $PbBr_2$ at the temperature of 250°C in a platinum tube was described by Bhatnagar [191]. Br^- (1.95 Å) anions at the ***Z***-site in general formula of apatite ($Pb_{10}(PO_4)_6Z_2$) can be readily substituted by other usual monovalent anions (Cl^-, F^- and OH^-).

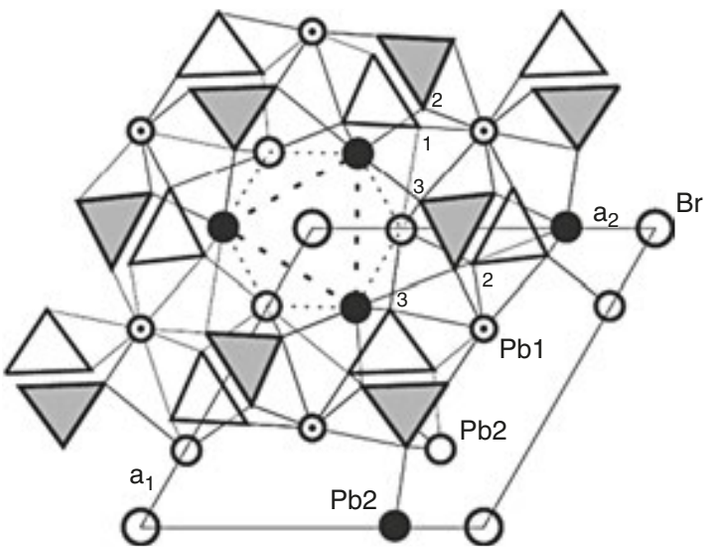

Fig. 30. The structure of lead bromapatite identifying the channel polyhedron (broken lines) formed by Pb(2) cations in apatite channel wall: open Pb(2) circles are at the height z = 1/4 and closed circles are at z = 3/4; triangles are PO_4 tetrahedra centered at z = 1/4 (open) and z = ¾ (shaded); numbers (1, 2, 3) identify oxygen atoms forming the corners of tetrahedra [190]

Liu et al [190] prepared synthetic lead bromapatite via solid-state reaction at pressure up to 1 GPa. In the structure of this phase (**Fig. 30**), isolated PO_4 tetrahedra centered at z = 1/4, 3/4 are linked by Pb(1) in nine-fold (6 + 3) coordination and Pb(2) in an irregular sevenfold (6 + 1) coordination. A prominent feature is large c-axis channel which is defined by tri-clusters of M(2) cations at z = 1/4, ¾ and accommodates a variety of anion components.

4.7.3 Strontium bromapatite

Strontium bromapatite (strontium bromoapatite) can be prepared via solid-state reaction (**Eq. 50**) and wet (solution) method (**Eq. 51**) according to the following reactions [135]:

$$6\ SrHPO_4 + 3\ SrCO_3 + SrBr_2 \xrightarrow{heat} Sr_{10}\left(PO_4\right)_6 Br_2 + 3\ CO_2 + 3\ H_2O \quad (49)$$

$$10\ SrBr_2(aq) + 6\ Na_3PO_4(aq) \rightarrow Sr_{10}(PO_4)_6Br_2(s) + 18\ NaBr(aq) \quad (50)$$

Since the precipitate contains Na^+ ions, it must be washed thoroughly to obtain pure product. A small amount of hydroxylapatite may also be present.

Strontium bromapatite forms softer crystal than fluorapatite or strontium chlorapatite. Since it is not stable under the mercury-vapor discharge in fluorescent lamp (**Section 10.6**), strontium bromapatite cannot be used for the production of lighting phosphor [135].

4.7.4 Other bromapatites

Other bromapatites are $Cd_5(PO_4)_3Br$ (a = 9.733 Å, c = 6.468 Å and Z = 2), $Cd_5(AsO_4)_3Br$ (a = 10.100 Å, c = 6.519 Å and Z = 2) and $Cd_5(VO_4)_3Br$ (a = 10.173 Å, c = 6.532 Å and Z = 2). They can be grown from melt in platinum crucible filled with $Cd_3(MO_4)_2$ (M = As, V and P) and the excess of $CdBr_2$. All phases belong to the space group of $P6_3/M$ [142],[143],[186].

4.8 Iodoapatites

Since, the apatite structure is capable of accommodating monovalent anions, strontium iodoapatites were investigated as a potential waste form to immobilize radioactive iodine [135],[192].

4.8.1 Calcium iodoapatite

Calcium iodoapatite ($Ca_5(PO_4)_3I$) does not exist as a separate phase but as oxoapatite. Iodo-oxyapatite (pentadecacalcium iodide oxide nanophosphate, $Ca_{15}(PO_4)_9(I,O)$) was synthesized by the flux method (**Section 4.2**). The crystal structure was refined in the space group $P6_3/M$ with lattice parameters ***a*** = 9.567 Å, ***b*** = 20.754 Å and ***Z*** = 2. Iodo-oxyapatite has typical hexagonal structure but the unit cell is tripled along the hexad (refer to **Footnote 16** in **Chapter 1**) and oxide ions along this direction [135].

4.8.2 Strontium Iodoapatite

Strontium iodoapatite (strontium iodoapatite, strontium iodine-apatite) is of academic interest due to large size of I^- ions compared to other halide ions. However, the thermodynamic functions determined for the alkaline earth apatite series preclude the formation of stable iodoapatite because the cationic size of Sr^{2+} or Ba^{2+} is too small relating to that of iodide ion which must fit upon the ***c***-axis of the structure next to the triads of Sr^{2+} or Ba^{2+} at (000), (010), and (001) positions in the lattice. Such crystals relevant to radioactive waste management include fluorapatite, and, in the end, iodoapatite which should be able to immobilize the radioactive species [135].

4.8.3 Lead vanado-iodoapatite

The preparation of lead vanado-iodoapatite ($Pb_{10}(VO_4)_6I_2$) by hot pressing (HP), isostatic hot pressing (HIP) and sealed-tube method (**Section 4.1.1**) were described in literature. $Pb_{10}(VO_4)_6I_2$ is thermally stable up to about 800 K. The thermal conductivity of hot-pressed sample, with the theoretical density of 82%, increases gradually with increasing temperature from 0.65 $W \cdot m^{-1} \cdot K^{-1}$ at room temperature to 0.78 $W \cdot m^{-1} \cdot K^{-1}$ at 523 K. The leaching rate of iodine for apatite was two orders of magnitude higher than that of AgI glass waste form. Despite the high leaching rate (compared to AgI embedded in glass), high chemical stability up to 800 K and acceptable mechanical properties of this apatite suggest that it be a good waste form when embedded in a suitable matrix material [135],[193].

Facile low temperature solid-state synthesis of iodoapatite by high-energy ball milling of PbI_2, PbO and V_2O_5 was described by Lu et al [195]. As-milled iodoapatite is in the form of amorphous matrix embedded with nanocrystals and can be readily crystallized by subsequent thermal annealing at low temperature of 200°C with minimal iodine loss.

4.8.4 Cadmium vanado-iodoapatite

Synthetic cadmium apatites containing iodine such as $Cd_5(VO_4)_3I$ (space group $P6_3/M$, a = 10.307 Å, c = 6.496 Å and Z = 2 [142],[143]) were prepared, but other apatites containing iodine are unknown [142],[194],[186]. $Cd_5(VO_4)_3I$ can be grown form the flux of $Cd_3(VO_4)_2$ and the excess of CdI_2 in the platinum crucible [142].

4.8.5 Radium iodoapatite

Radium iodoapatite, if could be formed, would have the formula $Ra_5(PO_4)_3I$ but it has not been prepared yet. This salt would be probably best prepared by solid-stare reaction [135]:

$$6\ RaHPO_4 + 3\quad RaCO_3 + RaI_2 \rightarrow Ra_{10}\left(PO_4\right)_6 I_2 + 3\ CO_2 + 3\ H_2O \tag{51}$$

Whether this compound can be formed remains speculative.[52]

4.9 Chalcogenide phosphate apatites

The preparation and the structure of chalcogenide phosphate apatites of the composition $Ca_{10}(PO_4)_6S$ (calcium sulfoapatite), $Sr_{10}(PO_4)_6S$ (strontium sulfoapatite), $Ba_{10}(PO_4)_6S$ (barium sulfoapatite) and $Ca_{10}(PO_4)_6Se$ (calcium selenoapatite) was reported by HENNING et al [196]. These apatite phases are isostructural and crystallize in the trigonal space group $P\bar{3}$.with the

[52] In human body radium behaves in a similar way as calcium. When ingested, it is readily adsorbed in bone where it may directly irradiate the bone and other tissues. This exposition may result in fatal disease as the tragic story of "*Radium girls*" working with luminous paint trade named: Undark (the mix of radium and zinc sulfide produced by U.S. Radium Corporation between 1917 and 1938) shows [136],[137].

chalcogenide ion positioned at (0 0 ½). The sulfoapatites show no ability to absorb H_2S in the way oxyapatite absorbs H_2O at elevated temperatures. This can be attributed to the position of sulfide ion and the way it influences the crystal structure around the vacant chalcogenide position at (000). Calcium sulfoapatites, $Ca_{10}(PO_4)_6S$, can be successfully synthesized only using oxide starting materials with sulfur vapor under H_2 atmosphere instead of toxic H_2S gas [197].

4.9.1 Anion deficient lacunar lead apatites

The apatitic structure can accommodate a great variety of other substituent's and vacancies in anionic sites (**Chapter 6**). Previous studies on apatites showed that the only system, where the compounds with the apatite structure could be prepared without ***Z*** anion, is the lead system. These apatites have the vacancies in Z anion sites (**Fig. 31**) with general formula $APb_4(XO_4)_3$, where A is monovalent cation Na, Ag, K, etc. Pb^{2+}on plays a crucial role allowing to preserve the ideal apatitic network. This role is related to the presence of lone $6s^2$pairs (**Section 2.1.2**) which can compensate for the Coulomb imbalance due to the existence of anion gaps in the tunnels of apatites [198],[199].

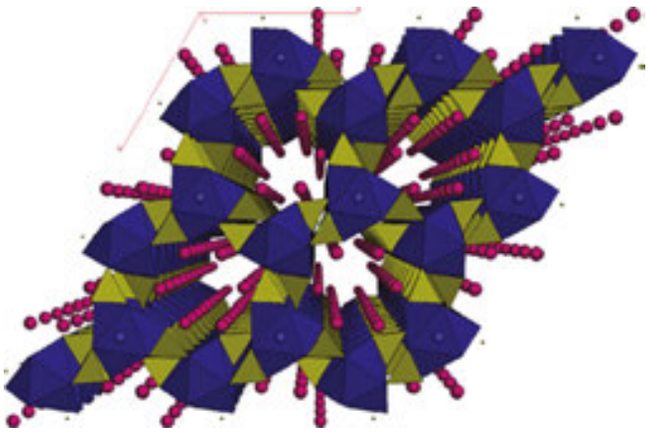

Fig. 31. Polyhedral view in the ab-plane of the crystal structure of $NaCaPb_3(PO_4)_3$ showing the tunnels [199].

Lead in apatite is of great interest from two points of view. First, lead is known as a "bone seeker" as it accumulates in bones and teeth, second, it may contribute to the deviation from the general formula of apatites. Moreover a new voltammetric sensor for the quantification of mercury based on $NaCaPb_3(PO_4)_3$ modified carbon paste electrode can be prepared. Because of the importance of these types of lacunar apatites and the problems which they may cause in biomaterial applications, particular attention has been paid during past few years to synthesize new lacunar anionic apatites [198],[199].

Silver lead apatite ($Ag_2Pb_8(PO_4)_6$, $P6_3/M$, a = 9.765 and c = 7.198 Å) and sodium lead apatite ($Na_2Pb_8(PO_4)_6$, $P6_3/M$, a = 9.731, c = 7.200 Å and Z = 2) were prepared by solid-state synthesis by Ternane et al [200] from the stoichiometric mixture of $Pb_3(PO_4)_2$ with Ag_3PO_4 (at 215°C and 100 atm.) and PbO, Na_2CO_3 and $(NH_4)_2HPO_4$, respectively. The synthesis of sodium lead apatite can be described by chemical equation:

http://dx.doi.org/10.5772/62212

$$8\ PbO + Na_2CO_3 + 6\ (NH_4)_2 HPO_4 \xrightarrow{\substack{500°C/3\ days \\ 700°C/2\ days}} Pb_8Na_2(PO_4)_6 + 12\ NH_3 + 9H_2O + CO_2 \quad (52)$$

The unit cell contains eight divalent Pb^{2+}cations, two monovalent cations (Na^+ or Ag^+) and six $[PO_4]^{3-}$ ions. The triangle sites, 6*h*, are occupied by Pb^{2+}ions only while the column positions, 4*f*, are occupied by nearly equal amounts of Pb^{2+} and monovalent ions (Na^+ or Ag^+).

The structure of this phase was also investigated by Koumiri et al [201]: ***a*** = 9.7249 Å, ***c*** = 7.190 Å and Z = 2. From the interatomic distances it appears that lead cations in the lacunar apatite $NaPb_4(PO_4)_3$ behave in two different ways:

i. Pb2(II) cations with stereochemically inactive lone $6s^2$ pairs are engaged in almost totally ionic bond Pb(2)/Na–O at the mixed site.

ii. Pb1(II) is engaged in a Pb(1)–O bond with more covalent character, where its lone $6s^2$ pair is stereochemically active and constitutes the seventh ligand of lead cation.

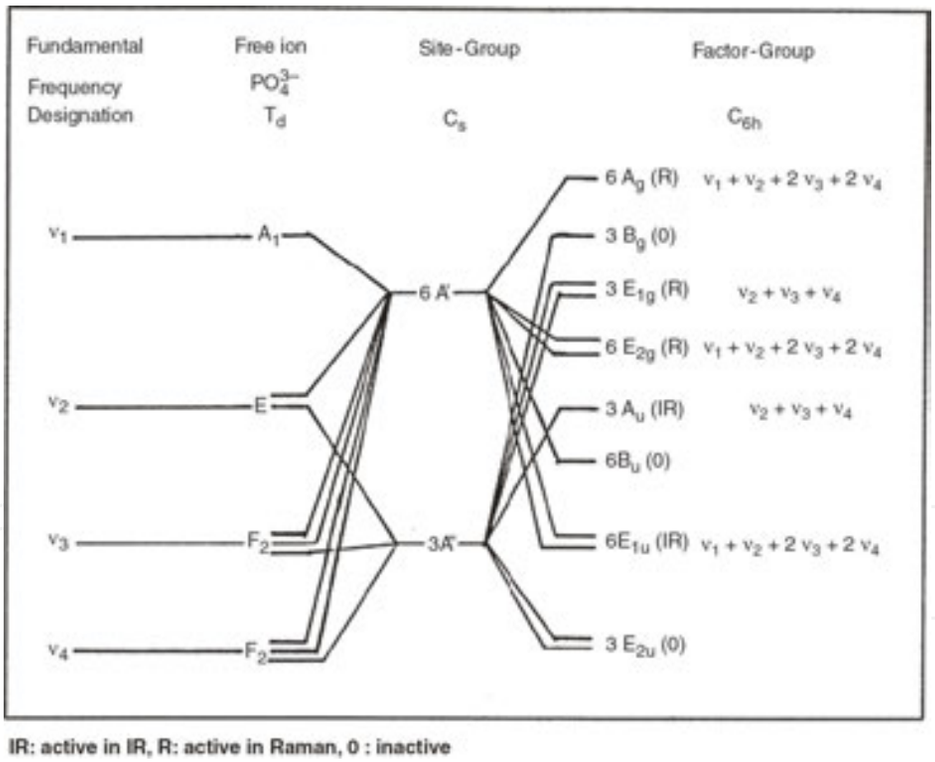

Fig. 32. The correlation chart for PO_4^{3-} fundamental modes under free-ion, site-group and factor group analyses in $Pb_8M_2(PO_4)_6$ where M = Ag and Na [200].

All $[PO_4]^{3-}$ groups are crystallographically equivalent in the cell and have C_s as the site group. P, O(1) and O(2) atoms are in 6*h* positions; remaining O(3) oxygen atoms occupy the (121) positions. On this basis, the optical modes at k = 0 are distributed as follows [200]:

$$\Gamma_{opt} = 12\ A_g + 8\ E_{1g} + 13\ E_{2g} + 8\ A_u + 12\ E_{1u} \tag{53}$$

where A_g, E_{1g} and E_{2g} are Raman-active normal modes, A_u and E_{1u} normal modes are infrared active. The internal modes from tetrahedral phosphate ions, six per unit cell, can be deduced by the group factor analysis given in **Fig. 32**.

Naddari et al [202] performed the solid-state synthesis of colorless calcium-lithium lead apatite ($Pb_6Li_2Ca_2(PO_4)_6$, LCPbAp, $P6_3/M$, $a = 9.679$ and $c = 7.113$ Å, $V = 577.09$ Å^3, $Z = 1$ and $\rho_{calc.} = 5.48$ g·cm^{-3}) via the thermal treatment of mixture of Li_2CO_3, $(NH_4)_2HPO_4$, $CaCO_3$ and PbO at 800°C in air for 12 h and subsequently at 900°C for 12 hours. The structure of $Pb_6Li_2Ca_2(PO_4)_6$ is shown in the perspective view in **Fig. 33**(**a**). Site (I) is occupied by 0.88 Ca^{2+}, 1.96 Li^+ and 1.148 Pb^{2+}. These cations are coordinated to nine oxide anions forming a tricapped trigonal prism. In the tunnel set around the *c* axis, site (II) is occupied by 4.98 Pb^{2+} and 1.02 Ca^{2+}. These cations constitute the walls of the tunnel and are arranged in equilateral triangles (**Fig. 33**(**b**)).

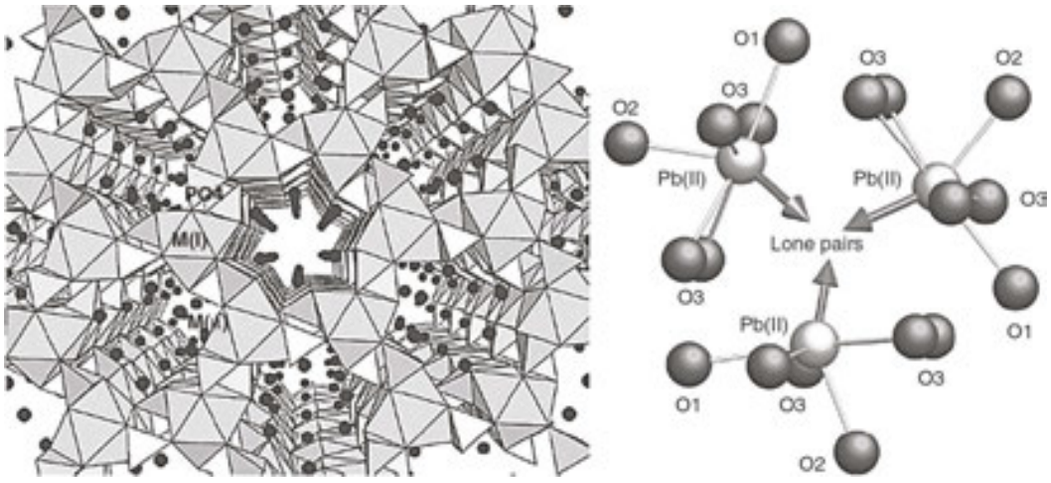

Fig. 33. Perspective view of $Pb_6Ca_2Li_2(PO_4)_6$ structure (a) and Pb(II)-Pb(II) stacking in $Pb_6Ca_2Li_2(PO_4)_6$ showing possible arrangement of electron lone pairs [202].

Lithium ions occupy preferentially site (I) and this structure is anionic lacunary apatite stabilized by the interaction of Pb(II) electron lone pair. The electrical conductivity as a function of temperature can be interpreted assuming a hopping mechanism of Li ions in the tunnels [202].

Tricationic lacunar apatites $Na_{1-x}K_xPb_4(AsO_4)_3$ ($0 \le x \le 1$) were synthesized as single phases by solid-state method at 700°C (48 h) by Manoun et al [198]:

$$\begin{aligned} &4\ PbO + 0.5x\ K_2CO_3 + 0.5(1-x)\ Na_2CO_3 + 3\ (NH_4)_2\ HAsO_4 \rightarrow \\ &Na_{1-x}K_xPb_4(AsO_4)_3 + 0.5\ CO_2 + 1.5\ H_2O + 3\ NH_3 \end{aligned} \tag{54}$$

It was found that Pb(II) ions in the solid solutions preferentially occupied the M(1) and M(2) sites in the lacunar anionic apatite structure. The structure contains the channels running along the *c*-axis and centered at (00z). The channels are most probably occupied by lone electron pairs of Pb^{2+} cations.

The factor group analysis [198] of the hexagonal structure ($P6_3/M$) shows that the normal modes of vibration can be classified among the irreducible representations of C_{6h} as follows:

$$\Gamma = 12A_g + 8E_{1g} + 13E_{2g} + 9A_u + 12B_u + 9B_g + 13E_{1u} + 8E_{2u} \tag{55}$$

where the internal mode contribution of (AsO_4) groups to the IR- and Raman-active vibrations is:

$$\begin{aligned}\Gamma_{AsO_4} &= 6Ag\left(\nu_1+\nu_2+2\nu_3+2\nu_4\right)+3E_{1g}\left(\nu_2+\nu_3+\nu_4\right)+\\ &6E_{2g}\left(\nu_1+\nu_2+2\nu_3+2\nu_4\right)+3A_u\left(\nu_2+\nu_3+\nu_4\right)+\\ &6E_{1u}\left(\nu_1+\nu_2+2\nu_3+2\nu_4\right)\end{aligned} \tag{56}$$

where *g* and *u* modes are Raman-and IR-active, respectively [198],[203],[204].

The syntheses of apatites, $Na_{1-x}K_xCaPb_3(PO_4)_3$ ($0 \le x \le 1$), with anion vacancy were carried out using the solid-state reactions at 700°C for 48 h [199]:

$$\begin{aligned}&\frac{1-x}{2}\ Na_2CO_3+\frac{x}{2}K_2CO_3+3\ PbO+Ca\left(NO_3\right)_2\cdot 4H_2O+\\ &3\ \left(NH_4\right)H_2PO_4\rightarrow Na_{1-x}K_xCaPb_3\left(PO_4\right)_3+0.5\ CO_2+\\ &3\ NH_3+NO_2+NO_3+8.5\ H_2O\end{aligned} \tag{57}$$

The lattice constants of the solid solutions varied linearly with x. It was found that Pb ions in the solid solutions occupied M(1) and M(2) sites in the lacunar apatite structure. The structure was described as built up from $[PO_4]^{3-}$ tetrahedra and Pb^{2+} of six-fold coordination cavities (*6h* positions), which delimit void hexagonal tunnels running along [001]. The tunnels are connected by cations of mixed sites (*4f*) half occupied by Pb^{2+} and half by Na^+/K^+ mixed alkali cations.

The factor group analysis of the hexagonal structure ($P6_3/M$) shows that the normal modes of vibration can be classified among the irreducible representations of C_{6h} by **Eq. 56** where the internal mode contribution of (PO_4) groups to the IR and Raman-active vibrations is [199]:

$$\begin{aligned}\Gamma_{PO_4} &= 6A_g\left(\nu_1+\nu_2+2\nu_3+2\nu_4\right)+3E_{1g}\left(\nu_2+\nu_3+\nu_4\right)\\ &+6E_{2g}\left(\nu_1+\nu_2+2\nu_3+2\nu_4\right)+3A_u\left(\nu_2+\nu_3+\nu_4\right)\\ &+6E_{1u}\left(\nu_1+\nu_2+2\nu_3+2\nu_4\right)\end{aligned} \quad (58)$$

4.10 Synthetic analogues of other minerals from the supergroup of apatite

These minerals were usually prepared in order to elucidate the structure of naturally occurring minerals or due to its potential applications in immobilization of nuclear and toxic waste (**Chapter 6**) and electrical properties (ionic conductivity). Synthetic analogues of ellestadite and britholite weren't included because they are described in **Chapter 5** and **6**, respectively. Rare earth apatites are described separately in next **Chapter 5**.

4.10.1 Cesanite

Synthetic cesanite as an analogue of mineral with the composition $Na_3Ca_2(SO_4)_3(OH)$ (**Section 2.1.7**) shows typical features of the apatite structure, as shown in **Fig. 34**. The symmetry reduction from the centrosymmetric space group $P6_3/M$ to the non-centrosymmetric space group $P\bar{6}$leads to a doubling of the number of crystallographically independent sites. The origin of the unit cell is shifted by Z + ¼ relating to the origin in the space group $P6_3/M$. Alternating pairs of isolated tetrahedral anions (the sulfate-groups) form ribbons running parallel to the ***c***-axis. As the sulfur atoms are located in special Wyckoff positions 3*j* and 3*k*, the tetrahedra have the point group symmetry *m* [205].

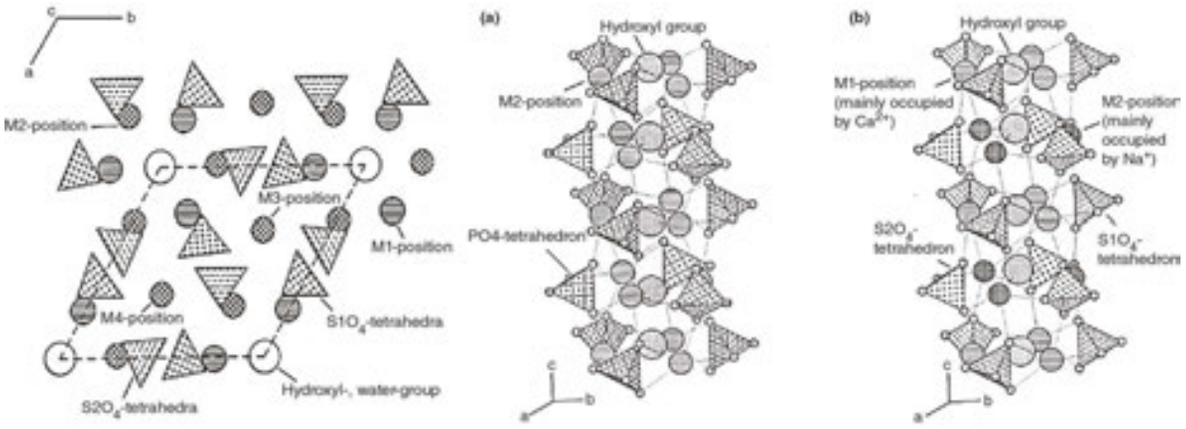

Fig. 34. The projection of the crystal structure of synthetic cesanite parallel to (001) (1) and the arrangement of cations and sulfate tetrahedra around the 6_3 and the 6◎ axes, respectively (2): phosphate apatite (a) and synthetic cesanite (b) [205].

Small spread in the S-O distances and O-S-O angles indicates only minor deviations from ideal tetrahedral symmetry. The sub-structure of the array of sulfate tetrahedra shows a distinct

pseudo-symmetry, closely mimicking $P6_3/M$. Maximal deviations from this symmetry occur at O(4) atom, which is shifted by 0.16 Å (synthetic) and 0.02 (natural) from its position in $P6_3/M$. Na and Ca cations are distributed either by six O atoms and one hydroxyl ion or water molecule (M(1) and M(2)) or by nine O atoms (M(3) and M(4) [205].

Synthetic analogues of minerals cesanite Halide sulfates have general formula [206]:

$$M_3^{+}M_2^{2+}\left(SO_4\right)_3 Z \tag{59}$$

where Z = OH, F and Cl. KLEMENT [207] synthesized sodium-calcium sulfatapatite, $Na_6Ca_4(SO_4)_6F_2$, by full substitution of S^{6+} for P^{5+} through the substitution scheme [208]:

$$S^{6+} + M^{+}\left(\text{e.g.,Na}\right) \Leftrightarrow P^{5+} + Ca^{2+} \tag{60}$$

where the hydroxyl equivalent is the equivalent to mineral cesanite, $Na_6Ca_4(SO_4)_6(OH)_2$. KREIDLER and HUMMEL [209] also synthesized $Na_6Ca_4(SO_4)_6F_2$ and $Na_6Pb_4(SO_4)_6F_2$ apatite-like phases. KNYAZEV et al [206] prepared the compounds of the composition of $Na_3Ca_2(SO_4)_3F$, $Na_3Cd_2(SO_4)_3Cl$, and $Na_3Pb_2(SO_4)_3Cl$ with the structure of apatite via the solid-state reactions:

$$Na_2SO_4 + 2\ CaSO_4 + NaF \rightarrow Na_3Ca_2\left(SO_4\right)_3 F \tag{61}$$

$$Na_2SO_4 + 2\ CdSO_4 + NaCl \rightarrow Na_3Cd_2\left(SO_4\right)_3 Cl \tag{62}$$

$$Na_2SO_4 + 2\ PbSO_4 + NaCl \rightarrow Na_3Pb_2\left(SO_4\right)_3 Cl \tag{63}$$

from the stoichiometric reaction mixture in a porcelain crucible. The mixtures of components were calcined in several steps at the temperatures of 570, 770 and 1020 K for 10 h, with intermediate grindings in agate mortar every 2 h [206].

The $Na_3Ca_2(SO_4)_3F:Ce^{3+}$ phosphor was prepared by NIKHARE et al [210] via the solid-state method according to the following reaction:

$$\begin{aligned} &2\ NaNO_3 + CaNO_3 + NaF + 3\ \left(NH_4\right)_2 SO_4 + Ce\left(NO_3\right)_3 \rightarrow \\ &Na_3Ca_2\left(SO_4\right)_3 F:Ce + 4\ NO + 8\ H_2O \end{aligned} \tag{64}$$

The pigment shows a single high intensity emission peak at 307 nm when excited by UV light of the wavelength of 278 nm

The compound having the formula: $K_3Ca_2(SO_4)_3F$, was identified in coatings of heat recovery cyclones of Portland clinker kiln. The structure of this phase (noncentrosymmetric, space group P_N2_1A, a = 13.415, b = 10.943 and c = 9.127 Å, $\boldsymbol{V}$ = 1284.75 Å^3, $\boldsymbol{Z}$ = 4 and $\boldsymbol{\rho}$ = 2.61 g·cm^{-3}) was reported as very distorted analogue of apatite where fluoride atoms are oriented along the pseudo-screw a-axis [211],[212].

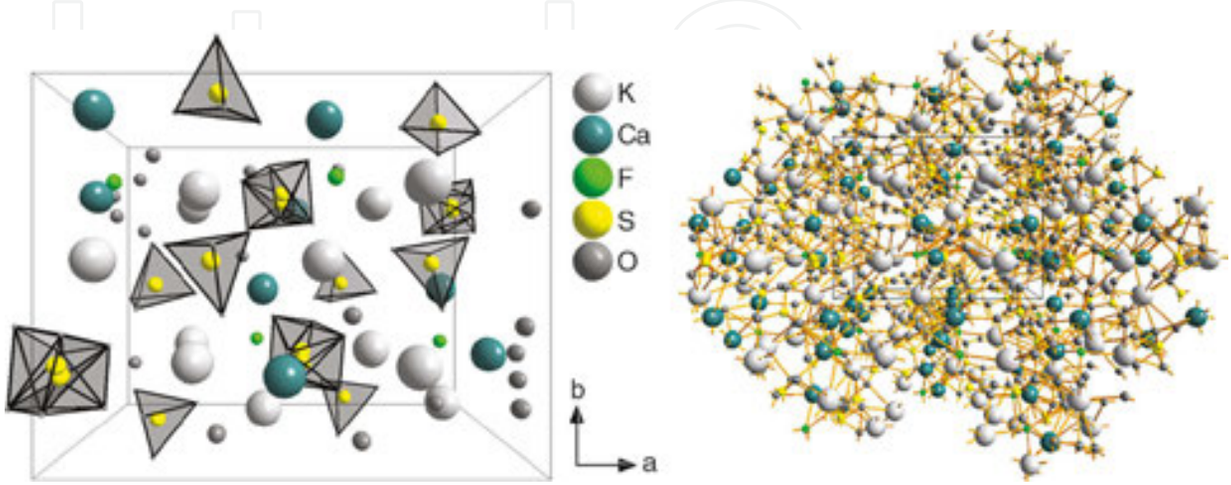

Fig. 35. The structure of $K_3Ca_2(SO_4)_3F$ according to Fayos et al [212] phase in the perspective view along the c-axis.

The activation by Eu or Ce leads to the phosphor: $K_3Ca_2(SO_4)_3F$:Ce, Eu, which was prepared by Poddar et al [213] via the precipitation method. The $K_3Ca_2(SO_4)_3F$:Ce luminescent pigment shows the emission at 334 nm when excited at 278 nm due to the $5d \rightarrow 4f$ transition of Ce^{3+} ions. The phases $K_3Ca_2(SO_4)_3F:Eu^{2+}$ and $K_3Ca_2(SO_4)_3F:Eu^{3+}$ show the emissions at 440 nm, and 596 and 615 nm via the transitions of $^5D_0 \rightarrow {}^7F_1$ and $^5D_0 \rightarrow {}^7F_2$ of Eu^{3+} ion, which are in blue and red region of the visible spectrum, respectively.

4.10.2 Bismuth calcium oxyapatites

The synthesis, the characterization and ionic conductivity of $Ca_{8-x}Sr_xBi_2(PO_4)_6O_2$ phase where x = 3, 4 and 5 was reported by Trabelsi et al [214]. Sr^{2+} ions were noted to occupy two sites (4f) and (6h), with a strong preference for (6h) sites. Heavy Bi^{3+} atoms preferentially occupied the (6h) site.

New bismuth calcium silicon oxide $Ca_4Bi_{4.3}(SiO_4)(HSiO_4)_5O_{0.95}$, with the apatite structure was synthesized by Uvarov et al [215]. The structure was refined from the powder X-ray diffraction data. The refinement revealed that the phase had the $P6_3/M$ space group with the unit cell parameters a = 9.6090 Å, c = 7.0521 Å, V = 563.9 Å^3 and c:a = 0.734.

Also the structure of bismuth calcium vanadium oxide ($BiCa_4V_3O_{13}$, $BiCa_4(VO_4)_3O$) was reported by Huang and Sleight [216] as apatite without an inversion center. The phase crystallizes in hexagonal system with the space group $P6_3$, a = 9.819 Å, b = 7.033 Å, $\boldsymbol{V}$ = 587.2 Å^3 and $\boldsymbol{Z}$ = 2. Calculated density is 4.129 g·cm^{-3}. Lower symmetry of the structure may be related to the site selective distribution of Bi atoms at the Ca sites.

http://dx.doi.org/10.5772/62212

4.10.3 Incorporation of 3d-metal ions to the hexagonal channel of apatite

The hexagonal channel in the structure of apatite can accommodate infinite linear chains of $[\text{-Me-O-}]_n^{n-}$, where Me = Cu, Zn, Ni, Co… (**Fig. 36**). The incorporation of *3d*-metal ions in the hexagonal channels of strontium phosphate apatite ($Sr_5(PO_4)_3OH$) was investigated by KAZIN et al [217].

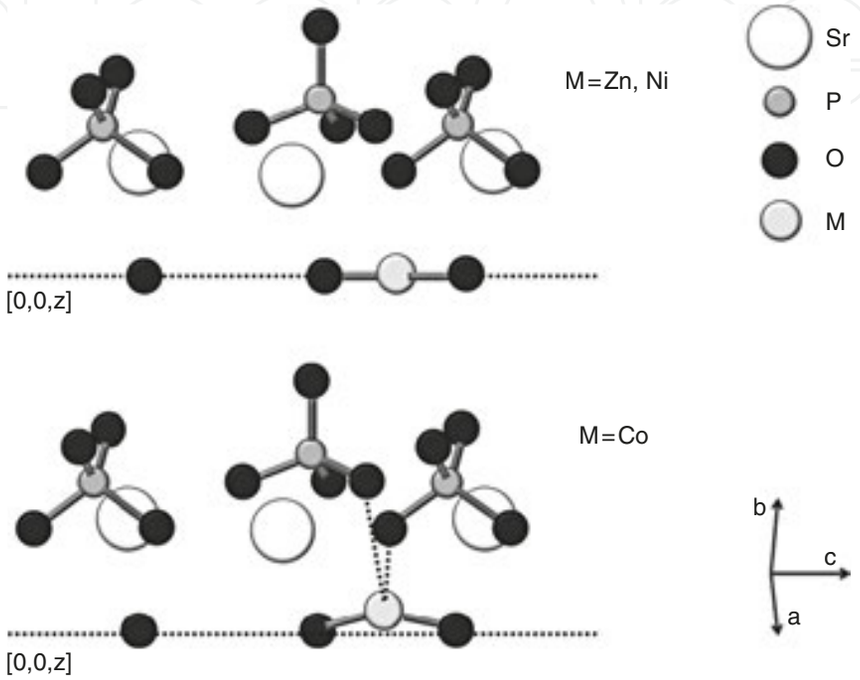

Fig. 36. Crystal structure fragments of doped apatite showing the atomic arrangement at the hexagonal channel where 3-d metal atoms are located [217].

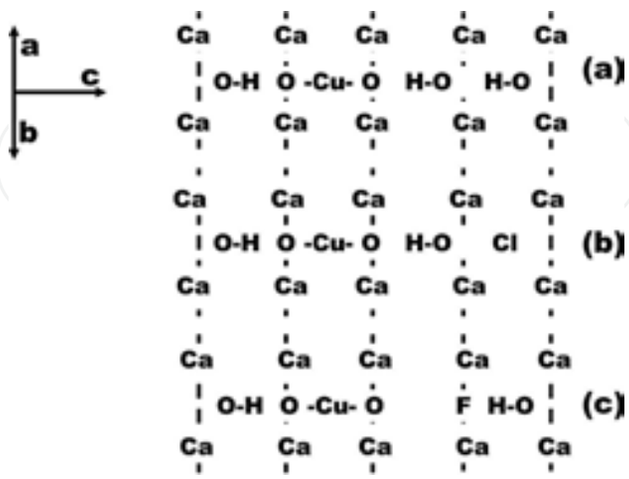

Fig. 37. Depiction of the structure in hexagonal channels (along the c-axis) in the lattice of copper-containing apatite: hydroxylapatite (a), hydroxylapatite with OH partially replaced by Cl and hydroxylapatite with OH partially replaced by F (c). The planes passing through Ca atoms depict the channel walls.

Doping of $Sr_5(PO_4)_3OH$ with ZnO, NiO and CoO at 1400°C in air resulted in the incorporation of 3d-ions entering the hexagonal channels of the apatite structure, formally substituting for protons in the OH groups. The structure of apatite channels in the phases with the composition of $Sr_5(PO_4)_3Zn_{0.15}O_{0.3}(OH)_{0.7}$ (white and shade of green), $Sr_5(PO_4)_3Ni_{0.2}\ O_{0.4}(OH)_{0.6}$ (green) and $Sr_5(PO_4)_3Co_{0.2}O_{0.5}(OH)_{0.4}$ (dark-violet) contains O-Me-O fragments separated by OH groups. Co atoms were localized in the position shifted by 0.5 Å from the center of channel. Their coordination can be described as distorted from linear O-Co-O probably by additional coordination to phosphate oxygen atoms [217].

In other work of Kazim et al [218], the synthesis and the properties of three compounds possessing the apatite structure with the composition of $Ca_5(PO_4)_3Cu_yO_{y+\delta}(OH)_{0.5-y-d}X_{0.5}$, where the parameter y = 0.01 - 0.3 for X = OH, y = 0.01 − 0.1 for X = F and y = 0.1 for X = Cl. Similar copper containing vanadates $Sr_5(VO_4)_3CuO$ are formed as co-products in the synthesis of vanadium doped superconductors [218],[219].

Author details

Petr Ptáček

Brno University of Technology, Czech Republic

References

[1] Daubrée A. Experiences sur la production artficielle de l'apatite, de la topaze, at de quelques autres métax fruorifés. Comptes rendus de l'Académie des Sciences 1851;32 625.

[2] Manross NS. Justus Liebig's Annalen der Chemie 1852;82 358.

[3] Briegleb H. Ueber die Einwirkung des phosphorsauren Natrons auf Flussspath in der Glühhitze. Justus Liebig's Annalen der Chemie 1856;97(1) 95–119.

[4] Forchhammer JG. Ann. d. Chem. u. Pharm. 1854;90 77.

[5] Deville HS-Claire, Caron H. Comptes Rendus 1858;17 985.

[6] Ditte A. Comptes Rendus 1882;94 1592.

[7] Clarke FW. The Data of Geochemistry. Bulletin (Geological Survey (U.S.)), U.S. Government Printing Office, 1920.

[8] Zambonini F. Quelques observations sur la composition des apatites. Acad. Sci. Paris Comptes Rendus 1916;162 919–921.

[9] Debray H. Comptes rendus 1861;52 44.

[10] Weinshenk E. Zeitschrift für Krystallographie und Mineralogie 1890;17 489.

[11] Cameron FK, McCaughey WJ. Jour. Phys. Chem. 1911;15 464–470.

[12] Hickok RL. Synthesis of calcium chlorspodiosite. United States Patent Office 3,378,354 Patented Apr. 16, 1968.

[13] Klement R, Gembruch F. Versuche über Isomorphie in der Wagneritgruppe. Naturwissenschaften 1941;29: 301–302.

[14] Mineralogical chemistry. Journal of the Chemical Society, Abstracts 1911;100 ii733-ii737. DOI: 10.1039/CA9110005733

[15] Hutchins WM. Occurrence of Apatite in Slag. Nature 1887;36 460.

[16] Voght JHL. Beiträge zur Kenntniss der Gesetze der Mineralbildung in Schmelzmassen und in den Neovulkanischen Ergussgesteinen. Kristiania, Alb. Cammermeyer´s verlag, Oslo 1852.

[17] Zambonini F. Uber die Mischristalle, welche die Verbindungen des Calciums, Strontiums, Bariums, und Bleis mit jenen der seltenen Erden bilden. Zeitschr. Kristallographie Band 1923;28 226–292.

[18] Jaffe EB. Abstract of the literature on synthesis of apatites and some related phosphates. Geological survey circular 135, 1951.

[19] Hendricks S, Jefferson ME, Mosely VM. The crystal structure of some natural and synthetic apatite-like substances. Zeitschr. Kristallographie 1932;81 352–369.

[20] Eitel W. Uber Karbonatphosphate der Apatitgruppe: Sehr. Königsberger Gelehrter Gesell. Naturwiss. 1924;4 159–177.

[21] Byrappa K, Yoshimura M. Handbook of Hydrothermal Technology. Materials Science and Process Technology. 2nd ed., William Andrew, 2012. ISBN: 978-1437778366

[22] Katashev A, Dekhtyar Y, Spigulis J. 14th Nordic-Baltic Conference on Biomedical Engineering and Medical Physics: NBC 2008. 16–20 June 2008. Riga, Latvia. IFMBE Proceedings-Volume 20. Springer Science & Business Media, 2008. ISBN: 978-3540693673

[23] West AR. Solid State Chemistry and its Applications. 2nd ed., John Wiley & Sons, 2014. ISBN: 978-1118676257

[24] Smart LE, Moore EA. Solid State Chemistry: An Introduction, Fourth Edition. CRC Press, 2012. ISBN: 978-1439847923

[25] Avvakumov GV, Senna M, Kosova NV. Soft Mechanochemical Synthesis: A Basis for New Chemical Technologies. Springer Science & Business Media, 2007. ISBN: 978-0306476464

[26] Dann SE. Reactions and Characterization of Solids. Tutorial chemistry texts - Volume 2. Royal Society of Chemistry, 2000. ISBN: 978-0854046126

[27] Mehrer H. Diffusion in Solids: Fundamentals, Methods, Materials, Diffusion-Controlled Processes. Springer Series in Solid-State Sciences - Volume 155. Springer Science & Business Media, 2007. ISBN: 978-3540714880

[28] Manickam S, Ashokkumar M. Cavitation: A Novel Energy-Efficient Technique for the Generation of Nanomaterials. CRC Press, 2014. ISBN: 978-9814411554

[29] van der Put PJ. The Inorganic Chemistry of Materials: How to Make Things Out of Elements. Plenum Series in Social/Clinical. Springer Science & Business Media., 1998. ISBN: 978-0306457319

[30] Rahaman MN. Ceramic Processing and Sintering. Materials Engineering. 2nd ed., CRC Press, 2003. ISBN: 978-0824709884

[31] Stojanovic BD, Skorokhod VV, Nikolic M. Advanced Science and Technology of Sintering. Springer Science & Business Media, 2011. ISBN: 978-1441986665

[32] Sadat-Shojai M, Mohammad-T Khorasani, Dinpanah-Khoshdargi E, Jamshidi A. Synthesis methods for nanosized hydroxyapatite with diverse structures. Acta Biomaterialia 2013;9() 7591–7621.(8)

[33] De Sénarmont HH. Sur la formation des mineraux par voie humide dans le gits metallifered concrectionnes. Annales de chimie et de physique 1851;32(3) 129–175.

[34] Acton QA. Magnesium Compounds - Advances in Research and Application: 2013 Edition. Scholarly Editions, 2013. ISBN: 978-1481677417

[35] Somiya S, Aldinger F, Spriggs RM, Uchino K, Koumoto K, Kaneno M. Handbook of Advanced Ceramics: Materials, Applications, Processing and Properties, Volume 2. Academic Press, 2003. ISBN: 978-0080532943

[36] Chattopadhyay R. Advanced Thermally Assisted Surface Engineering Processes. Springer Science & Business Media, 2004. ISBN: 978-1402076961

[37] Koizumi M, Nishihara M Isostatic Pressing: Technology and Applications. Elsevier applied science. Springer Science & Business Media. , 1991. ISBN: 978-1851665969

[38] Batsanov SS. Effects of Explosions on Materials: Modification and Synthesis Under High-Pressure Shock Compression High pressure shock compression of condensed matter. Shock Wave and High Pressure Phenomena. Springer Science & Business Media. , 1994. ISBN: 978-0387941233

[39] Ostwald W. Handbuch der allgemeinen Chemie, Band I, Academische Verlagsgesellschaft, Leipzig 1919.

[40] Block B. Verbesserungen an der Kolloidmühle, Chemische Apparatur 14, Heft 13 und 14, 1927.

[41] Balaz P. Mechanochemistry in Nanoscience and Minerals Engineering. Springer Science & Business Media, 2008. ISBN: 978-3540748557

[42] Bowden FP, Tabor D. The Friction and Lubrication of Solids, Volume 1. Oxford classic texts in the physical sciences. The international series of monographs on physics - Volume 9. Clarendon Press, 2001. ISBN: 978-0198507772

[43] Lea MC. Disruption of silver halides by mechanical force. The Journal of American Science 1892;43 527–531.

[44] Westbrook JH, Fleischer RL. Intermetallic Compounds, Crystal Structures of Intermetallic Compounds - Volume 1. Wiley, 2000a. ISBN: 978-0471608806

[45] Westbrook JH, Fleischer RL. Intermetallic Compounds, Basic Mechanical Properties and Lattice Defects of Intermetallic Compounds - Volume 2. Wiley, 2000b. ISBN: 978-0471611752

[46] Stoloff NS, Sikka VK. Physical Metallurgy and processing of Intermetallic Compounds. Springer Science & Business Media , 2012. ISBN: 978-1461312154

[47] Plauson H. Colloidal mill. Patent US2225797 A, 1940.

[48] Kelly WJ. Plauson Colloid Mill. Industrial and Engineering Chemistry 1923;15(9) 926–928.

[49] Parker LH. Reactions by trituration. Journal of the Chemical Society, Transactions 1914;105 1504–1516

[50] Sakka S. Handbook of Sol-gel Science and Technology. 1. Sol-gel processing. Springer Science & Business Media, 2005. ISBN: 978-1402079696

[51] Aegerter MA, Leventis N, Koebel MM. Aerogels Handbook Advances in Sol-Gel Derived Materials and Technologies. Springer Science & Business Media. , 2011. ISBN: 978-1441975898

[52] Brinker CJ, Scherer GW. Sol-Gel Science: The Physics and Chemistry of Sol-Gel Processing. Academic Press, 2013. ISBN: 978-0080571034

[53] Ring TA. Fundamentals of Ceramic Powder Processing and Synthesis. Academic Press, 1996. ISBN: 978-0080532196

[54] Youssef HA, El-Hofy HA. Ahmed MH. Manufacturing Technology: Materials, Processes, and Equipment. CRC Press, 2011. ISBN: 978-1439810859

[55] Xu R, Pang W, Huo Q. Modern Inorganic Synthetic Chemistry. Elsevier, 2011. ISBN: 978-0444535993

[56] Association Management, Resources Information. Nanotechnology: Concepts, Methodologies, Tools, and Applications: Concepts, Methodologies, Tools, and Applications. IGI Global, 2014. ISBN: 978-1466651265

[57] Schubert U, Hüsing N. Synthesis of Inorganic Materials. John Wiley & Sons, 2012. ISBN: 978-3527327140

[58] Tavadze GF, Shteinberg A. Production of Advanced Materials by Methods of Self-Propagating High-Temperature Synthesis. Springer Science & Business Media, 2013. ISBN: 978-3642352058

[59] Borisov AA, De Luca LT, Merzhanov AG. Self-Propagating High-Temperature Synthesis of Materials. Combustion science and technology book series - Volume 5. CRC Press, 2002. ISBN: 978-1560329787

[60] U.S.S.R. Inventor's Certificate 225 221 (1967).

[61] Merzhanov AG, Borovinskaya IP. elf-propagated high-temperature synthesis of refractory inorganic compounds. Doklady Akademii Nauk SSSR 1972;204(2) 366–369.

[62] Rao CNR, Thomas PJ, Kulkarni GU. Nanocrystals: Synthesis, Properties and Applications. Springer Series in Materials Science - Volume 95. Springer Science & Business Media, 2007. ISBN: 978-3540687528

[63] Schneller T, Waser R, Kosec M, Payne D. Chemical Solution Deposition of Functional Oxide Thin Films. Springer Science & Business Media, 2014. ISBN: 978-3211993118

[64] Lee B, Komarneni S. Chemical Processing of Ceramics, 2nd ed., CRC Press, 2005. ISBN: 978-1420027334

[65] Knyazev AV, Chernorukov NG, Bulanov EN. Apatite-structured compounds: Synthesis and high-temperature investigation. Materials Chemistry and Physics 2012 132(2–3) 773–781.

[66] Chernorukov NG, Knyazev AV, Bulanov EN. Phase transitions and thermal expansion of apatite-structured compounds. Inorganic Materials 2011;47(2) 172–177.

[67] Frank-Kamenetskaya O, Kol'tsov A, Kuz'mina M, Zorina M, Poritskaya L. Ion substitutions and non-stoichiometry of carbonated apatite-(CaOH) synthesised by precipitation and hydrothermal methods. Journal of Molecular Structure 2011;992(1–3) 9–18.

[68] Drouet Ch. A comprehensive guide to experimental and predicted thermodynamic properties of phosphate apatite minerals in view of applicative purposes. The Journal of Chemical Thermodynamics 2015;81 143–159.

[69] Derek EC. Chemistry, Biochemistry and Technology, Sixth Edition. CRC Press, 2013. ISBN: 978-1439840887

[70] Van Wazer JR. Phosphorus and its Compounds, Volume 1. Wiley-Interscience, New York, 1985.

[71] Brown PW, Hocker N, Hoyle S. Variations in Solution Chemistry During the Low-Temperature Formation of Hydroxyapatite. Journal of the American Ceramic Society 1991;74(8) 1848–1854.

[72] Brown PW. Phase Relationships in the Ternary System CaO-P_2O_5-H_2O at 25°C. Journal of the American Ceramic Society 1992;75(1) 17–22.

[73] Biggar GM. Experimental Studies of Apatite Crystallization in Parts of the System CaO-P_2O_5-H_2O at 1000 Bars Mineralogical Magazine 1966;35 1110–1115.

[74] Feng SS, Rockett TJ. The System CaO-P_2O_5-H_2O at 200°C. Journal of the American Ceramic Society 1976;62 619–620.

[75] Lantelme F, Groult H. Molten Salts Chemistry: From Lab to Applications. Newnes, 2013. ISBN: 978-0124017221

[76] Bengisu M. Engineering Ceramics. Engineering Materials Springer Science & Business Media, 2013. ISBN: 978-3662043509

[77] Morey GW, Niggli P. The Hydrothermal Formation of Silicates, A Review. Journal of the American Ceramic Society 1913;35 1086–1130.

[78] Rabenau A. The Role of Hydrothermal Synthesis in Preparative Chemistry. Angewandte Chemie International Edition in English 1985;24 1026–1040.

[79] Roy R. Acceleration the Kinetics of Low-Temperature Inorganic Syntheses. Journal of Solid State Chemistry 1994;111(1) 11–17.

[80] Baumer A, Argiolas R. Hydrothermal synthesis and characterization by X-ray of chlor, fluor or hydroxyapatite crystals. Neues Jahrbuch Fur Mineralogie-Monatshefte 1981a; 8 344–348.

[81] Jahnke RA. The synthesis and solubility of carbonate fluorapatite. American Journal of Science 1984;284 58–78.

[82] Deer WA. Rock-forming minerals: Non-silicates, volume 5B, second edition. Geological Society of London, 1998. ISBN: 978-1897799901

[83] Zhang H, Darvell BW. Synthesis and characterization of hydroxyapatite whiskers by hydrothermal homogeneous precipitation using acetamide. Acta Biomaterialia 2010;6(8) 3216–3222.

[84] Lin K, Chang J, Cheng R, Ruan M. Hydrothermal microemulsion synthesis of stoichiometric single crystal hydroxyapatite nanorods with mono-dispersion and narrow-size distribution. Materials Letters 2007;61(8–9) 1683–1687.

[85] Leal-Calderon F, Schmitt V, Bibette J. Emulsion Science: Basic Principles. Springer Science & Business Media, 2007. ISBN: 978-0387396835

[86] Rosen MJ, Kunjappu JT. Surfactants and Interfacial Phenomena. 4nd ed., John Wiley & Sons, 2012. ISBN: 978-1118229026

[87] Duffar T. Crystal Growth Processes Based on Capillarity: Czochralski, Floating Zone, Shaping and Crucible Techniques, John Wiley & Sons, 2010. ISBN: 978-1444320213

[88] Capper P. Bulk Crystal Growth of Electronic, Optical and Optoelectronic Materials. Wiley Series in Materials for Electronic & Optoelectronic Applications - Volume 14. John Wiley & Sons, 2005. ISBN: 978-0470012079

[89] Fukuda T, Rudolph P, Uda S. Fiber Crystal Growth from the Melt. Advances in Materials Research - Volume 6. Springer Science & Business Media, 2013. ISBN: 978-3662072141

[90] Verneuil A. Production artificielle du rubis par fusion. Comptes Rendus (Paris) 1902;135 791–794.

[91] Verneuil A. Mémoire sur la reproduction artificielle du rubis par fusion. Annales de chimie et de physique 1904;8(3) 20–48.

[92] Verneuil A. Comptes Rendus (Paris) 1910;151 131–132.

[93] Dobrovinskaya ER, Lytvynov LA, Pishchik V. Sapphire: Material, Manufacturing, Applications. Springer Science & Business Media, 2009. ISBN: 978-0387856957

[94] Czochralski J. Ein neues Verfahren zur Messung der Kristallisationsgeschwindigkeit der Metalle. Zeitschrift für Physikalische Chemie 1918;92 219–221.

[95] von Gomperz EV. Untersuchungen an Einkristalldrähten. Zeitschrift für Physikalische Chemie 1922;8 184–190.

[96] Kyropoulos S. Ein Verfahren zur Herstellung grosser Kristalle. Zeitschrift fur Anorganische und Allgemeine Chemie 1926;154 308–311.

[97] Kyropoulos S. Dielektrizitätskonstanten regulärer Kristalle. Zeitschrift fur Physik 1930;63 849–854.

[98] Morgenstern H.. Wachstumsbeobachtungen an Alkalihalogenidkristallen. Zeitschrift für Kristallographie 1938;100 221–227.

[99] Feigelson R. 50 Years Progress in Crystal Growth: A Reprint Collection. Elsevier, 2004. ISBN: 978-0080489933

[100] Bridgman PW. Proceedings of the American Academy of Arts and Sciences 1925;60 305–385.

[101] Pfann WG. Principles of Zone-Melting. Transactions of the Metallurgical Society of AIME 1952;154 747–753.

[102] Higuchi M, Katase H, Kodaira K, Nakayama S. Float zone growth and characterization of $Pr_{9.33}(SiO_4)_6O_2$ and $Sm_{9.33}(SiO_4)_6O_2$ single crystals with an apatite structure. Journal of Crystal Growth 2000;218(2–4) 282–286.

[103] Dietze W, Doering E, Glasow P, Langheinrich W, Schulz M, Ludsteck A, Mader H, Mühlbauer A, Weiss H, v. Münch W, Runge H, Schleicher L, Schnöller M, Sirtl E, Uden E, Zulehner W. Technology of Si, Ge, and SiC / Technologie Von Si, Ge und SiC. Landolt-Bornstein: New series. Numerical Data and Functional Relationshi - Volume 17, Part 3. Springer Science & Business Media, 1983. ISBN: 978-3540114741

[104] Rogers D. Einstein's Other Theory: The Planck-Bose-Einstein Theory of Heat Capacity. Princeton University Press, 2005. ISBN: 978-0691118260

[105] Bhat HL. Introduction to Crystal Growth: Principles and Practice. CRC Press, 2014. ISBN: 978-1439883334

[106] Jokić B, Mitrić M, Radmilović V, Drmanić S, Petrović R, Janaćković D. Synthesis and characterization of monetite and hydroxyapatite whiskers obtained by a hydrothermal method. Ceramics International 2011;37(1) 167–173.

[107] Ioku K, Yamauchi S, Fujimori H, Goto S, Yoshimura M. Hydrothermal preparation of fibrous apatite and apatite sheet. Solid State Ionics 2002;151(1–4) 147–150.

[108] Suchanek W, Yashima M, Kakihana M, Yoshimura M. Processing and mechanical properties of hydroxyapatite reinforced with hydroxyapatite whiskers. Biomaterials 1996;17(17) 1715–1723.

[109] Tas AC. Molten Salt Synthesis of Calcium Hydroxyapatite Whiskers. Journal of the American Ceramic Society 2001;84(2) 295–300

[110] Aizawa M, Ueno H, Itatani K, Okada I. Syntheses of calcium-deficient apatite fibres by a homogeneous precipitation method and their characterizations. Journal of the European Ceramic Society 2006;26(4–5) 501–507.

[111] Shyu JJ, Wu JM. Growth kinetics of spherulitic apatite in some MgO-CaO-SiO_2-P_2O_5 glasses. Journal of Materials Science 1994;29(12) 3167–3171.

[112] Stanton KT, O'Flynn KP, Kiernan S, Menuge J, Hill R. Spherulitic crystallization of apatite–mullite glass-ceramics: Mechanisms of formation and implications for fracture properties. Journal of Non-Crystalline Solids 2010;356(35–36) 1802–1813.

[113] Sommerauer J, Katz-Lehnert K. Trapped phosphate melt inclusions in silicate-carbonate-hydroxyapatite from comb-layer alvikites from the Kaiserstuhl carbonatite complex (SW-Germany). Contributions to Mineralogy and Petrology 1985;91(4) 354–359.

[114] Elliott JC. Recent progress in the chemistry, crystal chemistry and structure of the apatites. Calcified Tissue Research 1969;3(1) 293–307.

[115] Robert M, Robert OC. Fluorapatite laser material doped with neodymium and manganese. US patent US3504300 A, 1970.

[116] Prener JS. The growth and crystallographic properties of calcium fluor- and chlorapatite. Journal of the Electrochemical Society 1967;114(1) 77–83.

[117] Zeitschrift Für Kristallographie, Volume 207–208. Akademische Verlagsgessellschaft, 1993.

[118] Higuchi M, Masubuchi Y, Nakayama S, Kikkawa S, Kodaira K. Single crystal growth and oxide ion conductivity of apatite-type rare-earth silicates. Solid State Ionics 2004;174(1–4) 73–80.

[119] Higuchi M, Kodaira K, Nakayama S. Gowth of apatite-type neodymium silicate single crystals by the floating-zone method. Journal of Crystal Growth 1999;207(4) 298–302.

[120] Nakayama S, Sakamoto M, Higuchi M, Kodaira K, Sato M, Kakita S, Suzuki T, Itoh K. Oxide ionic conductivity of apatite type $Nd_{9.33}(SiO_4)_6O_2$ single crystal. Journal of the European Ceramic Society 1999;19(4) 507–510

[121] Koohpayeh SM, Fort D, Abell JS. The optical floating zone technique: A review of experimental procedures with special reference to oxides. Progress in Crystal Growth and Characterization of Materials 2008;54(3–4) 121–137.

[122] Masubuchi Y, Higuchi M, Kodaira K. Reinvestigation of phase relations around the oxyapatite phase in the Nd_2O_3-SiO_2 system 2003;247(1–2) 207–212.

[123] Yoshikawa A, Kochurikhin VV, Futagawa N, Shimamura K, Fukuda T. Growth of $Ca_8La_2(PO_4)_6O_2$ single crystals as substrates for GaN epitaxial growth. Journal of Crystal Growth 1999;204(3) 302–306.

[124] Masaoka M, Kyono A. Single crystal growth of lead vanado-chlorapatite $Pb_5(VO_4)_3Cl$ using CsCl flux method. Materials Letters 2006;60(29–30) 3922–3926.

[125] Roufosse A, Harvill ML, Gilliam OR, Kostiner E. The hydrothermal crystal growth of chlorapatite. Journal of Crystal Growth 1973;19(3) 211–212.

[126] Yu H, Zhang H, Wang X, Gu Z, Li X, Deng F. Local structure of hydroxyl-peroxy apatite: A combined XRD FT-IR, Raman, SEM and solid-state NMR study. Journal of Physics and Chemistry of Solids 2007;68(10) 1863–1871.

[127] Zhou H, Lee J. Nanoscale hydroxyapatite particles for bone tissue engineering. Acta Biomaterialia 2011;7(7) 2769–2781.

[128] Zhang C, Yang J, Quan Z, Yang P, Li C, Hou Z, Lin J. Hydroxyapatite nano-and microcrystals with multiform morphologies: controllable synthesis and luminescence properties. Cryst Growth Design 2009;9(6) 2725–2733.

[129] Kreidler ER, Hummel FA. The crystal chemistry of apatite: Structure fields of fluor- and chlorapatite. Journal of Physics and Chemistry of Solids 2007;68 1863–1871.

[130] Nacken R. The formation of apatite I. Zentralbl. Mineral., Geol. Paleontol. 1912; 545–559.

[131] Berak J. Rocz. Chem. 1961;35 23–30.

[132] Berak J, Tomczak-Hudina I. Phase equilibrium in the system of tricalcium phosphate-calcium fluoride. Rocz. Chem., 1972;46(12) 2157–2164.

[133] Alper A. Phase Diagrams 6-V: Materials Science and Technology, Volume - 5. Refractory materials - volume 6. Elsevier, 2012. ISBN: 978-0323154895.

[134] Wyllie PJ. Phase equilibria in system CaO-CO_2-H_2O and related systems, with implications form crystal growth of calcite and apatite. Journal of the American Ceramic Society 1967;50(1) 43–46.

[135] Ropp RC. Encyclopedia of the Alkaline Earth Compounds. Newnes, 2012. ISBN: 978-0444595539

[136] Sibtain A, Morgan A, MacDougall N. Physics for Clinical Oncology. OUP Oxford, 2012. ISBN: 978-0199573356

[137] Coleman ND. Expert Report Writing in Toxicology: Forensic, Scientific and Legal Aspects. John Wiley & Sons, 2014. ISBN: 978-1118432334

[138] Mathew M, Mayer I, Dickens B, Schroeder LW. Substitution in barium-fluoride apatite: The crystal structures of $Ba_{10}(PO_4)_6F_2$, $Ba_6La_2Na_2(PO_4)_6F_2$ and $Ba_4Nd_3Na_3(PO_4)_6F_2$. Journal of Solid State Chemistry 1979;28(1) 79–95.

[139] Fahami A, Nasiri-Tabrizi B, Ebrahimi-Kahrizsangi R. Mechanosynthesis and characterization of chlorapatite nanopowders. Materials Letters 2013;110 117–121.

[140] Baumer A, Argiolas R. Synthèses hydrothermals et determinations RX d´apatites chlorée, fluorée ou hydroxylée. Neues Jb Miner Mh 1981b;8 344–348.

[141] Nacken R. The formation of apatite I. Zentralbl.Mineral., Geol. Paleontol., 1912: 545–559.

[142] Sudarsanan K, Young RA, Wilson AJC. The structures of some cadmium `apatites' $Cd_5(MO_4)_3X$. I. Determination of the structures of $Cd_5(VO_4)_3I$, $Cd_5(PO_4)_3Br$, $Cd_3(AsO_4)_3Br$ and $Cd_5(VO_4)_3Br$. Acta Crystallographica Section B 1977;33(10) 3136–3142.

[143] Engel G. Z. anorg, allgem. Chem. 1968;362 273–280.

[144] Park HL, Jang MS. Phase transition in cadmium chlorapatite [$Cd_5(PO_4)_3Cl$]. Solid State Communications 1983;48(2) 109–110.

[145] Plaisier JR, de Graaff RAG, IJdo DJW. Structure determination of a new apatite: $Ba_5(OsO_5)_3Cl$. Materials Research Bulletin 1995;30(10) 1249–1252.

[146] Besse J.-P, Baud G, Levasseur G, Chevalier R. Structure cristalline de $Ba_5(ReO_5)_3C_1$: une nouvelle apatite contenant l'ion $(ReO_5)^{3-}$. Acta Crystallographica Section B 1979;35(8) 1756–1759.

[147] Baud G., Besse J.-P, Sueur G, Chevalier R. Structure de nouvelles apatites au rhenium contenant des anions volumineux: $Ba_{10}(ReO_5)_6X_2$ (X = Br, I). Materials Research Bulletin 1979;14(5) 675–682.

[148] Suzuki T, Kibe T. Specific surface free energy and morphology of chlorapatite crystals studied by modified Wilhelmy method. Journal of Crystal Growth 2010;312(20) 3025–3028.

[149] Ghosh P. Colloid and Interface Science. PHI Learning Pvt. Ltd., 2009. ISBN: 978-8120338579

[150] Han KN. Fundamentals of Aqueous Metallurgy. SME, 2002. ISBN: 978-0873352154

[151] Li NN, Fane AG, Ho WSW, Matsuura T. Advanced Membrane Technology and Applications, John Wiley & Sons, 2011. ISBN: 978-1118211540

[152] Suzuki T, Kumeda I, Teshima K, Oishi S. Specific surface free energies of strontium chlorapatite single crystal determined by contact angles of liquid droplets. Chemical Physics Letters 2006;421(4–6) 343–347.

[153] Wulff G.. Zur Frage dee Geschwindigkeit des Wachstums und der Auflösung de Krystallflächen. Zeitschrift für Kristallographie und Mineralogie 1901;34 449–530.

[154] Mutaftschiev B. The Atomistic Nature of Crystal Growth. Springer Series in Materials Science - Volume 43. Springer Science & Business Media, 2013. ISBN: 978-3662045916.

[155] Wopenka B, Pasteris JD. A mineralogical perspective on the apatite in bone. Materials Science and Engineering: C 2005;25(2) 131–143.

[156] Abouzeid Abdel-Z.M. Physical and thermal treatment of phosphate ores - An overview. International Journal of Mineral Processing 2008;85(4) 59–84.

[157] Pasero M, Kampf AR, Ferraris C, Pekov IV, Rakovan JR, White TJ. Nomenclature of the apatite supergroup minerals. European Journal of Mineralogy 2010;22 163–179.

[158] Fleet ME. Infrared spectra of carbonate apatites: ν2-Region bands. Biomaterials 2009;30(8) 1473–1481.

[159] Fleet ME, Liu X. Local structure of channel ions in carbonate apatite. Biomaterials. 2005;26(36) 7548–7554.

[160] Barralet J, Best S, Bonfield W. Carbonate substitution in precipitated hydroxyapatite: an investigation into the effects of reaction temperature and bicarbonate ion concentration. Journal of Biomedical Materials Research Part A 1998;41(1) 79–86.

[161] Penel G, Leroy G, Rey C, Bres E. MicroRaman spectral study of the PO_4 and CO_3 vibrational modes in synthetic and biological apatites. Calcified Tissue International 1998;63(6) 475–481.

[162] Dowker SEP, Anderson P, Elliott JC, Gao XJ. Crystal chemistry and dissolution of calcium phosphate in dental enamel. Mineralogical Magazine 1999;63(6) 791–800.

[163] Suchanek WL, Shuk P, Byrappa K, Riman RE, TenHuisen KS, Janas VF. Mechanochemical-hydrothermal synthesis of carbonated apatite powders at room temperature. Biomaterials 2002;23(3) 699–710.

[164] McClellan GH, Lehr JR. Crystal chemical investigation of natural apatites. The American Mineralogis 1969;54 1374–1391.

[165] Englert KM, McAteer JA, Lingeman JE. Williams Jr JC. High carbonate level of apatite in kidney stones implies infection, but is it predictive? Urolithiasis 2013;41(5) 389–394.

[166] Bazin D, Carpentier X, Brocheriou I, Dorfmuller P, Aubert S, Chappard C, Thiaudière D, Reguer S, Waychunas G, Jungers P, Daudon M. Revisiting the localisation of Zn^{2+} cations sorbed on pathological apatite calcifications made through X-ray absorption spectroscopy. Biochimie 2009;91(10) 1294–1300.

[167] Fleet ME, Liu X, Penelope LK. Accommodation of the carbonate ion in apatite: An FTIR and X-ray structure study of crystals synthesized at 2–4 GPa. American Mineralogist 2004;89 1422–1432.

[168] Grunenwald A, Keyser C, Sautereau AM, Crubézy E, Ludes B, Drouet C. Revisiting carbonate quantification in apatite (bio)minerals: a validated FTIR methodology. Journal of Archaeological Science 2014;49 134–141.

[169] Fleet ME, Liu X. Location of type B carbonate ion in type A–B carbonate apatite synthesized at high pressure. Journal of Solid State Chemistry 2004;177(9) 3174–3182.

[170] Ren F, Lu X, Leng Y. Ab initio simulation on the crystal structure and elastic properties of carbonated apatite. Journal of the Mechanical Behavior of Biomedical Materials 2013;26 59–67.

[171] Suetsugu Y, Takahashi Y, Okamura FP, Tanaka J. Structure Analysis of A-Type Carbonate Apatite by a Single-Crystal X-Ray Diffraction Method. Journal of Solid State Chemistry 2000;155(2) 292–297.

[172] Tonegawa T, Ikoma T, Suetsugu Y, Igawa N, Matsushita Y, Yoshioka T, Hanagata N, Tanaka J. Thermal expansion of type A carbonate apatite. Materials Science and Engineering: B 2010;173(1–3) 171–175

[173] Fleet ME, Liu X. Carbonate apatite type A synthesized at high pressure: new space group ($P3^{-}$) and orientation of channel carbonate ion. Journal of Solid State Chemistry 2003;174(2) 412–417.

[174] Elliott JC, Bonel G, Trombe JC. Space group and lattice constants of $Ca_{10}(PO_4)_6CO_3$. Journal of Applied Crystallography 1980;13(6) 618–621.

[175] Elliott JC. Structure and Chemistry of the Apatites and Other Calcium Orthophosphates, Elsevier Press, Amsterdam, 1994. ISBN: 978-0-444-81582-8

[176] Lafon JP, Champion E, Bernache-Assollant D. Processing of AB-type carbonated hydroxyapatite $Ca_{10-x}(PO_4)_{6-x}(CO_3)_x(OH)_{2-x-2y}(CO_3)_y$ ceramics with controlled composition. Journal of the European Ceramic Society 2008;28(1) 139–147.

[177] Yao F, LeGeros JP, LeGeros RZ. Simultaneous incorporation of carbonate and fluoride in synthetic apatites: Effect on crystallographic and physico-chemical properties. Acta Biomaterialia 2009;5(6) 2169–2177.

[178] Peroos S, Du Z, de Leeuw NH. A computer modelling study of the uptake, structure and distribution of carbonate defects in hydroxy-apatite. Biomaterials 2006;27(9) 2150–2161.

[179] Elliott JC. Some observations on the crystal chemistry of carbonate-containing apatites. Archives of Oral Biology 1962;7 277–282.

[180] Nasiri-Tabrizi B, Fahami A. Mechanosynthesis of nanosized B-type carbonated fluorapatite. Materials Letters 2014;134 42–46.

[181] Fahami A, Beall GW, Nasiri-Tabrizi B, Pingguan-Murphy B. Effect of high-energy ball milling on the formation and microstructural features of carbonated chlorapatite nanopowders. Ceramics International 2015a;41(3) 4750–4758.

[182] Fahami A, Nasiri-Tabrizi B, Beall GW, Pingguan-Murphy B. Effect of ion concentration on mechanosynthesis of carbonated chlorapatite nanopowders. Materials Letters 2015b;146 16–19.

[183] Kannan S, Rocha JHG, Ferreira JMF. Synthesis of hydroxy-chlorapatites solid solutions. Materials Letters 2006a;60(7) 864–868.

[184] Kannan S, Rebelo A, Ferreira JMF. Novel synthesis and structural characterization of fluorine and chlorine co-substituted hydroxyapatites. Journal of Inorganic Biochemistry 2006b;100(10) 1692–1697.

[185] Yoder CH, Pasteris JD, Krol KA, Weidner VL, Schaeffer RW. Synthesis, structure, and solubility of carbonated barium chlor- and hydroxylapatites. Polyhedron 2012;44(1) 143–149.

[186] Elliott JC, Dykes E, Mackie PE. Structure of bromapatite and the radius of the bromide ion. Acta Crystallographica Section B 1981;37(2) 435–438.

[187] Cruz FJAL, da Piedade MEM, Calado JCG. Standard molar enthalpies of formation of hydroxy-, chlor-, and bromapatite. The Journal of Chemical Thermodynamics 2005;37(10) 1061–1070.

[188] Cruz FJAL, da Piedade MEM, Calado JCG. Erratum to "Standard molar enthalpies of formation of hydroxy-, chlor-, and bromapatite" J. Chem. Thermodyn. 37 (2005) 1061–1070]. The Journal of Chemical Thermodynamics 2006;38(7) 938.

[189] Dykes E. Preparation and characterisation of calcium bromapatite. Materials Research Bulletin 1974;9(9) 1227–1236.

[190] Liu X, Fleet ME, Shieh SR, He Q. Synthetic lead bromapatite: X-ray structure at ambient pressure and compressibility up to about 20 GPa. Physics and Chemistry of Minerals 2011;38(5) 397–406.

[191] Bhatnagar VM. Lead bromapatite, $Pb_{10}(PO_4)_6Br_2$. Inorganic and Nuclear Chemistry Letters 1971;7(3) 231–232.

[192] Ojovan MI. Handbook of Advanced Radioactive Waste Conditioning Technologies. Woodhead Publishing Series in Energy. Elsevier, 2011. ISBN: 978-0857090959

[193] Uno M, Shinohara M, Yamanaka S, Kurosaki K. Some properties of a lead vanado-iodoapatite $Pb_{10}(VO_4)_6I_2$. Journal of Nuclear Materials 2001;294(1–2) 119–122.

[194] Cockbain AG. The crystal chemistry of the apatites. Mineralogical Magazine 1968;36(281) 654–660.

[195] Lu F, Yao T, Xu J, Wang J, Scott S, Dong Z, Ewingc RC, Lian J. Facile low temperature solid state synthesis of iodoapatite by high-energy ball milling. RSC Advances 2014;4 38718–38725.

[196] Henning PA, Erik Adolfsson E, Grins J. The chalcogenide phosphate apatites $Ca_{10}(PO_4)_6S$, $Sr_{10}(PO_4)_6S$, $Ba_{10}(PO_4)_6S$ and $Ca_{10}(PO_4)_6Se$. Zeitschrift für Kristallographie International journal for structural, physical, and chemical aspects of crystalline materials 2008;215(4) 226–230.

[197] Junga SH, Hana SH, Leeb JS, Kimb YJ. Synthesis and Phase Transformation of $Ca_{10}(PO_4)_6S$ Sulfoapatite by Solid-state Reaction with Sulfur Vapor. Synthesis and Reactivity in Inorganic Metal-Organic and Nano-Metal Chemistry 2008;38(3) 303–306.

[198] Manoun B, Azdouz M, Azrour M, Essehli R, Benmokhtar S, El Ammari L, Ezzahi A, Ider A, Lazor P. Synthesis, Rietveld refinements and Raman spectroscopic studies of tricationic lacunar apatites $Na_{1-x}K_xPb_4(AsO_4)_3$ ($0 \le x \le 1$). Journal of Molecular Structure 2011;986(1–3) 1–9.

[199] Lahrich S, Elmhammedi MA, Manoun B, Tamraoui Y, Mirinioui F, Azrour M, Lazor P. Elaboration, Rietveld refinements and vibrational spectroscopic study of $Na_{1-x}K_xCaPb_3(PO_4)_3$ lacunar apatites ($0 \le x \le 1$). Spectrochimica Acta Part A: Molecular and Biomolecular Spectroscopy 2015;145 493–499.

[200] Ternane R, Ferid M, Trabelsi-Ayedi M, Piriou B. Vibrational spectra of lead alkali apatites $Pb_8M_2(PO_4)_6$ with M = Ag and Na. Spectrochimica Acta Part A: Molecular and Biomolecular Spectroscopy 1999;55(9) 1793–1797.

[201] El Koumiri M, Oishi S, Sato S, El Ammari L, Elouadi B. The crystal structure of the lacunar apatite $NaPb_4(PO_4)_3$. Materials Research Bulletin 2000;35(4) 503–513.

[202] Naddari T, Savariault Jean-M., El Feki H, Salles P, Salah AB. Conductivity and Structural Investigations in Lacunary $Pb_6Ca_2Li_2(PO_4)_6$ Apatite. Journal of Solid State Chemistry 2002;166(1) 237–244.

[203] Azdouz M, Manoun B, Azrour M, Bih L, El Ammari L, Benmokhtar S, Lazor P. Synthesis, Rietveld refinements and Raman spectroscopy studies of the solid solution $Na_{1-x}K_xPb_4(VO_4)_3$ ($0 \le x \le 1$). Journal of Molecular Structure 2010;963(2–3) 258–266.

[204] Toumi M, Smiri L, Bulou A. Crystal Structure and Polarized Raman Spectra of $Ca_6Sm_2Na_2(PO_4)_6F_2$. Journal of Solid State Chemistry 2000;149(2) 308–313.

[205] Piotrowski A , Kahlenberg V , Fischer RX , Lee Y , Parise JB. The crystal structures of cesanite and its synthetic analogue - A comparison. American Mineralogist 2002;87 715–720.

[206] Knyazev AV, Bulanov EN, Korokin VZ. Synthesis and Thermal Expansion of $(SO_4)_3L$ (L = Halogen) compounds with the Apatite Structure. Inorganic materials 3013;49(11) 1133–1137.

[207] Klement R. Sodium calcium sulfate apatite, $Na_6Ca_4(SO_4)_6F_2$. Naturwissenschaften 1939;27(33) 568.

[208] Sha Lian-K, Chappell BW. Apatite chemical composition, determined by electron microprobe and laser-ablation inductively coupled plasma mass spectrometry, as a probe into granite petrogenesis. Geochimica et Cosmochimica Acta 1999;63(22) 3861–3881.

[209] Kreidler ER, Hummel FR. The crystal chemistry of apatite: Structure fields of fluor- and chlorapatite. The American Mineralogist 1970;55 170–184.

[210] Nikhare GN, Gedam SC, Dhoble SJ. Luminescence characteristics of $Na_3Ca_2(SO_4)_3F$: Ce^{3+} fluoride material. Cement and Concrete Research 1985;15(4) 581–584.

[211] Vázquez FT. A new compound: $K_3Ca_2(SO_4)_3F$, identified in coatings of heat recover cyclones. Cement and Concrete Research 1985;115(4) 581–584.

[212] Fayos J, Watkin DJ, Perez-Mendez M. Crystal structure of the apatite-like compound $K_3Ca_2(SO_4)_3F$. American Mineralogist 1987;72 209–212.

[213] Poddar A, Gedamb SC, Dhoblec SJ. Luminescence of Eu and Ce in $K_3Ca_2(SO_4)_3F$ fluoride material. Luminescence 2014, DOI: 10.1002/bio.2839

[214] Trabelsi IT, Oueslati A, Mhiri T, Toumi M. Synthesis, characterization and ionic conductivity of $Ca_{8-x}Sr_xBi_2(PO_4)_6O_2$ for x = (3, 4, 5). Journal of Alloys and Compounds 2015;641 14–21.

[215] Uvarov V, Shenawi-Khalil S, Popov I. New bismuth calcium oxysilicate with apatite structure: Synthesis and structural characterization. Journal of Solid State Chemistry 2010;183(7) 1484–1489.

[216] Huang J, Sleight AW. The Apatite Structure without an Inversion Center in a New Bismuth Calcium Vanadium Oxide: $BiCa_4V_3O_{13}$. Journal of Solid State Chemistry 1993;104(1) 52–58.

[217] Kazin PE, Zykin MA, Tretyakov YD, Jansen M. Synthesis and properties of colored copper-containing apatites of composition $Ca_5(PO_4)_3Cu_yO_{y+\delta}(OH)_{0.5-y-\delta}X_{0.5}$ (X=OH, F, Cl). Synthesis and properties of inorganic compounds 2008;53(3) 409–414.

[218] Kazin PE, Gazizova OR, Karpov AS, Jansen M, Tretyakov YD. Incorporation of 3d-metal ions in the hexagonal channels of the $Sr_5(PO_4)_3OH$ apatite. Solid State Sciences 2007;9 82–87.

[219] Kazin PE, Uskova MA, Tretyakov YD, Jansen M, Scheurell S, Kemnitz E. Formation of Bi(Pb)-2223 with chemically compatible V-rich phase. Physica C 1998;301 185–191.